Fakultät für Chemie
Fachgebiet Industrielle Biokatalyse

A new synthetic biology methodology for the cell-free production of industrial alcohols

Bettina I. Sommer

Vollständiger Abdruck der von der Fakultät für Chemie der Technischen Universität München zur Erlangung des akademischen Grades eines Doktors der Naturwissenschaften genehmigten Dissertation.

Vorsitzender: Univ.-Prof. Dr. T. Nilges

Prüfer der Dissertation:

1. Univ.-Prof. Dr. Th. Brück
2. Univ.-Prof. Dr. V. Sieber

Die Dissertation wurde am 30.09.2013 bei der Technischen Universität München eingereicht und durch die Fakultät für Chemie am 20.11.2013 angenommen.

We shall not cease from our exploration
And at the end of all our exploring
Will be to arrive where we started
And know the place for the first time
T.S. ELIOT

ABSTRACT

A completely new concept for cell-free biosynthesis of hydrophobic platform chemicals was developed in a cooperation project between university and industry.

In the first step the primary substrate glucose was converted to the universal metabolic intermediate pyruvate by four enzyme systems. Subsequently, an aerobic enzyme cascade was constructed to selectively convert pyruvate to ethanol or isobutanol. Thereby, NAD^+ is the sole cofactor. A further advantage of cell-free biosynthesis pathways is a higher tolerance against toxic end products, like alcohols. Furthermore, no metabolic side-reactions occur and the chosen enzymes allow harsh reaction conditions, such as extended reaction times and high temperatures.

During this project isobutanol and ethanol could be synthesised with almost 50 % of the theoretical yield.

In this thesis a specific reaction in isobutanol biosynthesis cascade was studied, which can be catalysed by acetohydroxyacid synthases or by acetolactate synthases.

Next to isobutanol synthesis the cell-free n-butanol synthesis was studied. Here, two reactions originating from clostridial n-butanol biosynthesis pathway were considered: Firstly, the reduction of acetoacetyl-CoA to ß-hydroxybutyryl-CoA being catalysed by a ß-hydroxybutyryl-CoA dehydrogenase. Secondly, the reduction of crotonyl-CoA to butyryl-CoA, catalysed by a butyryl-CoA dehydrogenase (Bcd).

Clostridial Bcds require two electron transfer proteins for their activity. Therefore, a trans-2-enoyl CoA reductase was chosen for cell-free n-butanol biosynthesis.

Additionally, we were able to partly reconstruct an alternative n-butanol pathway by applying a non-natural enzyme cascade. This alternative pathway includes conversion of crotylalcohol to n-butanol and requires therefore less CoA- dependent substrates.

KURZFASSUNG

Ein komplett neues Konzept zur zellfreien Synthese von hydrophoben chemischen Bausteinen wurde in einem Kooperationsprojekt zwischen Universität und Industrie entwickelt.

Im ersten Schritt wird das Substrat Glukose durch vier Enzymsysteme in den universellen Metaboliten Pyruvat umgewandelt. In einer weiteren aeroben Konversionskaskade wird Pyruvat zu Ethanol oder Isobutanol umgewandelt. Dabei ist NAD^+ der einzige Cofaktor. Ein weiterer Vorteil der zellfreien Biosynthesewege ist eine verbesserte Toleranz gegenüber toxischen Endprodukten, wie zum Beispiel Alkoholen. Außerdem treten keine metabolischen Nebenreaktionen auf und die ausgewählten Enzyme erlauben harte Reaktionsbedingungen, wie lange Laufzeiten und hohe Temperaturen.

Im Rahmen dieses Projekts wurde Isobutanol und Ethanol mit etwa 50 % der theoretischen Ausbeute gebildet.

In dieser Arbeit wurde eine spezifische Reaktion der Isobutanolsynthese betrachtet, die von Acetohydroxyacid Synthasen und von Acetolaktat Synthasen katalysiert werden kann.

Neben der Isobutanolsynthese wurde auch an der zellfreien n-Butanolproduktion gearbeitet. Hierbei wurden zwei Reaktionen aus dem clostridiellen Butanolsyntheseweg näher betrachtet: Zum einen, die Reduktion von Acetoacetyl-CoA zu ß-Hydroxybutyryl-CoA, welche von einer ß-Hydroxybutyryl-CoA Dehydrogenase (Hbd) katalysiert wird. Zum anderen die Reduktion von Crotonyl-CoA zu Butyryl-CoA, katalysiert durch eine Butyryl-CoA Dehydrogenase (Bcd).

Clostridielle Bcds benötigen zwei Elektronentransportproteine für ihre Aktivität. Deshalb wurde für die zellfreie Butanolsynthese auf eine Trans-2-enoyl-CoA Reduktase von *Treponema denticola* zurückgegriffen.

Außerdem, konnten wir Teile eines alternativen n-Butanol Synthesewegs nachstellen, indem wir eine nicht natürliche Enzymkaskade nutzten. Dieser alternative Weg beinhaltet die Umwandlung von Crotylalkohol zu n-Butanol und benötigt dadurch weniger CoA-Substrate.

EIDESSTATTLICHE ERKLÄRUNG

Hiermit versichere ich, dass ich die vorliegende Dissertation selbstständig verfasst, sowie die Ausführungen und Gedanken, welche anderen Schriften sinngemäß oder wörtlich entnommen wurden, sowie weitere Quellen und Hilfsmittel kenntlich gemacht habe. Die vorliegende Arbeit wurde bisher weder in gleicher noch ähnlicher Form einer anderen Prüfungsbehörde vorgelegt oder anderweitig veröffentlicht.

München, den 30.09.2013

ACKNOWLEDGEMENTS

I am deeply thankful to my supervisors for their constant support.
Firstly, to Prof. Dr. Thomas Brück, who accepted me as a doctoral candidate and provided me with a fascinating research topic. He was always willing to help me with all thinkable questions and problems.
Secondly, to Prof. Dr. Volker Sieber, who hosted me for more than one year at his institute and supported me with his advice, whenever necessary.

Special thanks to Dr. Daniel Garbe, who always took time for my questions.
You had always helpful answers and advises on hand, thanks therefore.

Next, I would like to thank Dr. Bernhard Loll for crystallizing AlsS and for his additional support.

Thanks to my project partners of "Zellfreie Bioproduktion von hydrophoben Synthesebausteinen aus nachwachsenden Rohstoffen" to Dr. Jan-Karl Guterl, Dr. Daniel Garbe, Steven Reiße, Martina Haack, Jörg Carsten, Fabian Steffler and Anja Schmidt. I enjoyed the time with all of you.

Especially I want to thank Martina for her support in the lab as well as with chemical analyses and for her accompany in uncountable hours spent driving between Garching and Straubing.

Also many thanks to my lab-bench-mate Jogi. I enjoyed every "Käffchen", "Schifferl", "Äthiopier" and "Inder" with you.

I like to thank my office mates (Martina, Tom, Johannes and Mahmoud) for the pleasant atmosphere, all the nice conversations and photo sessions.

Finally yet importantly, I like to thank the two persons, who are most meaningful in my life.
To my mum, who supported me in every thinkable kind and whom I could always ask for advice.
Moreover to Bastian, thanks a lot for being there for me during the last years.
Thanks for a great time and thanks for your great support, while writing this thesis.

LIST OF CONTENTS

LIST OF TABLES

LIST OF FIGURES

LIST OF ABBREVIATIONS

A_8	eight alanines
ABE	acetone, butanol and ethanol
acacCoA	acetoacetyl-CoA
Adh	alcohol dehydrogenase
AHAS	acetohydroxyacid synthase
Ala / A	alanine
AlDH	glyceraldehyde dehydrogenase
Als	acetolactate synthase
AlsS	acetolactate synthase from *B. subtilis*
Asn / N	asparagine
BCAA	branched-chain amino acid
Bcd	butyryl-CoA dehydrogenase
B. stearothermophilus / Bs	*Bacillus stearothermophilus*
B. subtilis	*Bacillus subtilis*
c	concentration
C	crude extract
C. acetobutylicum / Ca	*Clostridium acetobutylicum*
C. beijerinckii	*Clostridium beijerinckii*
CD	circular dichroism
CECFs	crude extract cell-free systems
C. kluyveri	*Clostridium kluyveri*
CoA	coenzyme A
CO_2	carbon dioxide
C. saccharobutylicum	*Clostridium saccharobutylicum*
cv	column volume
d	distance (layer thickness)
DHAD	dihydroxyacid dehydratase
E. coli	*Escherichia coli*
E.C.	enzyme commission
ED	Entner-Doudoroff
e.g.	example given
et al.	and other authors, *et alii*
etfA/B	electron-transfer-protein A/B
F	flow through
FadB	ß-hydroxyacyl-CoA dehydrogenase
FADH/FAD^+	flavin adenine dinucleotide
FID	flame ionization detector

Fig.	figure
fs	femto second
g	gram
GC	gas chromatography
GDH	glucose dehydrogenase
Gln / Q	glutamine
Glu / E	glutamate
Gly / G	glycine
G. thermodenitrificans / Gth	*Geobacillus thermodenitrificans*
h	hour
H	crude extract incubated for 20 min at 60 °C
ß-hbCoA	ß-hydroxybutyryl-CoA
Hbd	ß-hydroxybutyryl-CoA dehydrogenase
His / H	histidine
His_6-tag	attachment of 6 histidines on a protein
HPLC	high-performance liquid chromatography
H_2SO_4	sulphuric acid
H. volcanii	*Haloferax volcanii*
i.e.	id est (that is)
ID	identification number
Ile / I	isoleucine
IPTG	isopropyl-ß-1-thiogalactopyranoside
Kari	ketol-acid reductoisomerase
k_{cat}	catalytic constant
kDa	kilo Dalton [$1*10^3$ g/mol]
KDGA	2-keto-3-desoxygluconate aldolase
K_i	dissociation constant
K_M	Michaelis Menten constant
$KMnO_4$	potassium permanganate
LB	Luria-Bertani broth
LDH	lactate dehydrogenase
Leu / L	leucine
Lys / K	lysine
M	protein ladder
M	molar [mol/l]
M. aeolicus	*Methanococcus aeolicus*
MD	molecular dynamics
mg	milligram
$MgCl_2$	magnesium chloride

min	minutes
ml	millilitre
mM	mini molar
Mr	molecular weight
M. ruber /Mr	*Meiothermus ruber*
MRW	mean residue weight
n	nano ($1*10^{-9}$)
NADH/NAD^+	nicotinamide adenine dinucleotide
NADPH/$NADP^+$	nicotinamide adenine dinucleotide phosphate
Ni^{2+}-NTA	nickel- nitrilotriacetic acid
nm	nano meter
np	non-phosphorylative
ns	nano second
OD	optic density
opt	optimum
OYE	old yellow enzyme
P	pellet (insoluble fraction of crude extract)
PCR	polymerase chain reaction
pdb	protein data bank
Pdc	pyruvate decarboxylase
pH	decimal logarithm of the hydrogen ion activity
Phe / F	phenylalanine
Pro / P	proline
r^2	coefficient for determination
RMSD	root-mean-square deviation
psi	pounds per square inch
RT	room temperature
S. cerevisiae	*Saccharomyces cerevisiae*
SDS	sodium dodecyl sulphate
SEPs	synthetic enzymatic pathways
Ser / S	serine
sp	species
S. solfataricus / Ss	*Sulfolobus solfataricus*
T	temperature
t	time
TB	Terrific broth medium
T. denticola / Td	*Treponema denticola*
Ter	trans-2-enoyl CoA reductase
TEV	tobacco etch virus

Thr / T	threonine
T_m	melting point
T_{opt}	optimum temperature
Tyr / Y	tyrosine
U	unit (One unit of enzyme activity is defined as the amount of enzyme necessary to convert 1 µmol substrate per minute)
v_{max}	maximal speed
(v/v)	volume per volume
(w/v)	weight per volume
YqjM	2-enoate reductase from *B. subtilis*
Å	Angstrom
ΔG^0	Gibbs-Energy
°C	degree Celsius
ε_M	extinction coefficient at x nm [$M^{-1}cm^{-1}$]
µ	micro ($1*10^{-6}$)
µg	micro gram
µl	micro litre
%	per cent

Chapter 1

Introduction

1.1 BIOFUELS

Before industrial revolution, the global economy was largely based on carbon sources extracted from plants either directly or indirectly via animals. Even at the beginning of the 20th century, many industrial materials (e.g. dyes and solvents) were produced from plants. This changed by the late 1960s, when most chemical products turned to be petroleum based. It is expected that fossil fuels, which formed during thousands of years, are being used up in a short time period. Furthermore, it is assumed, that energy demand will grow more than 50 % by 2025 especially due to increased demand of developing nations [1]. Therefore, in the near future increasing environmental problems will arise particularly from carbon dioxide (CO_2) produced during fossil fuels combustion. Shifting society's dependence from fossil fuels to renewable biomass resources is generally viewed as a possible solution to provide for a sustainable industrial society and an effective management of greenhouse gas emission.

A promising approach in biofuel production is recycling CO_2 by using naturally evolved photosynthesis. In this context, two possible, approaches exist. Firstly, CO_2 is fixated in biomass producing plants and subsequently converted in biological (microbial fermentation- or enzymatic) or thermochemical processes to liquid fuels. In the second, more direct approach CO_2 is incorporated by a photosynthetic, fuel-producing organism, i. e. algae [2]. The latter features advantages as no fertilizers and pesticides are necessary for growing the crops.

First generation biofuels are mostly bioalcohols (e.g. ethanol), biodiesel and vegetable oils. While lipids for biodiesel production are extracted from oil plants (e.g. soybean and palm) by transesterification [3], ethanol is traditionally produced by fermentation. *Saccharomyces cerevisiae* or *Zymomonas mobilis* converts with high product yields sugars (mostly hexose) via glycolysis to ethanol [4].

Summarized, biofuels serve two purposes: A) reducing dependency on expensive fossil fuels and B) decreasing emissions of greenhouse gases. However, considering biofuels the food versus fuel debate [5] arises. It might not be responsible to use biomass that could also be used as a food resource to accommodate global energy demands of a growing population. To avoid this conflict biofuels should be created from waste products rather than from crops.

Therefore, the use of lignocelluloses as well as low-input high-diversity mixtures of native grassland perennials [6] as carbon source can be possibilities for large-scale biofuel production. However, this option requires integrative consideration of land-use policy and water resource distribution [7].

1.1.1 Fuel Properties

Biofuels are designed to substitute petroleum-based fuels consisting primarily of alkanes with various carbon chain lengths branching and saturation patterns. It is desired that biofuels have equivalent physical and energetic characteristics as fossil fuels. This would allow the use of existing infrastructure and profiting from minimize greenhouse gas emissions. In general, longer carbon chains have lower octane numbers, while higher branching increases the octane number.

Gasoline

Conventional gasoline consists of smaller alkanes (6 - 9 carbons) with specific vapour pressure and octane number, which is important for automotive industry.

Diesel

In contrast to gasoline, diesel fuel consists of longer alkanes containing 12 to 20 carbons in length. Considering long-chain alkanes the freezing point is important, as they solidify at temperatures lower 10 °C.

Ethanol

Ethanol is no optimal gasoline replacement as it provides less energy per volume and a lower vapour pressure than conventional gasoline. In addition, its hygroscopicity is damaging existing pipelines and engine ducts (Table 1.1). Furthermore, blending gasoline with ethanol increases vapour pressure of the mixture and changes the gasoline fuel properties.

Table 1.1: Comparison of chemical properties of liquid fuels (inherited from [7]).

Fuel	Ethanol	n-Butanol	Isobutanol	Alkanes (gasoline)	Alkanes (diesel)	Fatty acid methyl esters (biodiesel)
Heating value (MJ/L)	21	29	29	32	39	37
Vapour pressure (psi)	1.1	0.077	0.17	0.1-30	<0.01	<0.01
Blended vapour pressure (psi)	20[a]	6.4[a]	6.8[a]	7.8-15		
Average of octane number[b]	116	87	110	90		
Hygroscopicity	High	Low	Low	Low	Very low	Very low
Fits current infrastructure?	No	Yes	Yes	Yes	Yes	No

[a] Alcohol blended at 10 % with gasoline.

[b] Average of research- and motor octane number.

n-Butanol

Advanced biofuels like n-butanol and isobutanol are better suitable than ethanol as gasoline equivalent. n-Butanol possesses a high heating value and a low hygroscopicity.

Isobutanol

Isobutanol has a higher octane number than n-butanol due to its carbon chain branching. Therefore, it allows more flexibility in fuel design. Additionally, isobutanol can serve as a precursor for the production of isobutene [8], which, at present, is exclusively produced in large scale by petroleum refining. Isobutene is used as a gasoline additive and for the production of butyl rubber and chemicals [9].

1.1.2 Biofuel Production in Cells

Advantages of native biofuel producers (like clostridia and yeast) in fermentation processes are at least initial higher production efficiency and higher tolerance of these organisms towards the toxic end product. These native producers are mostly not amenable to genetic manipulation and their physiological regulation is often poorly understood. This is especially important, as optimization of such a process is lab-intensive and time consuming. Additionally, effects of strain engineering are hardly predictable and results can, in general, not be transferred to other target products or organisms [10].

In fermentation processes product formation and cell growth are not correlated [11]. For cell growth feedstock is metabolised, which can consequently not be converted in target product. To overcome this problem fed-batch fermentations [12] were applied to uncouple cell growth from product formation. However, general problems of microbial fermentation systems remain, like phage infection, microbial contamination or cell sporulation.

However, in practice the theoretical yield (Table 1.2) in fermentation processes can often not be achieved.

Table 1.2: Energy yield of various fuels (inherited from [7]).

Fuel	Mass energy density (MJ kg^{-1})	Volumetric energy density (MJl^{-1})	Max biochemical yield (g g^{-1})[a]	Energy yield from glucose (%)[b]
Gasoline	42.7	32.0	/	/
Diesel	45.5	38.7	/	/
Ethanol	29.7	20.8	0.511	97.6
n-butanol	36.1	29.2	0.411	95.4
Isobutanol	36.1	29.0	0.411	95.4

[a] Theoretical yield based on best available cell metabolic pathways.

[b] Based on an energy density for glucose of 15.6 MJkg^{-1}, using pathway yield.

This might be due to a competition for substrate and cofactor use between endogenous and heterologous metabolic pathways [13]. Additionally, reaction rate at each step involves regulation at the level of gene transcription, which is dependent on mRNA stability and translation [14].
Furthermore, the produced compounds may be destructive for the microbial membrane and toxic for the host metabolism [15]. Additionally, low product titres demand cost and energy intensive product recoveries such as distillation.
When using lignocellulose hydrolysate as carbon source, toxicity may also arise from the physiochemical pre-treatment and depolymerisation procedures resulting in formation of degradation products such as furan derivatives, phenols and carboxylic acids [16].

1.1.2.1 State of the Art Isobutanol Production in Non-Natural Hosts

Since no native organisms have been identified to produce advanced biofuels in considerable quantities [17], synthetic metabolic pathways were introduced into non-natural hosts to catalyse new chemical reactions.
Additionally, to enhance the biofuel production competing reactions have to be eliminated from the metabolism and the metabolic flux of the system has to be streamlined towards higher production of the target. For isobutanol production, several organisms were engineered and optimized.
To produce C3 – C5 alcohols the enzymes ketoacid decarboxylase (Kdc) and alcohol dehydrogenase (Adh) were added to the naturally amino acid biosynthetic pathway (Ehrlich pathway) [18]. Due to the ubiquity of these pathways, this concept is working in many organisms and therefore shows significant promise for industrial applications.
In addition, Atsumi *et al.* (2009) introduced an acetolactate synthase from *Bacillus subtilis* (AlsS) (Chapter 4) to increase the affinity for pyruvate compared to an acetohydroxyacid synthase, that is involved in amino acid biosynthesis (Chapter 2 and 3). Therefore, the carbon flow was redirected towards isobutanol production instead of glycolysis [19].
Atsumi *et al.* (2008) were able to produce 22 g/l of isobutanol in 4.7 days under micro-aerobic conditions by deleting competing pathways in *E. coli*. This corresponds to a yield of 86 % of theoretical maximum [20]. Additionally, cell chemical mutagenesis approaches combined with amino acid analogue growth based selection were used to increase strain tolerance to the desired alcohol [21].
In a subsequent study, this improved strain produced more than 50 g/l isobutanol aerobically in three days with *in situ* product removal by using a gas stripping method [22, 23]. Therefore, *in situ* product removal might allow to overcome isobutanol toxicity in host organisms.

By resolving the cofactor imbalance in the isobutanol production pathway, Bastian *et al.* (2011) was able to achieve 100 % of the theoretical maximum under anaerobic conditions [24].

As demonstrated for the industrial production of bioethanol, *S. cerevisiae* is an ideal host for bio-refinery processes due to its capacity for cell-recycle fermentation and its remarkable tolerance against low pH, high temperature and various inhibitors [25]. Additionally, *S. cerevisiae* is an extremely well characterised model organism, with a large variety of research tools and resources simplifying metabolic engineering [26-28].
Chen *et al.* (2011) used enzymes involved in the valine biosynthesis in *S. cerevisiae* and was able to produce 4.12 mg of isobutanol per gram of glucose [29]. In contrast Kondo *et al.* (2012) were even able to produce 6.6 mg per gram of glucose, hereby the isobutanol titre was elevated to 143 mg/l [30].

Corynebacterium glutamicum was used for isobutanol production achieving titres up to 4.9 g/l in five days under aerobic conditions [31]. *C. glutamicum* is a Gram-positive bacterium, which is usually used for industrial amino acids production.

The photoautotroph cyanobacteria *Synechococcus elongatus* was able to produce 450 mg/l isobutanol with the same heterologous enzymes as *E. coli* [32]. Cyanobacteria are known to be more tolerant towards isobutanol. Therefore, *S. elongatus* was also engineered for isobutyraldehyde production, a molecule that can be easily removed from the fermentation approach with a gas stripping method [33]. Isobutyraldehyde could be produced with a maximum titre of 1.1 g/l in eight days [34].

Clostridium cellulolyticum is able to use crystallized cellulose without the need to chemically or exoenzymatically breakdown of polysaccharides [35]. *C. cellulolyticum* could be engineered to produce isobutanol at titres up to 0.66 g/l with crystallized cellulose as substrate [36].

1.1.2.2 State of the Art n-Butanol Production in Host Organism

Traditionally n-butanol is produced by the clostridial acetone, butanol and ethanol (ABE-) fermentation process [37].
Additionally, n-butanol has been produced in *E. coli* through the non-natural amino acid norvaline pathway with a maximum of 2 g/l [38].
In an alternative approach, five genes of the n-butanol producing pathway were introduced in *E. coli* for n-butanol production, resulting in a titre of 0.58 g/l [39]. For system optimization a chimeric pathway assembled from three different organisms was constructed, able to produce 4.65 g/l under semi-aerobic conditions [40].

Shen *et al.* (2011) achieved titres of 30 g/l with *E. coli* in seven days under anaerobic fermentation conditions with continuous removal of the product while 15 g/l were achieved in three days without product removal [41]. Therefore, they knocked out competing NADH consuming pathways and increased the acetyl-CoA driving force.
In summary, it was possible to produce n-butanol anaerobically in *E. coli* at reasonable biofuel production titres, when continuous product removal was applied.

1.1.3 Cell-Free Production Systems

In contrast to cell-based fermentation processes for biofuel production, also cell-free production systems are currently examined for application. In this context, it is possible to design non-natural metabolic pathways that are only restricted by thermodynamic limitations, enzyme performance and natural cofactor stability [42].
Generally, two types of enzymatic cell-free reaction concepts are distinguished: crude extract cell-free systems (CECFs) and synthetic enzymatic pathways (SEPs) [43]. CECFs are prepared by cell lysis and if necessary by subsequent removal of the cell debris. In contrast, SEPs consist of purified enzymes and cofactors, which have to be added to the system. This concept enables superior control on catalyst concentration and composition.
The decision for one of these concepts is based on the necessity of catalyst purity.
During the last few years enzymatic cascades were applied to produce chemicals and gained increasing popularity as restrictions derived from the microbial physiology could be circumvented.

However, cell-free systems are not a recent discovery. Eduard Buchner already fermented ethanol using cell-free yeast extract more than hundred years ago [44]. In his approach, glucose was converted to two molecules ethanol and carbon dioxide under formation of two molecules ATP (Figure 1.1).

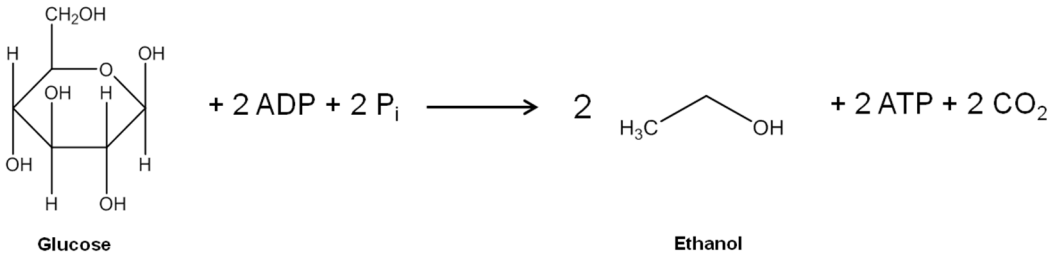

Figure 1.1: Conversion of glucose to ethanol.

1.1.3.1 Disadvantages of Cell-Free Production Systems

The major disadvantage of cell-free production systems is that they are more expensive than microbial fermentations due to enzyme production and purification.

Additionally, biofuels are low-value bulk products, therefore, it is not economical to use an expensive feedstock. Final production costs are also significantly impacted by the expensive cofactors.

However, enzyme production and purification costs can be decreased by consolidated expression of several enzymes in a single microbial host and/or by application of crude extract cell-free systems.

Additionally, biomimetic NAD^+/NADH coenzymes can be used [45, 46], which are in general much more stable compared to their native counterparts. Biomimetic cofactors can be recycled up to ~500,000 times [14] and thus the costs are negligible.

1.1.3.2 Advantages of Cell-Free Production Systems

Advantages of cell-free approaches are high product yields, fast reaction rates, high product titres, a broad range of reaction conditions and a simplified process control [47].

Additionally, *in vitro* biocatalytic cascades are less complex compared to *in vivo* systems. This fact is illustrated in Figure 1.2, where six subsequent biochemical reactions are shown.

Regarding the *in vitro* platform, it is assumed, that for every enzymatic step, five enzymes can be identified performing the same reaction. Following this assumption, 30 combinations are possible.

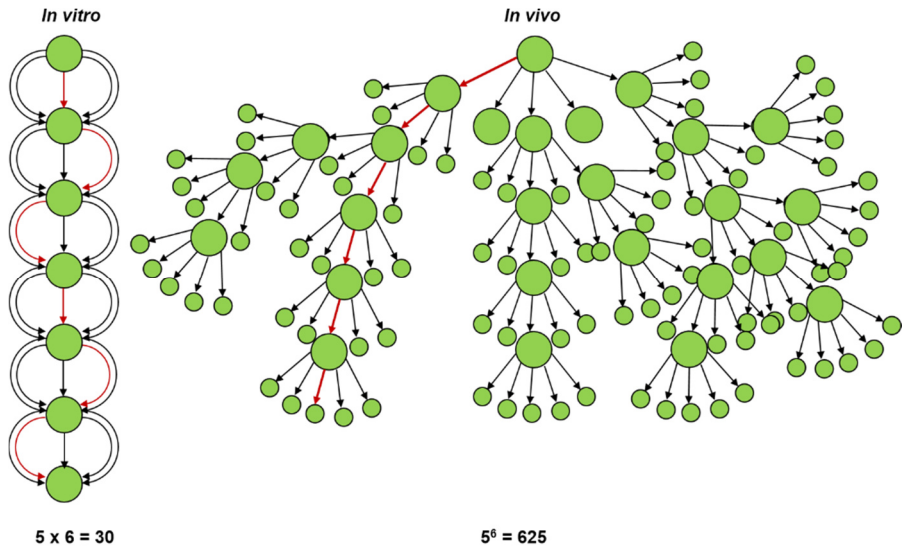

Figure 1.2: Comparison of *in vitro* and *in vivo* platforms.
Regarding six subsequent biochemical reactions the *in vitro* approach is with 30 possible combinations much less complex compared to the *in vivo* approach with 625 possible combinations. The red arrows represent the optimized pathway (inherited from [14]).

In vivo systems, given the same assumptions, are much more complex. Each enzymatic step is linked with other reactions and pathways combinations.

By application of simplified reaction systems, side reactions and substrate redirection are eliminated. Additionally, enzymes are able to work in presence of higher solvent concentrations compared to cell-based systems. Therefore, highly simplified product removal by phase separation is possible [48]. In optimized production systems continuous product recovery may be envisioned.

Enzymes originating from extremophilic organisms are able to tolerate higher process temperatures, thereby featuring higher reaction rates. These reaction systems also provide higher substrate diffusion, lower viscosities, better phase separation and decreased bacterial contamination of the reaction medium.

Enhanced enzyme stability, prevention of protein contamination in the product as well as easy separation of the enzymes from the reaction mixture can additionally be achieved by immobilizing enzymes [49].

1.2 PRODUCTION OF CHEMICALS VIA MINIMIZED REACTION CASCADES

In this study, a new, aerobic and cell-free reaction cascade is designed featuring a minimum of enzyme system components.

The preliminary work was published in 2012 and presented a cell-free approach featuring an artificial minimized glycolytic reaction cascade, which requires only NADH as cofactor [42]. Characteristically, the used toolbox forms the central intermediate pyruvate from the substrate glucose that enables an array of industrially relevant molecules. These are synthesised aerobically and cell-free, as reported for the biofuels ethanol and isobutanol [42]. Simultaneously, it was attempted to produce n-butanol.

For industrial application enzymes with improved tolerance to higher process temperatures as well as to higher solvent concentrations are required. Therefore, enzymes originating from extremophilic organism were preferentially chosen [50, 51]. Additionally, enzyme fidelity was selected according to the demand for substrate selectivity.

1.2.1 Pathway Design

Pyruvate, the central intermediate of the designed pathways, is produced from glucose using a modified non-phosphorylative Entner-Doudoroff-Pathway (np-ED) derived from hyperthermophilic archaea [52]. Therefore, one mol glucose is converted into two moles pyruvate by action of the following four enzymes: glucose dehydrogenase (GDH) [53], gluconate/glyceraldehyde dehydroxyacid dehydratase (DHAD) [54], 2-keto-3-desoxygluconate aldolase (KDGA) [55] and glyceraldehyde dehydrogenase (AlDH) [56, 57].

With the use of DHAD from *Sulfolobus solfataricus* (*Ss*DHAD) [54] dephosphorylation and phosphorylation steps included in the natural ED pathway could be eliminated. Additionally, the number of required enzymes could be reduced as *Ss*DHAD is able to perform two steps in pyruvate synthesis (Figure 1.3A) and one step in isobutanol synthesis (Figure 1.3B) (Research results of Jörg Carsten (Technische Universität München, Straubing, Germany)).

1.2.2 Ethanol Synthesis

For ethanol synthesis pyruvate was subsequently converted to acetaldehyde by a pyruvate decarboxylase (Pdc) [58] and then further elaborated to ethanol by an alcohol dehydrogenase (Adh) [59, 60].
Application of the enzyme cascade allowed conversion of 25 mM glucose to 28.7 mM ethanol in 19 h under adding of 5 mM NAD^+. The molar yield was 57.4 % [42]. Based on the initial substrate and coenzyme concentrations this result suggests NAD^+ and NADH recycling.
Summarized, we were able to produce 1.3 g/l ethanol without any enzyme or process optimization.

1.2.3 Isobutanol Synthesis

For the production of C3 – C5 alcohols by the Ehrlich pathway a ketoacid decarboxylase (Kdc) and an alcohol dehydrogenase (Adh) were added, as described for the isobutanol production in *E. coli* (1.1.2.1). In our approach, we advanced this concept and converted pyruvate to isobutanol using only four additional enzymes (Figure 1.3).
In a completely cell-free environment one molecule pyruvate was decarboxylated and ligated to another molecule of pyruvate by the action of an acetolactate synthase (Als, Chapter 4) [61]. The obtained acetolactate was further converted by ketol-acid reductoisomerase (Kari) [62] resulting in dihydroxyisovalerate. This natural DHAD substrate was then converted into 2-ketoisovalerate. Finally isobutanol was produced by 2-ketoacid decarboxylase (Kdc) [58, 63] and Adh [59, 60] via isobutyraldehyde.
Measurements showed that 19.1 mM glucose was converted to 10.3 mM isobutanol within 23 h corresponding to a molar yield of 53 %.
We were able to produce 0.8 g/l isobutanol in 23 h without optimization in a cell-free system. This conforms a higher amount of isobutanol than produced in fermentation processes using *C. cellulolyticum*, *S. elongates* or *S. cerevisiae* as host organism.

1.2.4 Butanol Synthesis

To produce n-butanol seven different reactions have to be catalysed (Figure 1.3). The pyruvate dehydrogenase complex transforms pyruvate into acetyl-CoA.

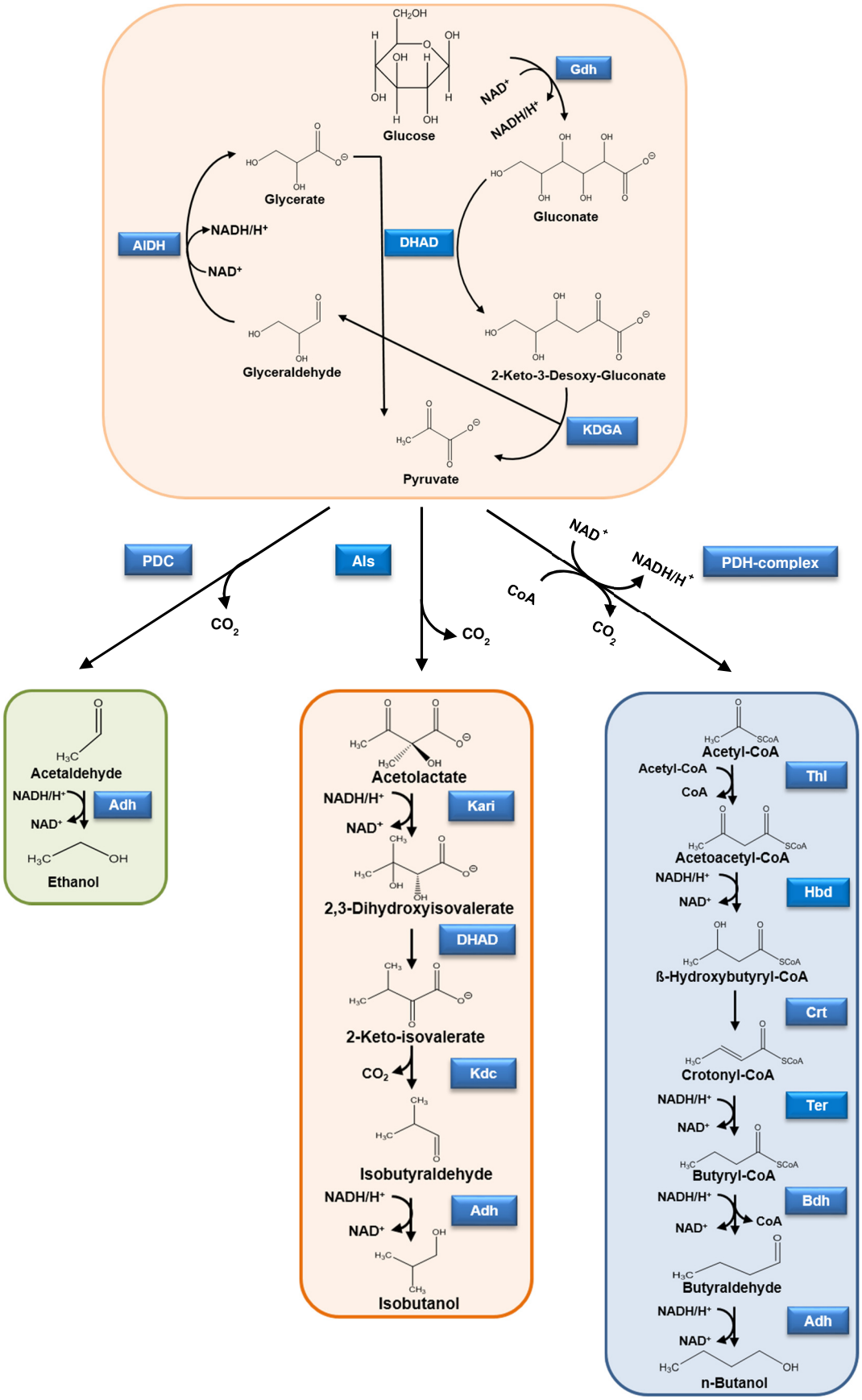

Figure 1.3: Schematic presentation of cell-free reaction pathways to produce ethanol, isobutanol and n-butanol starting from glucose.

Thiolase (Thl), also known as acetyl-CoA acetyltransferase, condenses two molecules of acetyl-CoA to one molecule of acetoacetyl-CoA. Afterwards acetoacetyl-CoA has to go through four steps of NADH-dependent reduction and one step of dehydration. First, ß-hydroxybutyryl-CoA dehydrogenase (Hbd) reduces acetoacetyl-CoA to ß-hydroxybutyryl-CoA (Chapter 5). Then, crotonase (Crt) dehydrates 3-hydroxybutyryl-CoA to crotonyl-CoA. Third, butyryl-CoA dehydrogenase (Bcd) or alternatively trans-2-enoyl-CoA reductase (Ter) converts crotonyl-CoA to butyryl-CoA (Chapter 6). Finally, an aldehyde dehydrogenase (Bhd) and an Adh form n-butanol in two consecutive reduction reactions.
Up to now no reliable cell-free n-butanol production was possible and further improvements will be subject to ongoing scientific research.

1.3 MOLECULAR HYDROGEN PRODUCTION BY A SYNTHETIC ENZYMATIC PATHWAY

The use of hydrogen as renewable biofuel enables a compelling energy vision, but there are several impediments like hydrogen production, storage, distribution, as well as fuel cells. Hydrogen production from renewable biomass could produce cheaper hydrogen compared to already applied systems, decrease reliance on fossil fuels and achieve zero net greenhouse gas emissions.
In 2000 Woodward and co-workers developed an enzymatic reaction pathway for the production of molecular hydrogen from the intermediate glucose-6-phosphate [64].
Zhang *et al.* (2007) demonstrated a synthetic enzymatic pathway consisting of 13 enzymes for producing hydrogen from glucose-6-phosphate derived from starch and water at 30 °C in the following reaction [65].

$$C_6H_{13}0_9P_i + 12\ NADP^+ + 7\ H_2O \rightleftharpoons 12NADPH + 12H^+ + 6CO_2 + P_i$$

The core part of this enzymatic toolbox is a synthetic, non-natural pathway resembling the pentose phosphate pathway consisting of 11 enzymes. Independent from the initial substrate, the main starting intermediate for this pathway is glucose-1-phosphate.
Because NADPH was used as universal electron carrier in this system, an expansion of this concept serving as a biomass-based NAD(P)H generation system for multiple purposes can be envisioned [10].
Hereby, the hydrogen yields were much higher than the theoretical limit ($4H_2$/glucose) of anaerobic fermentations. With technology improvements, i.e. hydrogen storage, distribution and infrastructure in the hydrogen economy and integration in fuel cells, this technology might be able to satisfy the growing energy demand.

Several attempts have been made to produce electricity by enzymatic fuel cells. A promising approach was done by Xu and Minteer (2011), yielding a maximum of 24 electrons by complete oxidation of glucose to CO_2 [66].

1.4 SCOPE OF THE WORK

In the context of a cooperation project between the Chair of Chemistry of Biogenic Resources (Technische Universität München, Straubing, Germany), the Division of Industrial Biocatalysis (Technische Universität München, Garching, Germany) and the industrial partner Clariant Produkte Deutschland GmbH (München, Germany) a completely new concept to produce in a cell-free reaction cascade chemical buildings blocks as well as biofuels from renewable resources was developed.

The aim of this research project was a more efficient as well as more versatile utilisation of biomass. Using the designed cell-free systems higher product titres can be achieved compared to conventionally used fermentation processes. The production of hydrophobic compounds above solubility limitations enables an easier and cheaper product separation, as products can easily be removed from reaction mixture.

With the start of this project the major focus was on the cell-free production of ethanol, isobutanol and n-butanol. Therefore, this thesis deals with three different reactions involved in aerobic, cell-free isobutanol and n-butanol production.

For isobutanol synthesis, enzymes suitable to join two molecules of pyruvate and form one molecule acetolactate were screened.

For n-butanol production two reactions were considered. One to reduce acetoacetyl-CoA to ß-hydroxybutyryl-CoA and the other to catalyse reduction of crotonyl-CoA to butyryl-CoA.

In a first step, suitable enzymes for each reaction were identified based on literature precedence. Genes were cloned in expression vectors with and without terminal His_6-tags. Subsequently, the enzymes were tested towards their expression and reactivity with the desired substrate.

If the enzymes were able to catalyse the desired reactions and could be expressed in reasonable amounts, the enzymes were further characterised. The main focus was laid on a biochemically characterisation towards their thermostability, solvent tolerance and fidelity.

Additionally, kinetic parameter like K_M, k_{cat} and K_i were determined, which enables bioinformatic studies on the pathways targeted identification of the optimal enzyme composition for large reaction scale ups.

In large reaction scale ups all enzymes of a biosynthetic pathway were assembled *in vitro* and the desired product was synthesised. Additionally, for all occurring intermediates appropriate GC and/or HPLC analyses methods have been developed.

1.5 REFERENCES

1. **Ragauskas AJ, Williams CK, Davison BH, Britovsek G, Cairney J, Eckert CA, Frederick WJ, Jr., Hallett JP, Leak DJ, Liotta CL, Mielenz JR, Murphy R, Templer R, Tschaplinski T.** 2006. The path forward for biofuels and biomaterials. Science **311:**484-489.
2. **Wackett LP.** 2011. Engineering microbes to produce biofuels. Curr Opin Biotechnol **22:**388-393.
3. **Leung DY, Wu X, Leung M.** 2010. A review on biodiesel production using catalyzed transesterification. Applied Energy **87:**1083-1095.
4. **Dien B, Cotta M, Jeffries T.** 2003. Bacteria engineered for fuel ethanol production: current status. Applied microbiology and biotechnology **63:**258-266.
5. **Zhang Z, Lohr L, Escalante C, Wetzstein M.** 2010. Food versus fuel: What do prices tell us? Energy Policy **38:**445-451.
6. **Tilman D, Hill J, Lehman C.** 2006. Carbon-negative biofuels from low-input high-diversity grassland biomass. Science **314:**1598-1600.
7. **Li H, Cann AF, Liao JC.** 2010. Biofuels: biomolecular engineering fundamentals and advances. Annu Rev Chem Biomol Eng **1:**19-36.
8. **Macho Vn, Králik M, Jurecekova E, Hudec J, Jurecek L.** 2001. Dehydration of C_4 alkanols conjugated with a positional and skeletal isomerisation of the formed C_4 alkenes. Applied Catalysis A: General **214:**251-257.
9. **Gogerty DS, Bobik TA.** 2010. Formation of isobutene from 3-hydroxy-3-methylbutyrate by diphosphomevalonate decarboxylase. Appl Environ Microbiol **76:**8004-8010.
10. **Guterl JK, Sieber V.** 2013. Biosynthesis "debugged": novel bioproduction strategies. Engineering in Life Sciences **13:**4-18.
11. **Parekh S, Vinci V, Strobel R.** 2000. Improvement of microbial strains and fermentation processes. Applied Microbiology and Biotechnology **54:**287-301.
12. **Yee L, Blanch H.** 1992. Recombinant protein expression in high cell density fed-batch cultures of Escherichia coli. Nature Biotechnology **10:**1550-1556.
13. **Lee SK, Chou H, Ham TS, Lee TS, Keasling JD.** 2008. Metabolic engineering of microorganisms for biofuels production: from bugs to synthetic biology to fuels. Curr Opin Biotechnol **19:**556-563.
14. **Zhang YH, Sun J, Zhong JJ.** 2010. Biofuel production by in vitro synthetic enzymatic pathway biotransformation. Curr Opin Biotechnol **21:**663-669.
15. **Fischer CR, Klein-Marcuschamer D, Stephanopoulos G.** 2008. Selection and optimization of microbial hosts for biofuels production. Metab Eng **10:**295-304.
16. **Nichols NN, Dien BS, López MJ, Moreno J.** 2010. Use of Coniochaeta ligniaria to detoxify fermentation inhibitors present in cellulosic sugar streams. Biocatalysis and Biomolecular Engineering**:**253-263.
17. **Clomburg JM, Gonzalez R.** 2010. Biofuel production in Escherichia coli: the role of metabolic engineering and synthetic biology. Applied microbiology and biotechnology **86:**419-434.
18. **Hazelwood LA, Daran JM, van Maris AJ, Pronk JT, Dickinson JR.** 2008. The Ehrlich pathway for fusel alcohol production: a century of research on Saccharomyces cerevisiae metabolism. Appl Environ Microbiol **74:**2259-2266.
19. **Atsumi S, Li Z, Liao JC.** 2009. Acetolactate synthase from Bacillus subtilis serves as a 2-ketoisovalerate decarboxylase for isobutanol biosynthesis in Escherichia coli. Appl Environ Microbiol **75:**6306-6311.
20. **Atsumi S, Hanai T, Liao JC.** 2008. Non-fermentative pathways for synthesis of branched-chain higher alcohols as biofuels. Nature **451:**86-89.

21. **Atsumi S, Wu TY, Machado IM, Huang WC, Chen PY, Pellegrini M, Liao JC.** 2010. Evolution, genomic analysis, and reconstruction of isobutanol tolerance in Escherichia coli. Mol Syst Biol **6:**449.

22. **Baez A, Cho KM, Liao JC.** 2011. High-flux isobutanol production using engineered Escherichia coli: a bioreactor study with in situ product removal. Appl Microbiol Biotechnol **90:**1681-1690.

23. **Atsumi S, Wu TY, Eckl EM, Hawkins SD, Buelter T, Liao JC.** 2010. Engineering the isobutanol biosynthetic pathway in Escherichia coli by comparison of three aldehyde reductase/alcohol dehydrogenase genes. Appl Microbiol Biotechnol **85:**651-657.

24. **Bastian S, Liu X, Meyerowitz JT, Snow CD, Chen MM, Arnold FH.** 2011. Engineered ketol-acid reductoisomerase and alcohol dehydrogenase enable anaerobic 2-methylpropan-1-ol production at theoretical yield in Escherichia coli. Metab Eng **13:**345-352.

25. **Hasunuma T, Kondo A.** 2012. Development of yeast cell factories for consolidated bioprocessing of lignocellulose to bioethanol through cell surface engineering. Biotechnol Adv **30:**1207-1218.

26. **Cherry JM, Hong EL, Amundsen C, Balakrishnan R, Binkley G, Chan ET, Christie KR, Costanzo MC, Dwight SS, Engel SR, Fisk DG, Hirschman JE, Hitz BC, Karra K, Krieger CJ, Miyasato SR, Nash RS, Park J, Skrzypek MS, Simison M, Weng S, Wong ED.** 2012. Saccharomyces Genome Database: the genomics resource of budding yeast. Nucleic acids research **40:**D700-705.

27. **Krivoruchko A, Siewers V, Nielsen J.** 2011. Opportunities for yeast metabolic engineering: Lessons from synthetic biology. Biotechnology journal **6:**262-276.

28. **Nielsen J, Jewett MC.** 2008. Impact of systems biology on metabolic engineering of Saccharomyces cerevisiae. FEMS Yeast Res **8:**122-131.

29. **Chen X, Nielsen KF, Borodina I, Kielland-Brandt MC, Karhumaa K.** 2011. Increased isobutanol production in Saccharomyces cerevisiae by overexpression of genes in valine metabolism. Biotechnol Biofuels **4:**2089-2090.

30. **Kondo T, Tezuka H, Ishii J, Matsuda F, Ogino C, Kondo A.** 2012. Genetic engineering to enhance the Ehrlich pathway and alter carbon flux for increased isobutanol production from glucose by Saccharomyces cerevisiae. J Biotechnol **159:**32-37.

31. **Smith KM, Cho KM, Liao JC.** 2010. Engineering Corynebacterium glutamicum for isobutanol production. Appl Microbiol Biotechnol **87:**1045-1055.

32. **McEwen JT, Atsumi S.** 2012. Alternative biofuel production in non-natural hosts. Curr Opin Biotechnol **23:**744-750.

33. **Angermayr SA, Hellingwerf KJ, Lindblad P, de Mattos MJ.** 2009. Energy biotechnology with cyanobacteria. Curr Opin Biotechnol **20:**257-263.

34. **Atsumi S, Higashide W, Liao JC.** 2009. Direct photosynthetic recycling of carbon dioxide to isobutyraldehyde. Nat Biotechnol **27:**1177-1180.

35. **Payot S, Guedon E, Cailliez C, Gelhaye E, Petitdemange H.** 1998. Metabolism of cellobiose by Clostridium cellulolyticum growing in continuous culture: evidence for decreased NADH reoxidation as a factor limiting growth. Microbiology **144:**375-384.

36. **Higashide W, Li Y, Yang Y, Liao JC.** 2011. Metabolic engineering of Clostridium cellulolyticum for production of isobutanol from cellulose. Appl Environ Microbiol **77:**2727-2733.

37. **Jones DT, Woods DR.** 1986. Acetone-butanol fermentation revisited. Microbiol Rev **50:**484-524.

38. **Shen CR, Liao JC.** 2008. Metabolic engineering of Escherichia coli for 1-butanol and 1-propanol production via the keto-acid pathways. Metab Eng **10:**312-320.

39. **Nielsen DR, Leonard E, Yoon SH, Tseng HC, Yuan C, Prather KL.** 2009. Engineering alternative butanol production platforms in heterologous bacteria. Metab Eng **11:**262-273.

40. **Bond-Watts BB, Bellerose RJ, Chang MC.** 2011. Enzyme mechanism as a kinetic control element for designing synthetic biofuel pathways. Nat Chem Biol **7:**222-227.

41. **Shen CR, Lan EI, Dekishima Y, Baez A, Cho KM, Liao JC.** 2011. Driving forces enable high-titer anaerobic 1-butanol synthesis in Escherichia coli. Appl Environ Microbiol **77:**2905-2915.

42. **Guterl JK, Garbe D, Carsten J, Steffler F, Sommer B, Reisse S, Philipp A, Haack M, Rühmann B, Koltermann A, Kettling U, Brück T, Sieber V.** 2012. Cell-free metabolic engineering: production of chemicals by minimized reaction cascades. ChemSusChem **5:**2165-2172.

43. **Hodgman CE, Jewett MC.** 2012. Cell-free synthetic biology: thinking outside the cell. Metab Eng **14:**261-269.

44. **Buchner E, Rapp R.** 1897. Alkoholische Gährung ohne Hefezellen. Berichte der deutschen chemischen Gesellschaft **30:**2668-2678.

45. **Lo HC, Fish RH.** 2002. Biomimetic NAD(+) models for tandem cofactor regeneration, horse liver alcohol dehydrogenase recognition of 1,4-NADH derivatives, and chiral synthesis. Angew Chem Int Ed Engl **41:**478-481.

46. **Lutz J, Hollmann F, Schnyder A, Fish RH, Schmid A.** 2004. Bioorganometallic chemistry: biocatalytic oxidation reactions with biomimetic NAD^+/NADH co-factors and $[Cp^*\ Rh\ (bpy)\ H]^+$ for selective organic synthesis. Journal of organometallic chemistry **689:**4783-4790.

47. **Zhang YH.** 2010. Production of biocommodities and bioelectricity by cell-free synthetic enzymatic pathway biotransformations: challenges and opportunities. Biotechnol Bioeng **105:**663-677.

48. **Oudshoorn A, van der Wielen LA, Straathof AJ.** 2009. Assessment of options for selective 1-butanol recovery from aqueous solution. Industrial & Engineering Chemistry Research **48:**7325-7336.

49. **Tischer W, Kasche V.** 1999. Immobilized enzymes: crystals or carriers? Trends in Biotechnology **17:**326-335.

50. **Cowan D.** 1997. Thermophilic proteins: stability and function in aqueous and organic solvents. Comparative Biochemistry and Physiology Part A: Physiology **118:**429-438.

51. **Iyer PV, Ananthanarayan L.** 2008. Enzyme stability and stabilization—aqueous and non-aqueous environment. Process Biochemistry **43:**1019-1032.

52. **van der Oost J, Ahmed H, Ettema T, Tjaden B, Geerling A, Siebers B.** 2005. The semi-phosphorylative Entner-Doudoroff pathway in hyperthermophilic archaea: a re-evaluation. Biochem. J **390:**529-540.

53. **Milburn CC, Lamble HJ, Theodossis A, Bull SD, Hough DW, Danson MJ, Taylor GL.** 2006. The structural basis of substrate promiscuity in glucose dehydrogenase from the hyperthermophilic archaeon Sulfolobus solfataricus. Journal of Biological Chemistry **281:**14796-14804.

54. **Kim S, Lee SB.** 2006. Catalytic promiscuity in dihydroxy-acid dehydratase from the thermoacidophilic archaeon Sulfolobus solfataricus. Journal of biochemistry **139:**591-596.

55. **Wolterink-van Loo S, van Eerde A, Siemerink M, Akerboom J, Dijkstra B, van der Oost J.** 2007. Biochemical and structural exploration of the catalytic capacity of Sulfolobus KDG aldolases. Biochem. J **403:**421-430.

56. **Jung J, Lee S.** 2006. Identification and characterisation of Thermoplasma acidophilum glyceraldehyde dehydrogenase: a new class of NADP+-specific aldehyde dehydrogenase. Biochem. J **397:**131-138.

57. **Reher M, Bott M, Schönheit P.** 2006. Characterisation of glycerate kinase (2-phosphoglycerate forming), a key enzyme of the nonphosphorylative Entner–Doudoroff pathway, from the thermoacidophilic euryarchaeon Picrophilus torridus. FEMS microbiology letters **259:**113-119.

58. **Gocke D, Graf T, Brosi H, Frindi-Wosch I, Walter L, Müller M, Pohl M.** 2009. Comparative characterisation of thiamin diphosphate-dependent decarboxylases. Journal of Molecular Catalysis B: Enzymatic **61:**30-35.

59. **Fiorentino G, Cannio R, Rossi M, Bartolucci S.** 1998. Decreasing the stability and changing the substrate specificity of the Bacillus stearothermophilus alcohol dehydrogenase by single amino acid replacements. Protein engineering **11:**925-930.

60. **Guagliardi A, Martino M, Iaccarino I, Rosa MD, Rossi M, Bartolucci S.** 1996. Purification and characterisation of the alcohol dehydrogenase from a novel strain of *Bacillus stearothermophilus* growing at 70° C. The international journal of biochemistry & cell biology **28:**239-246.

61. **Wiegeshoff F, Marahiel MA.** 2007. Characterisation of a mutation in the acetolactate synthase of Bacillus subtilis that causes a cold-sensitive phenotype. FEMS microbiology letters **272:**30-34.

62. **Dumas R, Biou V, Halgand F, Douce R, Duggleby RG.** 2001. Enzymology, structure, and dynamics of acetohydroxy acid isomeroreductase. Accounts of chemical research **34:**399-408.

63. **Gocke D, Nguyen CL, Pohl M, Stillger T, Walter L, Müller M.** 2007. Branched-Chain Keto Acid Decarboxylase from Lactococcus lactis (KdcA), a Valuable Thiamine Diphosphate-Dependent Enzyme for Asymmetric C-C Bond Formation. Advanced Synthesis & Catalysis **349:**1425-1435.

64. **Woodward J, Orr M, Cordray K, Greenbaum E.** 2000. Biotechnology: enzymatic production of biohydrogen. Nature **405:**1014-1015.

65. **Zhang YH, Evans BR, Mielenz JR, Hopkins RC, Adams MW.** 2007. High-yield hydrogen production from starch and water by a synthetic enzymatic pathway. PLoS One **2:**e456.

66. **Xu S, Minteer SD.** 2011. Enzymatic biofuel cell for oxidation of glucose to CO2. ACS Catalysis **2:**91-94.

Chapter 2

Optimizing Expression and Purification of Acetohydroxyacid Synthases

2.1 INTRODUCTION

Branched-chain amino acids (BCAAs) biosynthesis is detected in plants, algae, fungi, bacteria and archaea, but not in animals. Therefore, enzymes of the BCAA biosynthetic pathway are an attractive target for herbicides, fungicides and antimicrobial compounds. Examples are sulfonylureas, imidazolinones, sulfonylaminocarbonyltriazolinones and pyrimidinylsalicylic acids [1-3], which are widely used in agriculture. These compounds do not resemble the natural substrate of BCAA biosynthetic enzymes and represent non-competitive or uncompetitive inhibitors. Consequently, they cannot bind at the enzyme's active site [2, 4-7]. Acetohydroxyacid synthase (anabolic AHAS; EC 2.2.1.6) catalyses the first step in the BCAA biosynthetic pathway (Figure 2.1). For catalytic activity AHAS requires thiamine pyrophosphate (TPP) and flavin adenine dinucleotide (FAD^+) as cofactors as well as a divalent metal ion (mostly Mg^{2+}).

2.1.1 AHASs Catalysed Reactions

The AHAS holoenzyme is composed of a large, catalytic and a small, regulatory subunit. In bacteria, the molecular weights of catalytic subunits range from 59 to 66 kDa and of regulatory subunits from 9 to 34 kDa [8]. The catalytic subunit alone shows activity which is significantly enhanced by addition of the regulatory subunit. Additionally, the regulatory subunit controls the catalytic subunit through feedback inhibition by BCAAs. AHAS is involved in valine, leucine and isoleucine biosynthesis, hereby valine followed by isoleucine is found to be the most potent inhibitor in bacteria [9-11].

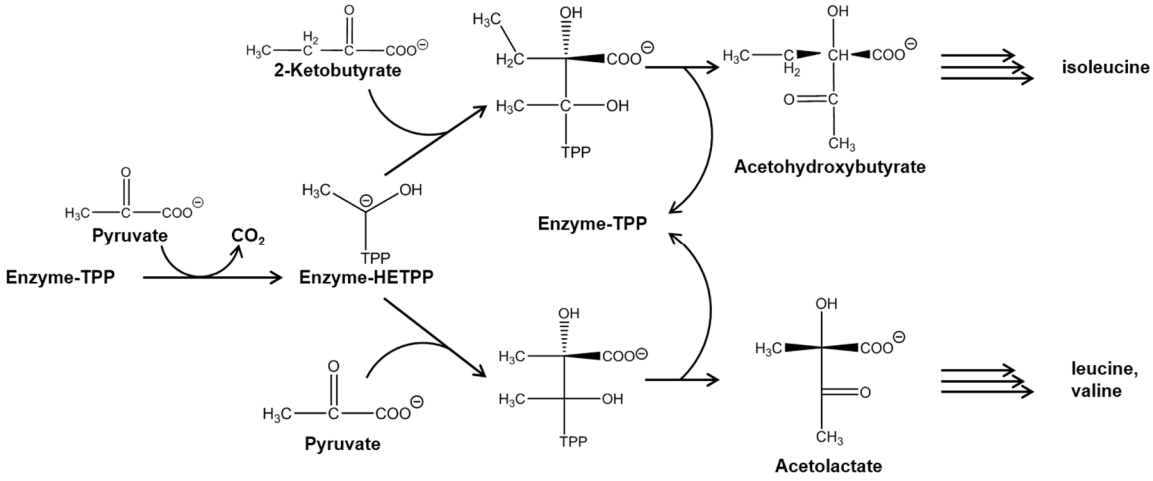

Figure 2.1: The two competing reactions catalysed by AHASs.

AHASs catalyse the decarboxylation of pyruvate and the condensation of the intermediate hydroxyethylthiamin pyrophosphate enamine (HE-TPP) with either pyruvate or 2-ketobutyrate

to form the valine- and leucine precursor acetolactate or the isoleucine precursor acetohydroxybutyrate, respectively (Figure 2.1).

2.1.2 X-Ray Structures of AHAS's - State of the Art

AHAS Catalytic Subunit

In 2002 the first X-ray crystal structure of the AHAS catalytic subunit from *S. cerevisiae* in complex with TPP, Mg^{2+} and FAD^{+} was published [12]. Beside a preliminary X-ray crystallographic study of the catalytic subunit of *E. coli* AHAS II [13], no bacterial AHAS catalytic subunit structure has been reported up to date.

AHAS Regulatory Subunit

The first X-ray crystal structure of a regulatory subunit was reported for *E. coli* AHAS III [14]. Later AHAS II regulatory subunits from *Thermotoga maritima* and *Nitrosomonas europea* were determined [15]. In all reports, the regulatory subunit was crystallized as a dimer including N- and C-terminal domains possessing a ferredoxin-like fold (ßαßßαß). Both domains significantly contribute to dimer stabilization [8]. In a previous study, it was suggested that the N-terminal domains of regulatory subunits alone are sufficient to completely activate the catalytic subunit and thus can from the holoenzyme [16].

AHAS Overall-Structure

The overall structure of AHAS catalytic subunit from *S. cerevisiae* considered to be a dimer consisting of two catalytic subunits [12]. Each subunit consists of three domains (α, ß and γ) and the active site is formed at the interface between two subunits.
AHAS contains the motif Gly-Asp-Gly-(X_{26})-Asn characteristic of all TPP enzymes [17] involved in coordination of the metal ion (Mg^{2+}), which binds to the diphosphate function of TPP [8].
FAD^{+} in AHAS keeps the active site of the enzyme in the necessary geometry for catalysis [12]. It is assumed that the FAD^{+} dependence is attributed to the AHAS ancestor pyruvate oxidase (POX) [18]. Unclear is how the FAD^{+}-independent acetolactate synthase can catalyse the same reaction without this cofactor (see Chapter 4).

Crystal structures of the catalytic and regulatory subunits of an AHAS, as a complex, would significantly improve the understanding of how the subunits interact and the mechanism of feedback regulation works.
Therefore, this study focussed on the crystallisation of two different AHASs, being enterobacterial AHAS II from *E. coli* and AHAS from *Bacillus stearothermophilus*. For

crystallization experiments, it is a necessity to obtain a soluble and active protein that can be purified in large amounts.
Crystallisation experiments were performed in collaboration with Dr. Bernhard Loll (FU Berlin, Germany). Therefore, purification strategies for the above-mentioned proteins were optimized in this section.

2.2 MATERIALS AND METHODS

2.2.1 Devices, Chemicals, Strains and Plasmids

A list with all used devices (Table 9.1), chemicals (Table 9.2) and strains (9.1.1) and plasmids (9.1.2) is attached in the Chapter 9.

2.2.2 Isolation of Genomic DNA

Genomic DNA from *B. stearothermophilus* and *E. coli* K12 was isolated with a genomic DNA isolation kit from Thermo Scientific according to the manual as well as by applying a slightly modified protocol from Jones and Bartlett [19].

2.2.3 Cloning – Plasmid Construction

The sequences for all named primers as well as all obtained plasmids in the following section are listed in the Chapter 9.

2.2.3.1 AHAS II from *E. coli*

pETGST1a_IlvG

To obtain IlvG with an N-terminal fused GST-tag, *E. coli ilvG* gene was cloned into the vector pETGST1a_BamHI using *Bam*HI and *Xho*I as restriction sites. PCR with genomic DNA from an *E. coli* K12 strain was performed with the primers 5′ IlvG_*Bam*HI and 3′ IlvG_*Xho*I. To restore the sequence of the original gene from the known deletion in the middle of the *ilvG* gene (at base pair 875) an overlap extension PCR was done [20]. In the first PCR two overlapping gene fragments were designed applying the primers 5′ IlvG_*Bam*HI and 3′ IlvG_875at as well as the primers 5′ IlvG_875at and 3′ IlvG_*Xho*I. In the second PCR the full-length original gene *ilvG* was obtained with the primers 5′ IlvG_*Bam*HI and 3′ IlvG_*Xho*I.

pCBR_IlvG_HisC

For IlvG fused to a C-terminal His_6-tag, the *ilvG* gene, without any deletions, was cloned into the pre-digested pCBR_HisNo vector (*Bsa*I and *Xho*I). PCR was performed using the primers 5′ IlvG_*Bsa*I and 3′ IlvG_Stop_*Xho*I.

2.2.3.2 AHAS from *B. stearothermophilus*

pCBR_IlvBN_HisNo

The *B. stearothermophilus ilvBN* gene was obtained by PCR with genomic DNA as template and with the primers 5′ IlvBN_pCBR and 3′ IlvBN_pCBR. Afterwards the gene was cloned into the vector pCBR_HisNo pre-digested with *Bfua*I and *Bsa*I.

pET28a_IlvBN_HisN

The gene *ilvBN* was fused together with an N-terminal His_6-tag using the vector pET28a and the restriction sites *Nde*I and *Xho*I. PCR was performed applying the primers 5′ IlvBN_pET28a and 3′ IlvBN_Stop_pET28a.

pETGST1a_IlvBN, pETGST1a_IlvB, pETGST1a_IlvN

The genes for the subunits *ilvB* and *ilvN* were both cloned separately or in combination in the pre-digested vector pETGST1a (*Nco*I and *Xho*I). PCR was performed with the primers 5′ IlvBN_pETGST1a_NcoI, 5′ IlvN_pETGST1a, 3′ IlvB_pETGST1a and 3′ IlvN_pETGST1a.

p613_IlvN

The gene for the regulatory subunit *ilvN* was additionally cloned in the vector p613 pre-digested with *Sma*I and *Xho*I. For PCR the primers 5′ ilvN_p613_6V and 3′ IlvN_p613 were used.

pETGST1a_IlvB_short, pET28a_IlvBN_short_HisNo

Construction of the truncated variants IlvB_short and IlvBN_short (both missing the first 13 amino acids) were applied by PCR using the template pCBR_IlvBN_NoHis and the primers 5′ IlvB_13AS_NcoI, 3′ IlvB_pETGST1a and 3′ IlvBN_Stop_pET28a. The truncated *ilvB* gene was cloned in pETGST1a vector and the truncated *ilvBN* gene in the pET28a vector pre-digested with the restriction sites *Nco*I and *Xho*I.

pTXB3_IlvB, pTXB3_IlvN, pTXB3_IlvB_short

Both genes for the subunits *ilvB* and *ilvN* as well as the truncated *ilvB* gene were cloned in the vector pTXB3 using the restriction sites *Nco*I and *Xho*I. PCR was performed with the primers 5′ IlvBN_pETGST1a_*Nco*I, 5′ IlvB_13AS_*Nco*I, 5′ IlvN_pETGST1a, 3′ IlvB_pTXB3 and 3′ IlvN_pTXB3.

IlvBN mutants

The exchanges Q28A_E30A, E185A_E186A and E491A_K492A were either introduced alone or in combination by using mega-primer PCR [21] applying listed primers (Table 2.1).
The resulting genes of the *ilvBN* variants were cloned in the pre-digested vector pET28a (*Nco*I and *Xho*I).

Table 2.1: Overview of used primers and templates for construction of IlvBN mutants.

mutated amino acids	template	forward primer	reverse primer	obtained plasmid
Q28A_E30A	pCBR_IlvBN _HisNo	5′ IlvBN_ pETGST1a_ *Nco*I	3′ IlvBN_Q28A _E30A_r 3′ IlvBN_Stop_ pET28a	pET28a_IlvBN_ Q28A_E30A_ HisNo
E185A_E186A	pCBR_IlvBN _HisNo	5′ IlvBN_ pETGST1a _*Nco*I	3′ IlvBN_E185A _E186A_r 3′ IlvBN_Stop_ pET28a	pET28a_IlvBN_ E185A_E186A_ HisNo
E491A_K492A	pCBR_IlvBN _HisNo	5′ IlvBN_ pETGST1a_ *Nco*I	3′ IlvBN_E491A _E492A_r 3′ IlvBN_Stop_ pET28a	pET28a_IlvBN_ E491A_K492A_ HisNo
Q28A_E30A_ E185A_E186A	pET28a_IlvBN_ Q28A_E30A _HisNo	5′ IlvBN_ pETGST1a _*Nco*I	3′ IlvBN_E185A _E186A_r 3′ IlvBN_Stop_ pET28a	pET28a_IlvBN_ Q28A_E30A_ E185A_E186A_ HisNo
Q28A_E30A_ E491A_E492A	pET28a_IlvBN_ Q28A_E30A_ HisNo	5′ IlvBN_ pETGST1a _*Nco*I	3′ IlvBN_E491A _K492A_r 3′ IlvBN_Stop_ pET28a	pET28a_IlvBN_ Q28A_E30A_ E491A_E492A_ HisNo
E185A_E186A_ E491A_K492A	pET28a_IlvBN_ E185A_E186A_ HisNo	5′ IlvBN_ pETGST1a _*Nco*I	3′ IlvBN_E491A _K492A_r 3′ IlvBN_Stop_ pET28a	pET28a_IlvBN_ E185A_E186A_ E491A_K492A_ HisNo
Q28A_E30A_ E185A_E186A_ E491A_K492A	pET28a_IlvBN_ Q28A_E30A_ E185A_E186A_ HisNo	5′ IlvBN_ pETGST1a_ *Nco*I	3′ IlvBN_E491A _K492A_r 3′ IlvBN_Stop_ pET28a	pET28a_IlvBN_ Q28A_E30A_ E185A_E186A_ E491A_K492A_ HisNo

2.2.4 Heterologous Protein Expression

2.2.4.1 AHAS II from *E. coli*

Enzyme expression was performed using *E. coli* BL21(DE3) as host strain. IlvG was expressed in TB medium [22] supplemented with 50 µg/ml kanamycin. After inoculation cells were grown to an OD_{600} = 0.5 – 0.7 at 37 °C and subsequently induced with 1 mM IPTG. The temperature was decreased to 16 °C and kept for 20 h. Afterwards the cells were harvested (4,500 g, 4 °C, 30 min) and stored at -20 °C.

2.2.4.2 AHAS from *B. stearothermophilus*

Enzyme expression was performed using *E. coli* HMS174(DE3) cells for all IlvBN variants (His_6_IlvBN, His_6_GST_IlvBN, IlvB_His_6, His_6_GST_IlvB, IlvN_His_6, IlvN_HisNo, and

His_6_GST_IlvN). IlvBN variants were expressed in TB medium supplemented with 50 µg/ml kanamycin. After inoculation cells were grown to an OD_{600} = 0.5 – 0.7 at 37 °C and subsequently induced with 1 mM IPTG. Afterwards the temperature was shifted to 16 °C to stay on this level for 48 h. Afterwards the cells were harvested (4,500 g, 4 °C, 30 min) and stored at -20 °C.

2.2.5 Enzyme Purification

After accomplishing the protein purification procedures described in the following sections all proteins were stored as liquid stocks with 10 % (v/v) glycerol at -80 °C.

2.2.5.1 Enzymes with Terminal His_6-tag

The cell pellets were resuspended in 50 mM Hepes pH 8.0, 20 mM imidazole. Cell lysates were prepared with Emulsiflex-B15 and cell debris removed by centrifugation (25,000 g, 4 °C, 20 min). A Ni^{2+}-NTA column (column volume (cv) ~ 4 ml; Thermo Scientific, Schwerte, Germany) was equilibrated with 50 mM Hepes pH 8.0, 20 mM imidazole. His_6 tagged enzymes were loaded on the column and washed with 3 cv of equilibration buffer. The tagged enzymes were eluted with 50 mM Hepes pH 8.0 and 500 mM imidazole. Desalting of the proteins was performed with PD-10 columns (GE Healthcare, Freiburg, Germany).

2.2.5.2 Enzymes with GST-tag

First, enzymes fused to a GST-Tag were purified as described in the above-mentioned section (see 2.2.5.1). After desalting TEV-protease was added in excess to the enzyme solution to cleave the affinity tag. For stabilisation of IlvN 150 mM glucose or a to IlvN equivalent amount of IlvB was added. GST-tag was cleaved by TEV-protease at 8 °C overnight. Afterwards imidazole was added to 20 mM for binding of the His_6 tagged GST-tag as well as the TEV-protease to the Ni^{2+}-NTA beads. The enzyme solution was loaded on a Ni^{2+}-NTA column. The flow through contained the enzymes without GST-tag. The tagged enzymes were eluted with elution buffer (50 mM Hepes pH 8.0, 500 mM imidazole). Desalting of the proteins was performed with PD-10 columns.

2.2.5.3 Enzymes Fused to *Mycobacterium xenopi* Intein/Chitin Binding Domain

The cell pellets, which contained enzymes fused on a *Mxe* intein/chitin binding domain, were resuspended in 20 mM Hepes pH 8.0 and 500 mM NaCl. Cell lysates were prepared with Emulsiflex-B15 and cell debris removed by centrifugation (25,000 g, 4 °C, 20 min). Washed chitin beads were mixed with cell lysate and the suspension was incubated at 8 °C for 2.5 h. Subsequently, the suspension was filled in a column, washed with 15 ml buffer followed by 3 ml DTT-buffer (20 mM Hepes pH 8, 500 mM NaCl and 100 mM DTT). Finally, the beads

were resuspended in the DTT-buffer, filled in a 50 ml reaction tube and slowly shaken overnight at 8 °C. Afterwards the solution was refilled in a column and the protein fraction was separated.

2.3 RESULTS AND DISCUSSION

2.3.1 AHAS II from *E. coli*

At present, no complete crystal structure for any bacterial AHAS is available (see 2.1.2). For AHAS II from *E. coli* a preliminary X-ray crystallographic study was reported in 2011 [13]. Niu *et al.* (2011) could obtain crystals of IlvG, but they were not able to solve the crystal structure. To finally solving the crystal structure of IlvG, the genomic DNA from an *E. coli* K12 strain was isolated. It is known that a frame shift mutation in isozyme II exists in common *E. coli* K12 strains [23]. Under appropriate growth conditions, a single isozyme is sufficient for non-auxotrophic growth and therefore the frame shift mutation, does not interfere with *E. coli* metabolism. This deletion in the cryptic *ilvG* gene was corrected by overlap extension PCR (see 2.2.3.1).

Subsequently, the gene was cloned in two different expression vectors (see 2.2.4.1). Expression tests showed that IlvG was soluble with a molecular weight of 59.4 kDa consistent with literature results [13].

The enterobacteriaceae *E. coli* and *S. typhimurium* are special among the bacteria as they possess three isozymes AHAS I, II and III, encoded in the ilvBN, ilvGMEDA and ilvIH operons [24-27]. Among these three isozymes, the catalytic subunits of AHAS I and II have the highest homology (46 %), whereas AHAS I and III are least homologous (37 %) [8]. Despite the similarities between the three isozymes, the expression of each is regulated in a different way [24, 28]. Specifically, they have different kinetic properties [8] and have slightly different metabolic roles [24, 28-30].

For example, AHAS II from *E. coli* requires, unlike the other two isozymes, the presence of the regulatory subunit for catalysis [7] and is completely insensitive to feedback inhibition by any of the BCAAs [25].

Many prokaryotes only possess a single AHAS, which is similar in sequence and properties to an enterobacterial AHAS III [31]. This feature limits growth to specific external conditions [32].

At the FU-Berlin IlvG_HisC and His_6_GST_IlvG are currently expressed, purified and crystallization experiments will be setup. A crystal structure of the catalytic subunit in complex with the regulatory subunit of AHAS II could help to understand why AHAS II is insensitive to inhibition by the BCAAs.

2.3.2 AHAS from *B. stearothermophilus*

AHAS from *B. stearothermophilus* is reported as a thermophilic AHAS [33] and is therefore interesting for industrial applications. *Bsahas* was cloned in different expression vectors. Subsequently, several approaches to improve expression and purification were performed.

2.3.2.1 Cloning and Expression of *Bs*AHAS with and without a Terminal His_6-tag

Genomic DNA from *B. stearothermophilus* was isolated. The *ilvBN* gene was then cloned in the expression vectors pCBR_NoHis and pET28a (with N-terminal histidine-tag). The genes encoding *ilvB* and *ilvN* were transferred in the vector pCBR_HisC (see 2.2.3.2). The resulting IlvB sequence contained the exchanges F79V, R463Q, P511A and S525A in contrast to the published sequence (accession No.: AY083837), while the IlvN sequence contained the exchanges F122V and K143E.

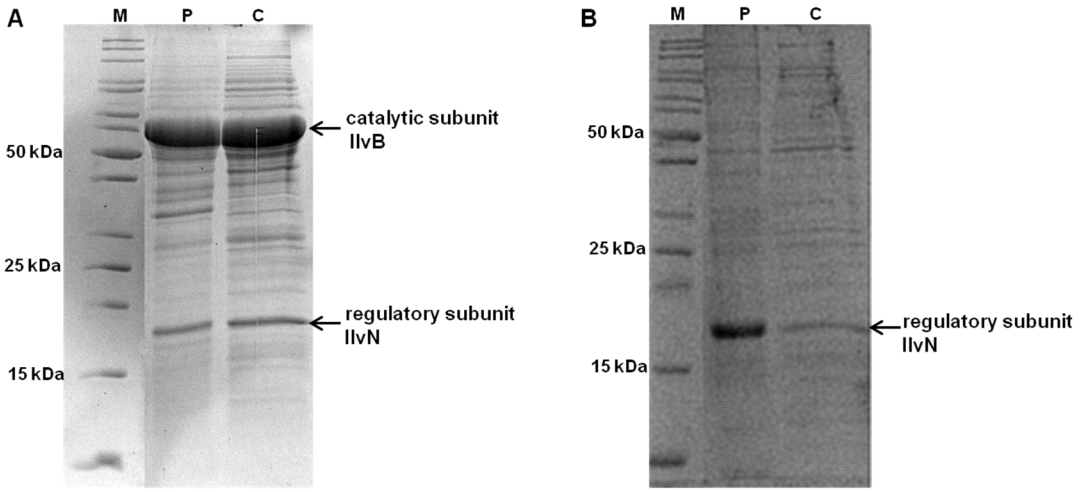

Figure 2.2: 12% SDS-pages show expressed catalytic- (IlvB) and regulatory (IlvN) subunit of *Bs*AHAS. A) Both subunits were simultaneously expressed in one organism. B) Expression of the small, regulatory subunit in an organism. M: unstained protein ladder; P: cell pellet; C: crude extract;

Expression of the holoenzyme (IlvBN) encompassing the catalytic- (IlvB) and the regulatory subunit (IlvN), in *E. coli* HMS174(DE3) cells, resulted in a soluble protein (Figure 2.2A). IlvB has a molecular weight of 62 kDa and IlvN of 19 kDa. However, IlvN alone is poorly expressed and the soluble fraction contains less protein compared to the simultaneous IlvBN expression (Figure 2.2B).

Even if IlvN was expressed in combination with IlvB, IlvB remained much more soluble than IlvN, as documented by literature precedence [7, 10, 33-37].

Reconstitution of the holoenzyme is accomplished by mixing equal amounts of IlvB and IlvN as described previously [9]. Therefore, the crude extract containing the holoenzyme (catalytic and regulatory subunit of *Bs*AHAS) had to be purified by gel chromatography.

To simplify the purification, IlvB was fused to an N-terminal His_6-tag by cloning IlvBN in a pET28a vector (see 2.2.3.2). During expression of both subunits, it was supposed that IlvB and IlvN could be reconstituted to one holoenzyme stable enough to persist the purification and desalting process.
It was reported that reconstitution of the two subunits will greatly enhance the specific activity of the enzyme [10, 33-37]. As displayed in Figure 2.2, for a complete reconstitution of the holoenzyme more IlvN was required than obtained by simultaneous expression of both subunits. This problem could not be solved by a simple purification method, but should be by optimization of IlvN expression.

To improve IlvN expression, the *ilvN* gene was transferred into expression vector p613 (see 2.2.3.2). During expression of proteins in the vector p613, porins will be co-expressed. Porins are proteins which cross the cellular membrane and act as a pore. Through these pores, proteins can diffuse and be secreted into the medium, from which the target protein can be purified. Unfortunately, the expression of IlvN was inefficient and multiple litres of medium would have been necessary to obtain a low amount of IlvN. Concentration of the medium is very time consuming and not suitable for sensitive enzymes. Therefore, another method to improve the expression of IlvN was evaluated.

2.3.2.2 Cloning and Expression of *Bs*AHAS with a N-terminal GST-tag

To improve IlvN expression, the *ilvN* gene was fused to a GST-tag by cloning in the vector pET-GST1a using the restriction sites *Nco*I and *Xho*I (Figure 2.3).

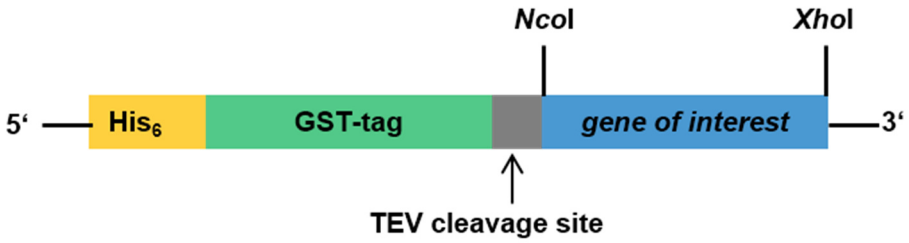

Figure 2.3: Cloning of genes in the expression vector pETGST1a.
The His_6-tag is represented in yellow, the GST-tag in green, the TEV cleavage site in grey and the *gene of interest* in blue.

When using *Nco*I as restriction enzyme an alanine as second amino acid of the protein sequence had to be included because of the recognition sequence and the digest of *Nco*I.

A GST-tag is used to enhance the folding and solubility of a target enzyme. Another advantage of this construct is the possibility to apply, Ni^{2+}-NTA- and glutathione- affinity chromatography as purification methods.

Proteases are highly specific for cleaving the sequence Glu-Asn-Leu-Tyr-Phe-Gln-I-(Gly/Ser) and are often used for removing affinity tags.
During purification the gene of interest was separated from the GST-tag and the His_6-tag by action of a specific protease, the TEV (Tobacco Etch Virus)- protease.

It was possible to improve the expression of IlvN by fusion to a GST-tag compared to expression with a C-terminal His_6-tag (Figure 2.4A).

In the next step the fusion protein His_6_GST_IlvN was purified and the GST-tag removed (Figure 2.4B). Purification of His_6_GST_IlvN could easily be accomplished by Ni^{2+}-chromatography. Subsequently, the protein was desalted and TEV-protease was added in an almost equivalent concentration compared to His_6_GST_IlvN. Additionally, 150 mM glucose or a to His_6_GST_IlvN equivalent amount of IlvB was supplied.

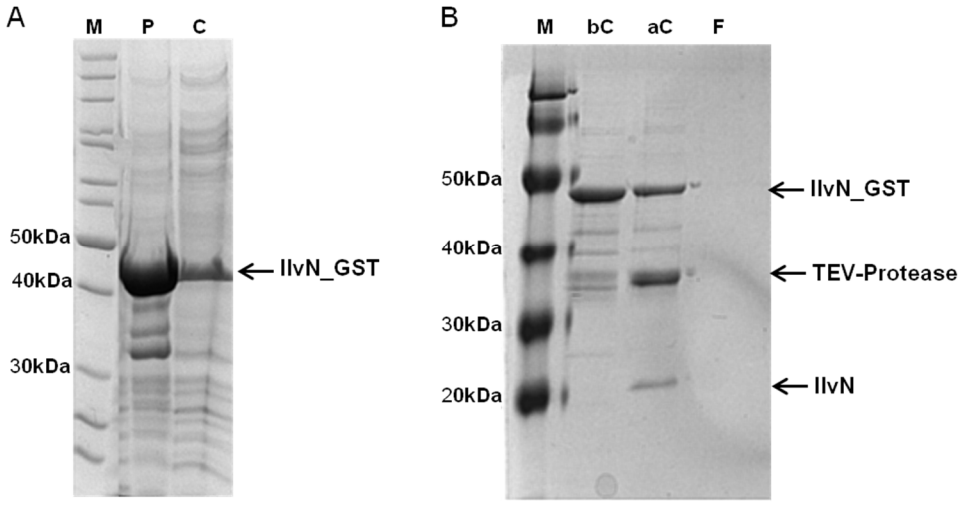

Figure 2.4: SDS-pages showing expressed His_6_GST_IlvN.
A) Expression of His_6_GST_IlvN, B) Purified His_6_GST_IlvN (lane 2) and digest of His_6_GST_IlvN by TEV-protease (lane 3). M: unstained protein ladder; P: cell pellet; C: crude extract; bC: before cleavage with TEV-protease; aC: after cleavage with TEV-protease; F: flow through.

The protein solution was stored overnight at 8 °C. If no glucose or IlvB was added IlvN precipitated overnight. Figure 2.4 shows that only a small amount of IlvN was cleaved off suggesting that the TEV cleavage site is hardly accessible for the TEV-protease.

Additionally, IlvB was cloned in vector pETGST1a (see 2.2.3.2).

2.3.2.3 Cloning and Expression of *Bs*AHAS with a Terminal Intein-Tag

As cleaving His_6_GST_IlvN with TEV-protease did not work well (see 2.3.2.2) another method to obtain a better-expressed and more soluble protein was applied, i.e. an intein mediated purification with an affinity chitin binding tag (IMPACT™ from New England Biolabs, Frankfurt am Main, Germany). Hereby the intein undergoes in the presence of thiols, e.g. DTT or by a

temperature/pH-shift, a specific self-cleavage that releases the target protein from the chitin-bound intein-tag.

For that, *ilvB* and *ilvN* were cloned in a pTXB3 vector using the restriction site *Nco*I and *Xho*I, as shown in Figure 2.5.

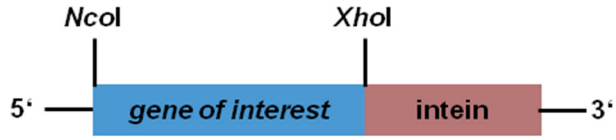

Figure 2.5: Cloning of genes in the expression vector pTXB3.
The *gene of interest* is represented in blue and the intein-tag in purple.

First the fusion protein IlvN_intein was expressed in *E. coli* HMS174(DE3) followed by cell disruption and addition of chitin beads. The intein-tag of the fusion protein sticks to the chitin beads allowing protein purification. Subsequently, 100 mM DTT was added and the solution was slowly inverted overnight at 8 °C. On the next day, cleaved protein was obtained as the intein-tag still stuck to the chitin beads.

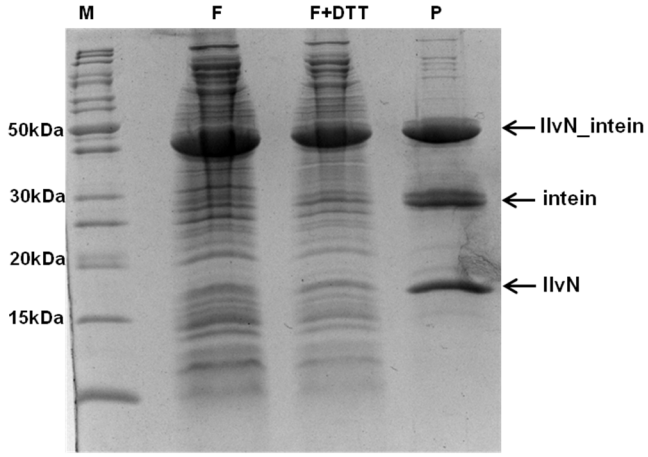

Figure 2.6: SDS page of IlvN purification by cleavage of the intein-tag.
M: unstained protein ladder, F: Flow through after adding chitin beads, F+DTT: Flow through after DTT addition; P: "purified" IlvN.

The expression of the IlvN_intein fusion protein worked well compared to the expression with GST-tag and results in a higher yield of IlvN.

Again, the majority of the fusion protein was not cleaved and the flow through contained fusion protein, intein-tag as well as IlvN (Figure 2.6). A subsequent gel chromatography would be implicitly required to obtain pure IlvN.

2.3.2.4 Truncated IlvB and IlvBN Variants

Preliminary X-ray crystallographic studies are available for the catalytic subunit from *E. coli* AHAS II [13]. As this is the only reported crystallized bacterial AHAS, the amino acid sequence

of IlvB from *B. stearothermophilus* and IlvG from *E. coli* were compared. The alignment (Figure 2.7) revealed that IlvG is 13 amino acids shorter at the N-terminus than IlvB.

```
                    10        20        30        40        50        60
           |....|....|....|....|....|....|....|....|....|....|....|....|.
IlvG       ------------MNGAQWVVHALRAQGVNTVFGYPGGAIMPVYDALYDGGVEHLLCRHEQ
IlvB       MAKMNVEEQTKTKMSGSMMLIEALKAEQVEVIFGYPGGAVLPLYDELYKAGVFHVLTRHEQ
```

Figure 2.7: Alignment of the N-terminus of *E. coli* IlvG with *B. stearothermophilus* IlvB.
Identical amino acids are highlighted in yellow.

Additionally, a prediction of the secondary structure of IlvB (done with phyre^2 [38]) showed no definite secondary structure for the first 13 amino acids of IlvB (Figure 2.8).

Figure 2.8: Predicted secondary structure of IlvB from *B. stearothermophilus*.
The first 13 amino acids of IlvB are coloured in red. This figure was prepared using PyMOL [39].

The truncation might improve the crystallizability of IlvB. Therefore, the truncated *ilvBN* gene was cloned in the vector pET28a and truncated *ilvB* gene alone was cloned in the vector pETGST1a (see 2.2.3.2). Both constructs were expressed and activity assays (3.2.4) were done in crude extract. In both samples, acetolactate was detected, suggesting that both enzymes are catalytically active. The obtained constructs were transferred to the FU-Berlin for crystallisation experiments.

2.3.2.5 Mutation of Surface Exposed Arginines and Lysines from IlvBN

Reduction of surface entropy can be obtained by mutation of the surface exposed arginines and lysines to alanines, which in consequence can lead to a higher probability of crystallization. The web-based application Ucla MBI-SERp was used to predict amino acid exchanges [40]. For IlvBN the mutation pairs Q28A_E30A, E185A_E186A and E491A_K492A were predicted. To increase the likelihood of IlvBN crystallization, these three mutation pairs

were cloned in separate and all possible combination setups by mega-primer PCR (see 2.2.3.2). The constructs were transferred to FU Berlin for crystallisation experiments.

2.4 CONCLUSIONS

Branched-chain amino acids are synthesised by plants, algae, fungi, bacteria and archaea, but not by animals. Therefore, enzymes of the BCAA biosynthetic pathway are potential targets in the development of herbicides, fungicides and antimicrobial compounds.

The acetohydroxyacid synthase is important as it catalyses the first common step in the BCAA biosynthetic pathway. Pyruvate is decarboxylated to yield acetolactate with a second molecule of pyruvate or acetohydroxybutyrate with a molecule of ketobutyrate. For catalytic activity AHAS requires TPP and FAD^+ as well as a divalent metal ion (mostly Mg^{2+}). Structurally AHASs are composed of catalytic and regulatory subunits and only the holoenzyme exhibits maximum activity and is inhibited by at least one of the BCAAs. Up to now, no crystal structure of a bacterial AHAS is available, although the crystal structures of the catalytic and regulatory subunits of an AHAS would significantly improve the understanding of how the subunits interact and how the mechanism of feedback regulation works.

Therefore, this study considered two different bacterial AHAS from *E. coli* (AHAS II) and from *B. stearothermophilus*.

The cloned constructs were tested for enzyme expression and subsequently relevant constructs were transferred to our cooperation partner from the FU Berlin (Germany) to obtain crystallographic data. In a first approach, AHAS II from *E. coli* (IlvG) was chosen because preliminary crystallisation studies of *E. coli* AHAS II were described already [13]. Therefore, *IlvG* was cloned with and without GST-tag.

Additionally, the AHAS from *B. stearothermophilus* (IlvBN) was tested, as it is known to be a thermophilic enzyme that is especially interesting for industrial applications. Therefore, intensive efforts were undertaken to express both subunits in equal amounts. *IlvBN* was cloned in pET-vectors with an N- and C-terminal His_6-tag as well as without a tag. Unfortunately, IlvB showed in all approaches a much higher solubility than IlvN.

To improve IlvN expression *ilvN* was cloned in the expression vector pETGST1a. This enhanced IlvN expression, but purification of IlvN was aggravated, because cleaving of the GST-tag was hardly possible. It can be suggested that the TEV-cleavage site is buried in the folded protein. Subsequently, *ilvN* was cloned in the expression vector pTXB3. Again, the expression of IlvN could be improved and also the cleavage of the tag could be enhanced. Although cleavage and purification of IlvN still has to be improved.

An alignment between IlvB and IlvG revealed that IlvG is 13 amino acids shorter than IlvB. As it is published that IlvG was crystallized, a truncated variant of *ilvB* was cloned.

Finally, surface exposed arginines and lysines were mutated to alanines to reduce surface entropy. Therefore, three mutation pairs were cloned in separate and in all possible combinations in *ilvBN*.

Altogether eighteen plasmids, i.e. pCBR_IlvG_HisC, pETGST1a_IlvG, pCBR_IlvBN_HisNo, pCBR_IlvB_HisC, pCBR_IlvN_HisNo, pET28a_IlvBN_HisN, pETGST1a_IlvBN, pETGST1a_IlvN, pETGST1a_IlvB, pET28a_IlvBN_short_HisNo, pETGST1a_IlvB_short, pET28a_IlvBN_Q28A_E30A_HisNo, pET28a_IlvBN_E185A_E186A_HisNo, pET28a_IlvBN_E491A_K492A_HisNo, pET28a_IlvBN_Q28A_E30A_E185A_E186A_HisNo, pET28a_IlvBN_Q28A_E30A_E491A_E492A_HisNo, pET28a_IlvBN_E185A_E186A_E491A_K492A_HisNo and pET28a_IlvBN_Q28A_E30A_E185A_E186A_E491A_K492A_HisNo were transferred to our cooperation partner Dr. Bernhard Loll (FU Berlin, Germany) and awaiting their further crystallisation studies.

2.5 REFERENCES

1. **LaRossa RA, Schloss JV.** 1984. The sulfonylurea herbicide sulfometuron methyl is an extremely potent and selective inhibitor of acetolactate synthase in Salmonella typhimurium. The Journal of biological chemistry **259:**8753-8757.
2. **Shaner DL, Anderson PC, Stidham MA.** 1984. Imidazolinones: potent inhibitors of acetohydroxyacid synthase. Plant Physiol **76:**545-546.
3. **Shimizu T, Nakayama I, Nakao T, Nezu Y, Abe H.** 1994. Inhibition of plant acetolactate synthase by herbicides, pyrimidinylsalicylic acids. Journal of Pesticide Science **19**.
4. **Schloss JV, Ciskanik LM, Van Dyk DE.** 1988. Origin of the herbicide binding site of acetolactate synthase. Nature **331:**360-362.
5. **Chang AK, Duggleby RG.** 1997. Expression, purification and characterisation of Arabidopsis thaliana acetohydroxyacid synthase. Biochem J **327 (Pt 1):**161-169.
6. **Durner J, Gailus V, Boger P.** 1991. New aspects on inhibition of plant acetolactate synthase by chlorsulfuron and imazaquin. Plant Physiol **95:**1144-1149.
7. **Hill CM, Pang SS, Duggleby RG.** 1997. Purification of Escherichia coli acetohydroxyacid synthase isoenzyme II and reconstitution of active enzyme from its individual pure subunits. Biochem J **327 (Pt 3):**891-898.
8. **Gedi V, Yoon MY.** 2012. Bacterial acetohydroxyacid synthase and its inhibitors--a summary of their structure, biological activity and current status. FEBS J **279:**946-963.
9. **McCourt JA, Duggleby RG.** 2006. Acetohydroxyacid synthase and its role in the biosynthetic pathway for branched-chain amino acids. Amino Acids **31:**173-210.
10. **Choi KJ, Yu YG, Hahn HG, Choi JD, Yoon MY.** 2005. Characterisation of acetohydroxyacid synthase from Mycobacterium tuberculosis and the identification of its new inhibitor from the screening of a chemical library. FEBS Lett **579:**4903-4910.
11. **Leyval D, Uy D, Delaunay S, Goergen JL, Engasser JM.** 2003. Characterisation of the enzyme activities involved in the valine biosynthetic pathway in a valine-producing strain of Corynebacterium glutamicum. J Biotechnol **104:**241-252.
12. **Pang SS, Duggleby RG, Guddat LW.** 2002. Crystal structure of yeast acetohydroxyacid synthase: a target for herbicidal inhibitors. J Mol Biol **317:**249-262.
13. **Niu X, Liu X, Zhou Y, Niu C, Xi Z, Su XD.** 2011. Preliminary X-ray crystallographic studies of the catalytic subunit of Escherichia coli AHAS II with its cofactors. Acta Crystallogr Sect F Struct Biol Cryst Commun **67:**659-661.
14. **Kaplun A, Vyazmensky M, Zherdev Y, Belenky I, Slutzker A, Mendel S, Barak Z, Chipman DM, Shaanan B.** 2006. Structure of the regulatory subunit of acetohydroxyacid synthase isozyme III from Escherichia coli. J Mol Biol **357:**951-963.
15. **Petkowski JJ, Chruszcz M, Zimmerman MD, Zheng H, Skarina T, Onopriyenko O, Cymborowski MT, Koclega KD, Savchenko A, Edwards A, Minor W.** 2007. Crystal structures of TM0549 and NE1324--two orthologs of E. coli AHAS isozyme III small regulatory subunit. Protein Sci **16:**1360-1367.
16. **Mendel S, Vinogradov M, Vyazmensky M, Chipman DM, Barak Z.** 2003. The N-terminal domain of the regulatory subunit is sufficient for complete activation of acetohydroxyacid synthase III from Escherichia coli. J Mol Biol **325:**275-284.
17. **Hawkins CF, Borges A, Perham RN.** 1989. A common structural motif in thiamin pyrophosphate-binding enzymes. FEBS Lett **255:**77-82.
18. **Chang YY, Cronan JE, Jr.** 1988. Common ancestry of Escherichia coli pyruvate oxidase and the acetohydroxy acid synthases of the branched-chain amino acid biosynthetic pathway. J Bacteriol **170:**3937-3945.
19. **Maloy SR.** 1989. Experimental Techniques in Bacterial Genetics.192.

20. **Ho SN, Hunt HD, Horton RM, Pullen JK, Pease LR.** 1989. Site-directed mutagenesis by overlap extension using the polymerase chain reaction. Gene **77:**51-59.

21. **Sailen B.** 2002. Megaprimer PCR, p. 189-196, methods in Molecular Biology.

22. **Schrimpf G.** 2002. Gentechnische Methoden: Eine Sammlung von Arbeitsanleitungen für das molekularbiologische Labor vol. 3. Spektrum Akademischer Verlag.

23. **Lawther RP, Calhoun DH, Adams CW, Hauser CA, Gray J, Hatfield GW.** 1981. Molecular basis of valine resistance in Escherichia coli K-12. Proc Natl Acad Sci U S A **78:**922-925.

24. **Barak Z, Chipman DM, Gollop N.** 1987. Physiological implications of the specificity of acetohydroxy acid synthase isozymes of enteric bacteria. J Bacteriol **169:**3750-3756.

25. **Lawther RP, Wek RC, Lopes JM, Pereira R, Taillon BE, Hatfield GW.** 1987. The complete nucleotide sequence of the ilvGMEDA operon of Escherichia coli K-12. Nucleic acids research **15:**2137-2155.

26. **Squires CH, De Felice M, Devereux J, Calvo JM.** 1983. Molecular structure of ilvIH and its evolutionary relationship to ilvG in Escherichia coli K12. Nucleic acids research **11:**5299-5313.

27. **Wek RC, Hauser CA, Hatfield GW.** 1985. The nucleotide sequence of the ilvBN operon of Escherichia coli: sequence homologies of the acetohydroxy acid synthase isozymes. Nucleic acids research **13:**3995-4010.

28. **Epelbaum S, LaRossa RA, VanDyk TK, Elkayam T, Chipman DM, Barak Z.** 1998. Branched-chain amino acid biosynthesis in Salmonella typhimurium: a quantitative analysis. J Bacteriol **180:**4056-4067.

29. **Dailey FE, Cronan JE, Jr.** 1986. Acetohydroxy acid synthase I, a required enzyme for isoleucine and valine biosynthesis in Escherichia coli K-12 during growth on acetate as the sole carbon source. J Bacteriol **165:**453-460.

30. **Dailey FE, Cronan JE, Jr., Maloy SR.** 1987. Acetohydroxy acid synthase I is required for isoleucine and valine biosynthesis by Salmonella typhimurium LT2 during growth on acetate or long-chain fatty acids. J Bacteriol **169:**917-919.

31. **Belenky I, Steinmetz A, Vyazmensky M, Barak Z, Tittmann K, Chipman DM.** 2012. Many of the functional differences between acetohydroxyacid synthase (AHAS) isozyme I and other AHASs are a result of the rapid formation and breakdown of the covalent acetolactate-thiamin diphosphate adduct in AHAS I. FEBS J **279:**1967-1979.

32. **Chipman D, Barak Z, Schloss JV.** 1998. Biosynthesis of 2-aceto-2-hydroxy acids: acetolactate synthases and acetohydroxyacid synthases. Biochim Biophys Acta **1385:**401-419.

33. **Porat I, Vinogradov M, Vyazmensky M, Lu CD, Chipman DM, Abdelal AT, Barak Z.** 2004. Cloning and characterisation of acetohydroxyacid synthase from Bacillus stearothermophilus. J Bacteriol **186:**570-574.

34. **Vyazmensky M, Sella C, Barak Z, Chipman DM.** 1996. Isolation and characterisation of subunits of acetohydroxy acid synthase isozyme III and reconstitution of the holoenzyme. Biochemistry **35:**10339-10346.

35. **Pang SS, Duggleby RG.** 1999. Expression, purification, characterisation, and reconstitution of the large and small subunits of yeast acetohydroxyacid synthase. Biochemistry **38:**5222-5231.

36. **Hershey HP, Schwartz LJ, Gale JP, Abell LM.** 1999. Cloning and functional expression of the small subunit of acetolactate synthase from Nicotiana plumbaginifolia. Plant Mol Biol **40:**795-806.

37. **Lee YT, Duggleby RG.** 2001. Identification of the regulatory subunit of Arabidopsis thaliana acetohydroxyacid synthase and reconstitution with its catalytic subunit. Biochemistry **40:**6836-6844.

38. **Kelley LA, Sternberg MJ.** 2009. Protein structure prediction on the Web: a case study using the Phyre server. Nat Protoc **4:**363-371.

39. **DeLano W.** The PyMOL Molecular Graphics System on World Wide Web. 2002. There is no corresponding record for this reference.

40. **Goldschmidt L, Cooper DR, Derewenda ZS, Eisenberg D.** 2007. Toward rational protein crystallization: A Web server for the design of crystallizable protein variants. Protein Sci **16:**1569-1576.

Chapter 3

Catalytic Activity of Acetohydroxyacid Synthases

3.1 INTRODUCTION

Acetohydroxyacid synthase (AHAS) catalyses the first step in the branched-chain amino acid (BCAA) biosynthetic pathway (see Chapter 2). AHAS is a thiamine pyrophosphate (TPP)- and flavin adenine dinucleotide (FAD^+)- dependent enzyme and also requires a divalent metal ion (mostly Mg^{2+}) for catalytic activity. AHAS catalyses the decarboxylation of pyruvate and the condensation of the intermediate hydroxyethylthiamin pyrophosphate enamine (HE-TPP) with either pyruvate or 2-ketobutyrate, to form the valine- and leucine precursor acetolactate or the isoleucine precursor acetohydroxybutyrate (Figure 2.1).

Reported AHAS Assays

For determination of enzymatic activities a reliable and fast assay is crucial. For the detection of catalytic AHAS activity several assays are reported. These are introduced in the following section.

Voges Proskauer Assay

The Voges Proskauer assay is a discontinuous colorimetric assay. Hereby the samples, containing buffer, enzyme, substrates and cofactors, are incubated for a fixed time from 30 min to 2 h. Subsequently, the reaction is terminated by adding sulphuric acid (H_2SO_4) and heating at 60 °C for 15 min to convert acetolactate to acetoin, which is then converted to a coloured product of unknown structure ($\varepsilon_M = 2 \times 10^4$ $m^{-1}cm^{-1}$ at 525 nm) by a reaction with creatin and α-napthol [1]. This assay allows highly sensitive enzyme activity measurements as low as 10^{-4} units.

Photometrical Assay at 333 nm

The photometrical assay at 333 nm is a continuous assay based on the decrease in absorbance due to pyruvate consumption ($\varepsilon_M = 17.5$ $M^{-1}cm^{-1}$) [2].
The assay requires high amounts of pyruvate and enzyme and thus shows only low sensitivity.

Coupled AHAS Assay with Kari

In the BCAA biosynthesis pathway the ketol-acid reductoisomerase (Kari) catalyses the reduction of acetolactate to acetohydroxybutyrate by NADPH consumption. This NADPH consumption can directly be measured in a photometer at 340 nm. A coupled assay, consisting of AHAS and Kari, has been explored by Hill and Duggleby (1999). Unfortunately, Hill *et al.* (1999) reported that Kari from *E. coli* has an intrinsic lactate dehydrogenase activity that results in NADPH oxidation by pyruvate [3].

Isobutanol is a hydrophobic alcohol with significant importance as renewable biofuel and chemical building block. In artificial isobutanol biosynthesis pathways (Chapter 1), AHASs (Chapter 2) or acetolactate synthases (Chapter 3) are key enzymes as they convert pyruvate to acetolactate.

Industrial applications require highly stable enzyme systems to achieve relevant production rates. Therefore, it is crucial to determine AHAS thermostability, temperature optima and half-life. Additionally, a high solvent tolerance of the enzyme is desired.

This study was conducted to evaluate a suitable assay to determine thermo- as well as solvent stability of two AHASs from *Bacillus stearothermophilus* (Chapter 2) and from *Sulfolobus solfataricus*.

3.2 MATERIALS AND METHODS

3.2.1 Devices, Chemicals, Strains and Plasmids

A list with all used devices (Table 9.1), chemicals (Table 9.2), strains (9.1.1) and plasmids (9.1.2) is attached in Chapter 9.

3.2.2 Cloning – Plasmid Construction

The sequences for all in the following section mentioned primers (9.1.3) and the resulting plasmids (9.1.2) are listed in Chapter 9.

3.2.2.1 AHAS from *B. stearothermophilus*

pET28a_IlvB_A_8_IlvN_HisN

Overlap extension PCR was applied to construct the variant IlvB_A_8_IlvN [4]. PCR was performed in two steps. In the first PCR the genes *ilvB_A_8* and *A_8_ilvN* were obtained with the primers 5′ IlvBN_pET28a, 5′ A_8_IlvN_2, 3′ IlvB_A_8_2 and 3′ IlvN_pETGST1a. In the second PCR the full-length *IlvB_A_8_ilvN* gene was produced with the primers 5′ IlvBN_pET28a and 3′ IlvN_pETGST1a.

pETGST1a_IlvB_A_8_IlvN

Subsequently, the gene *ilvB_A_8_IlvN* was cloned in the vector pETGST1a digested with the restriction enzymes *Nco*I and *Xho*I. Primers 5′IlvBN_pETGST1a_NcoI and 3′IlvN_pETGST1a led to the full-length product.

3.2.2.2 AHAS from *S. solfataricus*

pCBR_*Ss*AHAS_HisC, pCBR_*Ss*AHAS_HisNo

The *Ssahas* gene was *E. coli* codon optimised prior to its synthesis by Geneart (Regensburg, Germany). The published *Ss*AHAS amino acid sequence served as template (accession NP_342102). *Ssahas* was cloned in the vector pCBR_HisC and pCBR_HisNo pre-digested with *Bfua*I and *Bsa*I.

3.2.3 Heterologous Protein Expression

3.2.3.1 AHAS from *S. solfataricus*

Enzyme expression of *Ss*AHAS was performed using *E. coli* BL21(DE3) as host strain. *Ss*AHAS was expressed in LB medium supplemented with 50 µg/ml kanamycin. After inoculation cells were grown to an OD_{600} = 0.5 – 0.7 at 37 °C and subsequently induced with 1 mM IPTG. For further cultivation temperature was hold at 37 °C for 4 h. The cells were harvested (4,500 g, 4 °C, 30 min) and stored at -20 °C.

3.2.3.2 IlvB_A_8_IlvN from *B. stearothermophilus*

His_6_IlvB_A_8_IlvN and His_6_GST_IlvB_A_8_IlvN were expressed in *E. coli* HMS174(DE3) cells using TB medium supplemented with 50 µg/ml kanamycin. After inoculation cells were grown to an OD_{600} = 0.5 – 0.7 at 37 °C and subsequently induced with 1 mM IPTG. For further cultivation, temperature was lowered to 16 °C for 48 h. Afterwards the cells were harvested (4,500 g, 4 °C, 30 min) and stored at -20 °C.

3.2.4 Enzyme Assay

3.2.4.1 Photometrical AHAS Assay

The lactate dehydrogenase (LDH)-assay is a photometrical enzyme assay. It was performed in microtiter plate format using an Enspire 2 plate reader. The pH-value of the buffer was adjusted to the corresponding temperature according to Stoll [5]. The reaction mixtures contained 50 mM Hepes (pH 7 at desired temperature), 0.1 mM TPP, 10 mM $MgCl_2$ and 15 mM sodium pyruvate. The activity of IlvB was measured by assaying the pyruvate consumption at 50 °C and 60 °C in a water bath, in a standardized LDH assay in triplicates [6]. 4 µl samples of each assay were taken every five minutes and the remaining pyruvate was immediately converted to lactate by LDH. The volume 4 µl corresponds to 0.3 mM sodium pyruvate in the control without enzyme, which was transferred to the LDH assay (25 mM Hepes (pH 7.4 at RT), 0.3 mM NADH, up to 0.3 mM sodium pyruvate). The absorbance was determined at 340 nm.

3.2.4.2 GC-FID Analysis

Acetolactate can be detected neither by GC nor HPLC. However, the conversion of acetolactate with $KMnO_4$ (7.2 mM) leads to the instable acetoin, which is further oxidized to diacetyl. The accumulating diacetyl can be quantified by a Trace GC Ultra, equipped with a Headspace Tri Plus auto sampler, an agitator and a flame ionization detector. The GC analysis was performed on an Optima-5 MS column (length 30 m, internal diameter 0.25 mm, film thickness 0.25 µm (Macherey-Nagel, Düren, Germany), with helium (1 ml min^{-1}) as carrier gas. Injector and detector temperature were 200 °C, whereas the oven temperature programme was 60 °C for 2 min, raised to 150 °C with a ramp of 10 °C min^{-1}, the end temperature was held for 1 min. The samples (500 µl in a 10 ml gas-tight headspace vial) were incubated at 40 °C for 15 min. For the analysis 700 µl of the headspace were injected (headspace syringe 100 °C) in the split mode with a flow of 10 ml min^{-1}. The assay mixture contained 50 mM Hepes pH 7, 40 mM pyruvate, 10 mM $MgCl_2$ and 0.1 mM TPP.

3.3 RESULTS AND DISCUSSION

3.3.1 Selection of an AHAS Activity Assay

An activity assay suitable for determination of temperature and solvent stability was established. This assay allowed to test AHASs for their industrial applicability. Therefore, in literature reported assays (see 3.1) were screened for their advantages and disadvantages.

Voges Proskauer Assay

The Voges Proskauer assay is a discontinuous assay, resulting in inaccurate activity determination when product formation is not linear over time [7]. Additionally, no proof that A) all acetolactate is converted to acetoin by sulphuric acid and B) all acetoin is converted to the coloured product by creatin and α-napthol exists. This assay is suited for qualitative detection of acetolactate in environmental samples or tissue extracts, when a high sensitivity is necessary.

Photometrical Assay at 333 nm

In the photometrical pyruvate assay at 333 nm high amounts of substrate and enzyme are required. 60 mM pyruvate are necessary to achieve a value of 0.5 absorbance units at 333 nm. To achieve a change in the absorbance units a lot of pyruvate has to be consumed and therefore high amounts of enzyme are required, even if the enzyme is highly active. These high amounts cause problems when enzymes are exposed to higher organic solvent concentrations or higher temperatures for extended time periods. Agglutination or precipitation of the enzyme occurs and affects the absorption of pyruvate at 333 nm.

Furthermore, high protein amounts cause an enlargement of the signal at 280 nm in the absorbance spectra, which might influence the measurement at 333 nm.
Therefore, this assay is neither suitable to determine pH-, solvent- or thermostability of the protein of interest nor can the protein's half-live activity be analysed exactly.

Coupled Assay with Kari

This coupled assay combines high sensitivity and continuity. Bastian *et al.* (2011) were able to change the cofactor dependency of *E. coli* Kari (*Ec*Kari) [8]. Therefore, NADH could be chosen as cofactor instead of NADPH. NADH is more stable and cost efficient than NADPH. Furthermore, the problematic intrinsic lactate dehydrogenase activity could be avoided by selecting Kari from *Meiothermus ruber* (*Mr*Kari), which shows almost no lactate dehydrogenase activity. Additionally, *Mr*Kari's cofactor dependency could also be changed towards NADH (personal communication S. Reiße [9]).
A remaining problem is the 13 times lower activity of *Mr*Kari compared to *Bs*AHAS (9.2 U/mg). Therefore, in a coupled assay, Kari, the enzyme for detection, had to be applied in excess and is not commercially available.

3.3.1.1 Optimization of a Reported Lactate Dehydrogenase Assay

As the previous assays were not applicable a discontinuous, pyruvate decarboxylase assay [6] was chosen to determine AHASs activity.
The remaining pyruvate, after termination of AHAS activity, is consumed by a lactate dehydrogenase (LDH) leading to a corresponding decrease in the initial amount of detectable NADH at 340 nm (Figure 3.1) [6]. Every five minutes a sample was taken and the reaction was immediately stopped by adding a volume corresponding to the amount of sodium pyruvate in the control without enzyme to the LDH assay.

The major advantage of this assay compared to the Voges Proskauer assay is the one step conversion of acetolactate in a visible product. Additionally, its formation can be easily and continuously controlled during the reaction. By using the appropriate amount of enzyme, it was possible to obtain a slope due to several measured points (Figure 3.3). Additionally, both reactions (conversion of pyruvate to acetolactate and conversion of pyruvate to lactate) are setup independently. Consequently, no interference resulting in a decreased activity of the detection enzyme occurs.

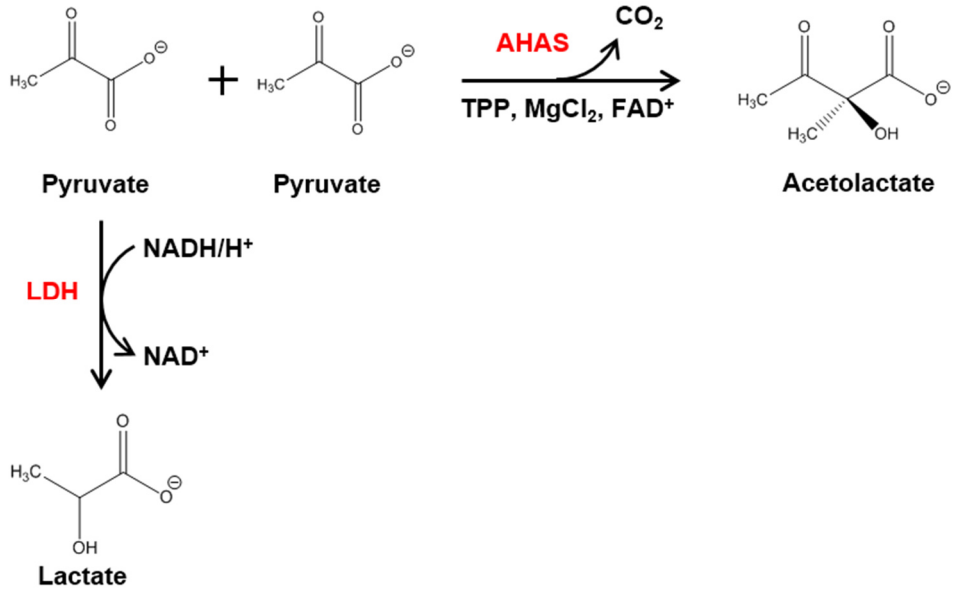

Figure 3.1: Principle of the coupled AHAS assay with LDH.
Pyruvate is converted to acetolactate by AHAS. In a second step remaining pyruvate is converted to lactate by LDH.

3.3.1.2 Detection of AHAS Activity by GC Measurements

Although the photometrical lactate dehydrogenase assay (3.3.1.1) is working quite well, GC measurements are advisable to confirm the formation of the desired end product, especially when working with cell extracts. As acetolactate can neither be measured by gas chromatography (GC) nor by HPLC acetolactate is commonly converted to acetoin by sulphuric acid [10]. Diacetyl, an undesired side product, is formed through an overreaction from acetoin moieties and inhibits calibration and calculation of the enzyme activity.

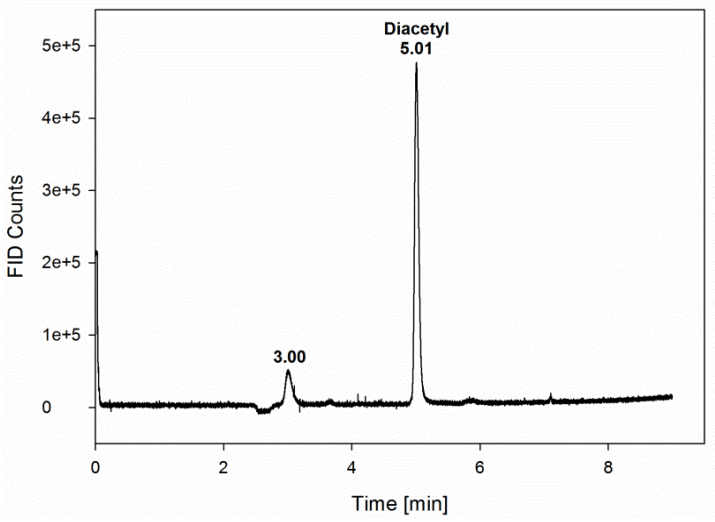

Figure 3.2: Chromatogram of GC-pyruvate assay;
At retention time 5.01 min diacetyl is eluted. The peak at retention time 3.00 min originates from injection.

Therefore, we established a protocol to convert almost all acetolactate to diacetyl prior to GC analysis by incubation with the strong oxidizing agent potassium permanganate at room temperature (Figure 3.2).
To terminate AHAS activity 7.2 mM potassium permanganate was added to an AHAS assay. This reaction is completed after a few seconds when small pieces of pyrolusite occurred.

3.3.2 AHAS from *B. stearothermophilus*

The already mentioned AHAS activity assay was needed to characterise AHASs with respect to their half-lives and thermostabilities for isobutanol production.
For a stable isobutanol production process the application of enzyme systems with high half-lives and enhanced thermostability are required to achieve relevant production rates [11]. Therefore, IlvBN from *B. stearothermophilus,* a thermophilic organism, seems to be suitable for cell-free isobutanol biosynthesis. A T_{opt} of 55 °C is published for *Bs*AHAS [12].

3.3.2.1 Determination of Catalytic Activity and Half-Life of IlvB

To validate the reported activity and thermostability of IlvB, pETGST1a_IlvB was cloned. Subsequent expression of His_6_GST_IlvB in HMS174(DE3) cells and purification of IlvB (without any tag) was achieved (see Chapter 2, 2.3.2.2).
IlvB activity was determined by using a coupled, photometric assay with LDH from porcine heart at 50 °C (see 3.3.1.1). Over a period of 30 min, each five minutes a sample was taken and remaining pyruvate converted via LDH to lactate (Figure 3.3).

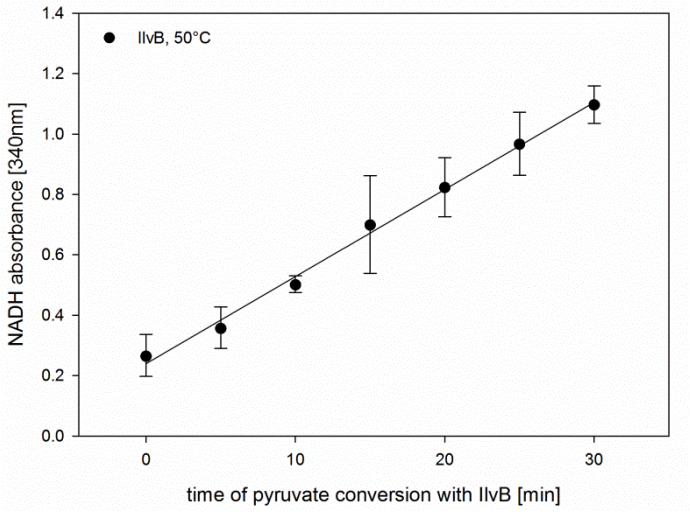

Figure 3.3: Determination of IlvB activity at 50 °C with LDH assay measured at 340 nm.
Shown is the trend line and the standard error of three measurements.

The trend line represents the increase in NADH-concentration calculated by a linear function (r^2-value = 0.99) (Figure 3.3) resulting in an IlvB activity of 4.6 U/mg. This value is consistent with literature precedence (3 U/mg) [12].
Further experiments were done to determine the half-life of IlvB at 50 °C and 60 °C. Results showed that IlvB was unstable without the regulatory subunit. The measured IlvB activity strongly fluctuated even in triplicate setups of one assay with the same conditions. This result was affirmed by the dissociation constants for the reconstituted enzyme, which indicated a tight association between the two subunits [13-15]. For a continuous stability and a reliable result, the regulatory subunit is implicitly required and therefore the expression of IlvN had to be improved (see 2.3.2). Nevertheless, Porat *et al.* (2004) purified the holoenzyme by gelfiltration and published a specific activity of 9.2 U/mg as well as a half-life of 5 min at 65 °C. For the large, catalytic subunit IlvB a T_{opt} of 50 °C was described [12].

3.3.2.2 Fusion of Catalytic and Regulatory Subunit of *Bs*AHAS

As shown in chapter 2 (see 2.3.2) expression of IlvB and IlvN in equimolar amounts was impossible. To obtain an IlvBN variant enabling a complete characterisation of IlvBN thermo- and solvent stability, IlvB was fused with IlvN spaced over eight alanines. The linker was required to ensure correct protein folding. A problem herein was to correlate the length of the linker with respect to the cloning efficiency.
The fusion gene *ilvB* aligned with *ilvN* spaced over an A_8-linker (*ilv*B_A_8_*ilv*N) was cloned in the vector pET28a by overlap extension PCR (see 3.2.2.1). To improve cloning likelihood different codons corresponding to the A_8-linker were applied.

The fused protein His_6_IlvB_A_8_IlvN was not very soluble, therefore *ilvB_*A_8*_ilvN* was also cloned in the vector pETGST1a to increase solubility.
With this soluble protein, contained in crude extract, initial activity assays were conducted. The assay was incubated overnight in a water bath at 50 °C. Subsequently, 7.2 mM $KMnO_4$ was added to convert acetolactate to diacetyl.
The chromatogram of the GC measurement showed a small diacetyl peak (at 4.88 min). Therefore, it can be deduced that the fustion protein His6_GST_IlvB_A8_IlvN had almost completely lost its ability to ligate two molecules pyruvate to one molecule acetolactate, thus no further experiments with this protein were conducted.

3.3.3 AHAS from *S. solfataricus*

Thermostability of IlvBN was hard to determine as IlvB can only exhibit its optimal activity in presence of IlvN and is instable without IlvN. Additionally, expression of IlvB and IlvN in

equimolar amounts was not possible (Chapter 2, 2.3.2) and a fusion enzyme consisting of IlvB linked to IlvN over an A_8-linker lost its ability to form acetolactate (see 3.3.2.2).

Therefore, an adequate enzyme originating from a thermo- or hyperthermophilic organism was searched.

Archaeal AHAS are special, as they might not have a regulatory subunit. However, it is reported for AHAS from *M. aeolicus* and *H. volcanii* that they are still sensitive to feedback inhibition by BCAAs [16, 17].

Due to its thermopilic origin and the possibility, that archaeal AHASs might not require a regulatory subunit the gene *ahas* from *Sulfolobus solfataricus* was cloned in pCBR- expression vectors (see 3.2.3.1). *Ss*AHAS was expressed in *E. coli* BL21(DE3) cells (3.3.3). After cell disruption, a small soluble fraction of *Ss*AHAS could be identified on a 12 % SDS-gel at approximately 64 kDa (Figure 3.4). Assays with cell lysates were carried out at different temperatures (40 °C – 80 °C) and detected no enzyme activity at all.

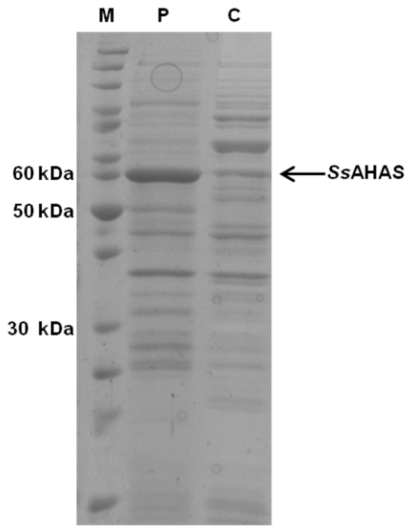

Figure 3.4: 10% SDS-page showing expressed *Ss*AHAS at approximately 64 kDa.
M: unstained protein ladder; P: cell pellet; C: crude extract;

It is possible, that the codon-optimization of *Ssahas* resulted in a loss of activity. Bowen *et al.* (1997) reported the identification of a putative regulatory subunit gene from *M. aeolicus* [18]. So it is likely that archaeal AHAS regulatory subunits exist and maybe this subunit is implicitly required for *Ss*AHAS activity. Additionally, it is reported that AHAS from *M. aeolicus* is oxygen sensitive [16] and thus it is likely that *Ss*AHAS also require an anaerobic environment.

3.4 CONCLUSIONS

AHAS catalyse the decarboxylation of one molecule pyruvate and transfer the remaining cofactor-bound hydroxyethyl group to a second molecule of pyruvate producing acetolactate. This is a key step in artificial isobutanol biosynthesis. For industrial applicability of AHAS a highly thermostable and solvent tolerant variant is required.

Therefore, we conducted a literature study to identify an optimal AHAS assay. Subsequently, a pyruvate decarboxylase assay was chosen to determine activity and thermostability of AHAS from *B. stearothermophilus* and *S. solfataricus*. Additionally, a known GC assay for acetolactate detection was improved by using potassium permanganate instead of sulphuric acid.

IlvB from *B. stearothermophilus* without the regulatory subunit exhibits an activity towards pyruvate of 4.6 U/mg, which is consistent with literature results [12]. Unfortunately, no thermostability measurements could be conducted with IlvB as it is instable in the absence of IlvN.

A fusion enzyme consisting of IlvB and IlvN, linked via eight alanines, was cloned to determine the IlvBN activity. However, IlvB_A_8_IlvN lost almost its ability to ligate two molecules pyruvate.

Therefore, an enzyme originating from a thermo- or hyperthermophilic organism with the ability to catalyse the decarboxylation of pyruvate to form acetolactate was searched.

AHAS from *S. solfataricus* seemed to be suitable regarding its thermostability and its easier purification as archaeal AHASs might not possess a regulatory subunit. However, after testing *Ss*AHAS in several different assay conditions, no activity could be detected. It might be possible that *Ss*AHAS inactivity was due to A) *Ssahas E. coli* codon-optimisation and/or B) *Ss*AHAS might be oxygen sensitive, as already shown for AHAS from *M. aeolicus* [16].

3.5 REFERENCES

1. **Westerfeld WW.** 1945. A colorimetric determination of paraldehyde. J Lab Clin Med **30:**1076.
2. **Schloss JV, Van Dyk DE, Vasta JF, Kutny RM.** 1985. Purification and properties of Salmonella typhimurium acetolactate synthase isozyme II from Escherichia coli HB101/pDU9. Biochemistry **24:**4952-4959.
3. **Hill CM, Duggleby RG.** 1999. Purified recombinant Escherichia coli ketol-acid reductoisomerase is unsuitable for use in a coupled assay of acetohydroxyacid synthase activity due to an unexpected side reaction. Protein Expr Purif **15:**57-61.
4. **Ho SN, Hunt HD, Horton RM, Pullen JK, Pease LR.** 1989. Site-directed mutagenesis by overlap extension using the polymerase chain reaction. Gene **77:**51-59.
5. **Stoll VS, Blanchard JS.** 2009. Buffers: Principles and Practice1. Methods in enzymology **463:**43-56.
6. **Wolterink-van Loo S, van Eerde A, Siemerink M, Akerboom J, Dijkstra B, van der Oost J.** 2007. Biochemical and structural exploration of the catalytic capacity of Sulfolobus KDG aldolases. Biochem. J **403:**421-430.
7. **Duggleby RG, Pang SS.** 2000. Acetohydroxyacid synthase. Journal of Biochemistry and Molecular Biology **33:**1-36.
8. **Bastian S, Liu X, Meyerowitz JT, Snow CD, Chen MM, Arnold FH.** 2011. Engineered ketol-acid reductoisomerase and alcohol dehydrogenase enable anaerobic 2-methylpropan-1-ol production at theoretical yield in Escherichia coli. Metab Eng **13:**345-352.
9. **Reisse S.** 2013. Personal communication, Industrial Biokatalysis, TU München.
10. **Holtzclaw WD, Chapman LF.** 1975. Degradative acetolactate synthase of Bacillus subtilis: purification and properties. J Bacteriol **121:**917-922.
11. **Guterl JK, Garbe D, Carsten J, Steffler F, Sommer B, Reisse S, Philipp A, Haack M, Rühmann B, Koltermann A, Kettling U, Brück T, Sieber V.** 2012. Cell-free metabolic engineering: production of chemicals by minimized reaction cascades. ChemSusChem **5:**2165-2172.
12. **Porat I, Vinogradov M, Vyazmensky M, Lu CD, Chipman DM, Abdelal AT, Barak Z.** 2004. Cloning and characterisation of acetohydroxyacid synthase from Bacillus stearothermophilus. J Bacteriol **186:**570-574.
13. **Pang SS, Duggleby RG.** 1999. Expression, purification, characterisation, and reconstitution of the large and small subunits of yeast acetohydroxyacid synthase. Biochemistry **38:**5222-5231.
14. **Lee YT, Duggleby RG.** 2001. Identification of the regulatory subunit of Arabidopsis thaliana acetohydroxyacid synthase and reconstitution with its catalytic subunit. Biochemistry **40:**6836-6844.
15. **Mendel S, Elkayam T, Sella C, Vinogradov V, Vyazmensky M, Chipman DM, Barak Z.** 2001. Acetohydroxyacid synthase: a proposed structure for regulatory subunits supported by evidence from mutagenesis. J Mol Biol **307:**465-477.
16. **Xing R, Whitman WB.** 1994. Purification and characterisation of the oxygen-sensitive acetohydroxy acid synthase from the archaebacterium Methanococcus aeolicus. J Bacteriol **176:**1207-1213.
17. **Vyazmensky M, Barak Z, Chipman DM, Eichler J.** 2000. Characterisation of acetohydroxy acid synthase activity in the archaeon Haloferax volcanii. Comp Biochem Physiol B Biochem Mol Biol **125:**205-210.
18. **Bowen TL, Union J, Tumbula DL, Whitman WB.** 1997. Cloning and phylogenetic analysis of the genes encoding acetohydroxyacid synthase from the archaeon Methanococcus aeolicus. Gene **188:**77-84.

Chapter 4

Detailed Structure-function Correlations of *Bacillus subtilis* Acetolactate Synthase

Acetolactate synthase from Bacillus subtilis (AlsS) has been used in the construction of artificial in vivo and in vitro biosynthesis pathways for production of isobutanol due to its favourable catalytic properties and stability. During isobutanol biosynthesis AlsS catalyses the condensation of two pyruvate units to acetolactate using TPP and $MgCl_2$ as cofactors. Recently, it was demonstrated that AlsS also catalyses the decarboxylation of the isobutanol precursor 2-ketoisovalerate (KIV) to isobutyraldehyde, which provides for significant consolidation of the enzyme cascade required to convert sugars into isobutanol. As the decarboxylation of KIV is rather inefficient, further efforts are required to enhance AlsS catalytic efficiency towards KIV without significantly affecting its native activity. Currently, optimization of AlsS enzyme activity is hampered by the lack of structural data for this enzyme family. For the first time this study describes a high resolution AlsS crystal structure (2.34 Å) and reports structure-function correlations focusing on key active site amino acid residues. Mutants were expressed in E. coli and thermalstability at 50 °C and 60 °C as well as catalytic properties towards pyruvate and KIV substrates were elucidated. Interestingly, a shift in the protein colour of $AlsS^{Q424S}$ and $AlsS^{Q424S\_Q487S}$ from white to bright red could be observed.

4.1 INTRODUCTION

Due to its hydrophobic properties and higher caloric value isobutanol is flagged as a novel renewable platform chemical and biofuel. Recently, both *in vivo* and *in vitro* isobutanol production processes have been reported [1-8].

The *in vitro* approach allows elimination of undesired metabolic side-reactions, which reduce molecular efficiencies. Cell based isobutanol yields are limited to about ~2 % (v/v) isobutanol due to toxic effects of the end product [1, 3]. By contrast, the *in vitro* isobutanol synthesis approach potentially allows for a yield of 12 % (v/v), which leads to spontaneous phase separation and simplified product recovery procedures [9].

An essential biocatalyst of isobutanol biosynthesis is TPP dependent acetolactate synthase (Als) (EC 2.2.1.6), which is naturally involved in butane-2,3-dione biosynthesis pathway [10, 11].

Als requires the cofactors TPP and $MgCl_2$ in order to catalyse the decarboxylation of one molecule pyruvate and transfer the remaining cofactor-bound hydroxyethyl group onto a second pyruvate molecule resulting in acetolactate (Figure 4.1A).

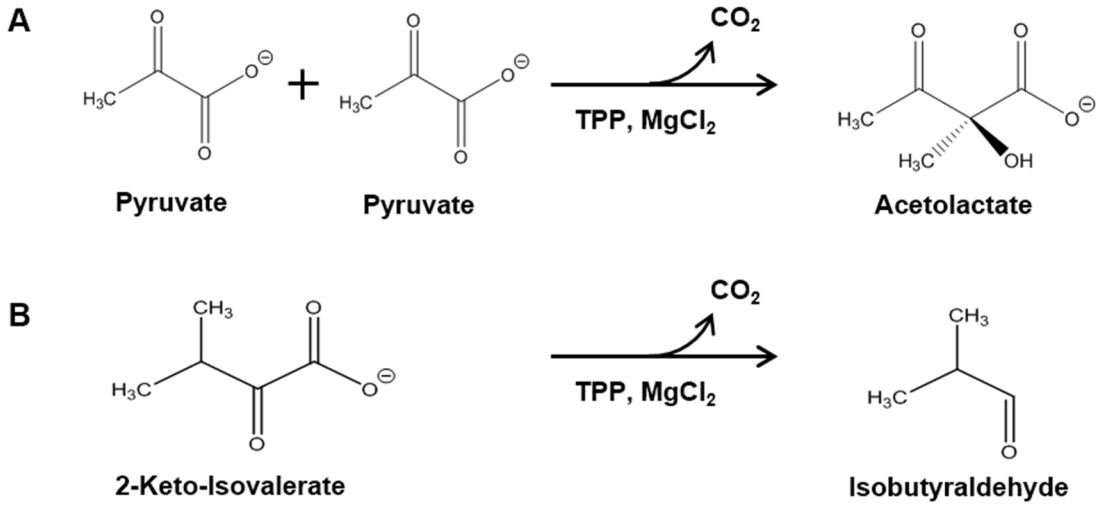

Figure 4.1: Reactivity of *B. subtilis* Als.
The main reaction catalyses the conversion of two molecules of pyruvate to acetolactate (A), whereas the side reaction (B) results in isobutyraldehyde.

A side reaction of Als from *Bacillus subtilis* (AlsS) also catalyses the decarboxylation of 2-ketoisovalerate (KIV) to isobutyraldehyde [2] (Figure 4.1B).

While pyruvate is an upstream intermediate in artificial isobutanol biosynthesis, KIV is a key downstream intermediate. Generally, the reaction with pyruvate is favoured by wild-type AlsS, which shows poor substrate selectivity and conversion rates towards KIV.

In addition, previously reported cell based isobutanol production efforts could not detect any 2-ketoacid decarboxylase (Kdc) activity of native AlsS [12].
As AlsS has a central role in synthetic isobutanol biosynthesis pathway [13], optimization of AlsS KIV selectivity would potentially lead to simplification of the cell-free reaction cascade as Kdc, an accessory enzyme, can be eliminated.

Structure guided mutagenesis of AlsS might be helpful to improve AlsS KIV selectivity. However previously, structural information for Als was limited to the crystal structure of Als from *Klebsiella pneumoniae* (pdb-ID: 1OZF) [14] and the crystal structures of the acetohydroxyacid synthase (AHAS) catalytic subunit from *Saccharomyces cerevisiae* (pdb-ID: 1T9A) [15] and *Arabidopsis thaliana* (pdb-ID: 1YHZ) [16].
AHAS (Chapter 2) is a related enzyme family, which catalyses the same reaction as Als but in a different biochemical context. AHAS catalyses the first step in the branched-chain amino acid biosynthesis pathway of valine, leucine and isoleucine [17] and additionally requires flavin adenine dinucleotide (FAD^+) cofactor for catalytic activity.
Although Als shares less than 30 % sequence identity with AHAS [18] the primary, secondary and also three-dimensional structures are very similar [14].

In this study, we obtained insights into the AlsS reaction mechanism. Additionally, we were able to solve the crystal structure of AlsS in the resting state by X-ray crystallography. The structural data were used to guide our mutagenesis efforts to obtain enzyme variants with improved activities and enhanced KIV selectivity. We substituted critical amino acids for catalysis and substrate recognition. These variants were probed for activity towards pyruvate and KIV as well as thermostability.

4.2 MATERIALS AND METHODS

4.2.1 Devices, Chemicals, Strains and Plasmids

A list with all used devices (Table 9.1), chemicals (Table 9.2), strains (9.1.1) and plasmids (9.1.2) is attached in Chapter 9.

4.2.2 Cloning –Plasmid Construction

The *E. coli* codon optimised *alsS* gene was synthesised by Geneart (Regensburg, Germany) using the published gene sequence of *alsS* as template (GenBank-nb.: CAB07802.1).

pCBR_AlsS_HisC and pCBR_AlsS_HisNo

AlsS was cloned into the vector pCBR_HisC and pCBR_HisNo using *Bfua*I and *Bsa*I restriction sites.

AlsS variants

AlsS mutants were constructed by applying mega-primer PCR [19]. Primer sequences are listed in Chapter 9 (9.1.3).

Table 4.1: Overview of used primers and templates for construction of AlsS variants.

mutated amino acids	template	forward primer	reverse primer	final construct
	pCBR_AlsS_HisC	5'AlsS_pETGST1a	3'AlsS_pETGST1a	pETGST1a_AlsS
K40H	pCBR_AlsS_HisC	5'AlsS_pETGST1a	3'AlsS_K40H 3'AlsS_pET28a	pET28a_AlsS_K40H_ HisC
K40I	pCBR_AlsS_HisC	5'AlsS_pETGST1a	3'AlsS_K40I 3'AlsS_pET28a	pET28a_AlsS_K40I_ HisC
K40Y	pCBR_AlsS_HisC	5'AlsS_pETGST1a	3'AlsS_K40Y 3'AlsS_pET28a	pET28a_AlsS_K40Y_ HisC
T84V	pCBR_AlsS_HisC	5'AlsS_pETGST1a	3'AlsS_T84V 3'AlsS_pET28a	pET28a_AlsS_T84V_ HisC
P87A	pCBR_AlsS_HisC	5'AlsS_pETGST1a	3'AlsS_P87A 3'AlsS_pET28a	pET28a_AlsS_P87A_ HisC
Q124S	pCBR_AlsS_HisC	5'AlsS_pETGST1a	3'AlsS_Q124S 3'AlsS_pET28a	pET28a_AlsS_Q124S_ HisC
Q424S	pCBR_AlsS_HisC	5'AlsS_Q424S 5'AlsS_pETGST1a	3'AlsS_pET28a	pET28a_AlsS_Q424S_ HisC
	pET28a_AlsS_ Q424S_HisC	5'AlsS_pETGST1a	3'AlsS_pETGST1a	pETGST1a_AlsS_ Q424S
Q424S_ Q487S	pET28a_AlsS_ Q424S_HisC	5'AlsS_Q487S 5'AlsS_pETGST1a	3'AlsS_pET28a	pET28a_AlsS_Q424S_ Q487S_HisC
	pET28a_AlsS_ Q424S_Q487S_ HisC	5'AlsS_pETGST1a	3'AlsS_pETGST1a	pETGST1a_AlsS_ Q424S_Q487S
Y481A	pCBR_AlsS_HisC	5'AlsS_Y481A 5'AlsS_pETGST1a	3'AlsS_pET28a	pET28a_AlsS_Y481S_ HisC
M483N	pCBR_AlsS_HisC	5'AlsS_M483N 5'AlsS_pETGST1a	3'AlsS_pET28a	pET28a_AlsS_M483N_ HisC
Q487S	pCBR_AlsS_HisC	5'AlsS_Q487S 5'AlsS_pETGST1a	3'AlsS_pET28a	pET28a_AlsS_Q487S_ HisC

In a first PCR the desired exchange was introduced in the mega-primer, which was further used for the second PCR to obtain the full-length product. Both pET28a/pETGST1a vector and full-length PCR product were digested with *Xho*I and *Nco*I and ligated together.

4.2.3 Protein Expression and Purification of AlsS for Crystallisation

The gene coding for *alsS* (AlsS_HisNo) or fused to a C-terminal His_6-tag (AlsS_HisC) was transformed with *E. coli* BL21 pLys Express cells. AlsS was cultured in 2xYT medium at 37 °C until an OD ~ 1.3 was reached and subsequently cooled down to 18 °C. Protein expression was induced by addition of 0.5 mM IPTG. Cells grew overnight and were harvested by centrifugation (10 min, 6,000 rpm at 4 °C). The pellet of AlsS was resuspended in 50 mM Tris/HCl pH 8.0, 500 mM NaCl, 1 mM $MgCl_2$. Cells were lysed by sonification at 4 °C and

the supernatant was cleared by 1 h centrifugation (20,000 rpm at 4 °C). A Ni^{2+}-NTA column (column volume (cv) ~ 1 ml; GE Healthcare, Dornstadt, Germany) was equilibrated with 20 mM Tris/HCl pH 8.0, 500 mM NaCl, 1 mM $MgCl_2$, 10 mM imidazole and 2 mM DTT. AlsS_HisC was loaded on the column and washed with 3 cv of equilibration buffer. AlsS_HisC was eluted in a linear gradient to 20 mM Tris/HCl pH 8.0, 500 mM NaCl, 1 mM $MgCl_2$, 2 mM DTT and 500 mM imidazole. In contrast, the cleared supernatant of AlsS_HisNo was diluted 1:10 with 50 mM Tris/HCl pH 8.0, 1 mM $MgCl_2$ and loaded on a 1 ml HisTrap Q XL column (GE Healthcare). AlsS_HisNo was eluted in a linear gradient from 100 to 1000 mM NaCl. The pooled fractions were diluted 1:10 with 50 mM Tris/HCl pH 8.0, 1 mM $MgCl_2$ and loaded on a MonoQ 10/100 column (GE Healthcare). AlsS_HisNo was eluted in a linear gradient from 100 to 1,000 mM NaCl. Size exclusion chromatography of AlsS_HisNo and AlsS_HisC was performed with a HighLoad Superdex S200 16/60 column (GE Healthcare), equilibrated with 50 mM Tris/HCl pH 8.0, 100 mM NaCl, 1 mM $MgCl_2$ and 2 mM DTT. Pooled protein fractions were concentrated with Amicon-Ultra 30,000 to 35 mg/ml as measured by the absorbance at 280 nm.

4.2.4 Crystallization and Crystal Cooling

For cofactor incorporation, AlsS_HisNo or AlsS_HisC with a concentration of 35 mg/ml was incubated for 3.5 hours at RT with 0.1 mM TPP and 10 mM Mg^{2+} and subsequently used for crystallization experiments. Crystals appeared after one day in a sitting drop setup with a reservoir solution composed of 30% (v/v) polyethylene glycol 300, 200 mM Ca acetate, and 100 mM Na cacodylate at pH 6.5. AlsS_HisNo crystallized with 45% (v/v) polyethylene glycol 200, 100 mM Tris/HCl pH 7.0 and 50 mM Li_2SO_4. Crystals grew to maximum size within three days and were sufficient in size for X-ray data collection. Without any additional cryo-protectant, crystals were flash cooled in liquid nitrogen.

4.2.5 X-Ray Data Collection, Structure Determination and Refinement

Synchrotron diffraction data were collected at the beamline 14.2 of the MX Joint Berlin laboratory at BESSY (Berlin, Germany) or beamline P14 of Petra III (Deutsches Elektronen Synchrotron, Hamburg, Germany). X-ray data collection was performed at 100 K. Diffraction data were processed with the XDS package [20, 21] (Table 4.2). For calculation of the free R-factor, a randomly generated set of 5 % of the reflections from the diffraction data set was used and excluded from the refinement. Initial phases of the AlsS_HisC were determined by molecular replacement PHASER [22] employing a search model of one monomer, that had been side chain and cofactor depleted, derived of the coordinates of the AlsS of *K. pneumoniae* (pdb-ID: 1OZF [14]). An initial, model was built with the program

BUCCANEER [23]. The structure was initially refined by applying a simulated annealing protocol and in later refinement cycles merely by maximum-likelihood restrained refinement implemented in PHENIX [24] followed by iterative model building cycles with COOT [25]. The structure of AlsS_HisNo was solved by molecular replacement using one protomer of the initially built AlsS_HisC with the program PHASER [22]. The structure was refined with PHENIX [24]. Water molecules were located with COOT [25] and manually inspected. The final model of AlsS_HisNo was used in the refinement of the AlsS_HisC against the medium resolution data set (Table 4.2). Model quality was evaluated with PROCHECK [26] and MolProbity [27]. Figures were prepared using PYMOL [28]. The active site tunnel was calculated using the PYMOL plug-in CAVER software tool [29].

4.2.6 Heterologous Expression and Protein Purification for Enzymatic Assays

Enzyme expression was performed using *E. coli* HMS174(DE3) as host strain. AlsS and all AlsS variants were expressed in TB media [30] supplemented with 50 µg/ml kanamycin. After inoculation cells were grown to an OD_{600} = 0.5 – 0.7 at 37 °C and subsequently induced with 1 mM IPTG. For further cultivation, the temperature was lowered to 16 °C for 48 h. Cell lysates were prepared with Emulsiflex-B15, cell debris was removed by centrifugation (25,000 g, 4 °C, 20 min). Protein purification was performed using Ni^{2+}-NTA column and proteins were desalted with PD-10 columns (GE Healthcare, Dornstadt, Germany). All variants were purified as described for the wild-type. AlsS and variants were stored as liquid stocks with 10 % (v/v) glycerol at -80 °C. Protein concentration was measured at 280 nm with unfolded protein in 8 M Urea [31]. The corresponding extinction coefficient was calculated by ExPASY ProtParam tool [32].

4.2.7 Enzyme Assays

Pyruvate- and KIV-assay are photometrical enzyme assays. They were performed in microtiter plate format using an Enspire 2 plate reader. The pH-values of the buffers were adjusted to the corresponding temperature according to Stoll [33]. For the pyruvate-assay, reaction mixtures contained 50 mM Hepes (pH 7 at current temperature), 0.1 mM TPP, 10 mM $MgCl_2$ and 15 mM sodium pyruvate. The activities of AlsS and variants were measured by assaying the pyruvate consumption at 50 °C or 60 °C in a water bath, in a standardized LDH assay in triplicates [34]. 4 µl samples of each assay were taken every five minutes and the remaining pyruvate was immediately converted to lactate by LDH (porcine heart). The volume 4 µl corresponds to 0.3 mM sodium pyruvate in the control without enzyme which was transferred to the LDH assay (25 mM Hepes (pH 7.4 at RT), 0.3 mM NADH, up to 0.3 mM sodium pyruvate). The absorbance was determined at 340 nm.

For thermal-stability assays, AlsS was stored over several days at 50 °C and 60 °C in a water bath.

For solvent-stability assays, the before mentioned reaction mixture contained the defined amount of n-butanol, ethanol or isobutanol. All assays were performed at 50 °C.

For determination of pH-optima, sodium acetate buffer was used for the pH range 4 – 5.5, sodium phosphate buffer for pH 6 and 6.5, Tris buffer for pH 7 – 9 and Caps buffer for pH 10 and 11 (50 °C).

For the KIV-assays, the reaction mixtures contained 50 mM Hepes (pH 7.0), 0.1 mM TPP, 2.5 mM $MgCl_2$, 30 mM KIV, 0.3 mM NADH and 0.25 U/ml ADH. The AlsS activity towards KIV was assayed at 40 °C and 340 nm.

4.2.8 Isoelectric Focusing

Isoelectric Focusing (IEF) was performed with Novex pH 3 - 7 IEF Gels 1.0 mm, 10 well (Life Technology GmbH, Darmstadt, Germany). Anode and cathode (pH 3 - 10) buffers as well as IEF sample buffer pH 3 – 10 were also bought from Novex. 1x IEF anode and 1x IEF cathode buffer were prepared as described from Novex. After prefocusing for 1 h at 100 V, proteins were focused for 1 h at 200 V and 30 min at 500 V. Subsequently, the IEF gel was fixed in 12 % TCA-solution for 30 min and the gel was stained with coomassie brilliant blue for further 30 min. For bleaching the gel was stored in hot water till the desired coloration was obtained.

4.3 RESULTS AND DISCUSSION

4.3.1 Structural Aspects of AlsS

Crystallisation of AlsS and assembly of the structure was performed by Dr. Bernhard Loll (FU Berlin, Germany).

4.3.1.1 Crystallisation of AlsS

AlsS_HisC and AlsS_HisNo were overexpressed in *E. coli* and purified to homogeneity for crystallization experiments. Prior to crystallization, the proteins were incubated with an excess of TPP and Mg^{2+}. Initially crystals of AlsS_HisC were obtained in the tetragonal space group $P4_12_12$ and the crystal structure could be solved at medium resolution (Table 4.2) by molecular replacement using a poly-alanine model derived from *K. pneumoniae* Als [14]. The asymmetric unit of AlsS_HisC contains one homo-tetramer with bound cofactors TPP and Mg^{2+}. Attempts to improve the diffraction quality of these crystals by manipulation of the initial crystallization condition failed. Therefore, we crystallized the untagged AlsS_HisNo, incubated with TPP and Mg^{2+}, under similar crystallization conditions as AlsS_HisC. These crystals had a different crystal morphology compared to AlsS_HisC and diffracted to 2.34 Å

resolution. Indexing of the diffraction data turned out to be very difficult, with various possibilities in monoclinic, orthorhombic and tetragonal space groups.

Table 4.2: Data collection and refinement statistics.

Data collection	**AlsS_NoHis-TPP small unit cell**	**AlsS_HisC-TPP**
Space group	$P2_122_1$	$P4_12_12$
Wavelength [Å]	0.9184	0.9184
Unit cell a; b; c [Å]	111.3; 170.0; 340.0	141.7; 141.7; 239.0
α; β; γ [°]	90.0; 90.0; 90.0	90.0; 90.0; 90.0
Resolution [Å] [a]	30.00 - 2.34 (2.48 - 2.34)	30.00 - 3.20 (3.39 - 3.20)
Unique reflections	268024 (41131)	258055 (40326)
Completeness [a]	98.4 (94.3)	99.5 (98.9)
$<I/\sigma(I)>$ [a]	11.5 (3.0)	11.3 (2.5)
R_{meas} [a, b]	0.108 (0.490)	0.183 (0.785)
CC1/2 [a]	99.6 (80.6)	99.4 (79.4)
Redundancy [a]	4.5 (4.1)	7.2 (7.1)
Refinement		
Non-hydrogen atoms	36644	16994
R_{work} [a, c]	0.172 (0.233)	0.187 (0.252)
R_{free} [a, d]	0.217 (0.297)	0.253 (0.329)
No. of protein chains	8	4
Protein residues	4416 / 24.2	2208 / 64.5
TPP molecules	8 / 24.4	4 / 74.1
Mg^{2+} cations	8 / 28.3	4 / 59.6
Ligand molecules	33 / 37.7	1 / 84.4
Water molecules	1955 / 24.9	23 / 26.1
RMSD [e] bond length [Å]	1.177	0.890
bond angles [°]	0.009	0.005
Ramachandran outliers [%]	0.1	0.1
Ramachandran favoured [%]	98.0	97.8

[a] values in parentheses refer to the highest resolution shell

[b] $R_{sym} = \Sigma_h [n/(n-1)]^{1/2} \Sigma_i | I_h - I_{h,i}| / \Sigma_h \Sigma_i I_{h,i}$.where I_h is the mean intensity of symmetry-equivalent reflections and n is the redundancy

[c] $R_{work} = \Sigma_h |F_o - F_c| / \Sigma F_o$ (working set, no σ cut-off applied)

[d] R_{free} is the same as R_{cryst}, but calculated on 5% of the data excluded from refinement

[e] Root-mean-square deviation (RMSD) from target geometries

In addition, careful analysis of the intensity distribution showed a clear modulation in intensities, i.e. h=2n+1 are much weaker then k=2n+1, indicating the presence of two different lattices within one crystal. Indeed, we could index our diffraction data in two different space groups, which we designate the small and the big unit cell. The small unit cell can be indexed in $P2_122_1$ with unit cell parameters a=111.3; b=170.0; c=340.0, whereas the large unit cell can be indexed in $P2_12_12_1$ with unit cell parameters and a=111.2; b=340.0; c=341.0 (Table 4.2).

Using the coordinates of AlsS_HisC as search model for molecular replacement, derived from our previously solved medium resolution data set, we could solve the structure of the small and large unit cell. In the small unit cell we could locate eight monomers in the asymmetric unit, arranged as one full and two partial tetramers that are complemented by symmetry-related AlsS_HisNo molecules. The structure of AlsS_HisNo in the small unit cell was refined to R/R_{free} of 0.172/0.217 with excellent geometry (Table 4.2). In the large unit cell we could locate 16 monomers, arranged as two complete tetramers and four dimers forming tetramers with symmetry related molecules.

4.3.1.2 Overall Structure of AlsS

The apparent biological unit of AlsS is a homo-tetramer formed by dimers of dimers (Figure 4.2A) as reported previously for the *K. pneumoniae* Als [14] and other TPP-dependent enzymes such as the pyruvate oxidase [35]. This feature contrasts the homo-dimer structure of *S. cerevisiae* [36] and *A. thaliana* AHAS [16]. For the structural description we will solely focus on the highest resolution structure of the complete tetramer in the asymmetric unit of the small unit cell. One monomer of the AlsS is composed of 571 amino acids. The first 13 N-terminal residues and at C-terminus the last five residues could not be modelled due to the lack of interpretable electron density and are likely to be flexible. Each monomer is composed of three domains (Figure 4.2B). The α-domain ranges from the N-terminus to N181 connected via a random coil to the central ß-domain spanning from P195 to A346. The C-terminal γ-domain starts at residue H376 and is connected to the central ß-domain by a mainly α-helix proceeded by a random coil linker. Overall, the monomers of one tetramer are practically indistinguishable with an RMSD of less than 0.3 Å. The *B. subtilis* and *K. pneumoniae* Als share a sequence identity of 51% and superimposing 512 pairs of Cα-atoms of both structures yields in a RMSD of 1.8 Å. Yet there are major structural differences in *B. subtilis* and *K. pneumoniae* Als. In the α-domain of *B. subtilis* Als the loop from K120 to S125 adopts a strikingly different conformation, enabling Q124 to point into the active site. In contrast, this region is occupied by water molecules in *K. pneumoniae* Als. Compared to the *K. pneumoniae* Als, we could model the linker between the α- and ß-domain completely as random coil.

Further differences are in the linker region connecting the α- and ß-domain from Q365 to D373 and in a loop in the γ-domain (R409 to T416) that adopts a different conformation.

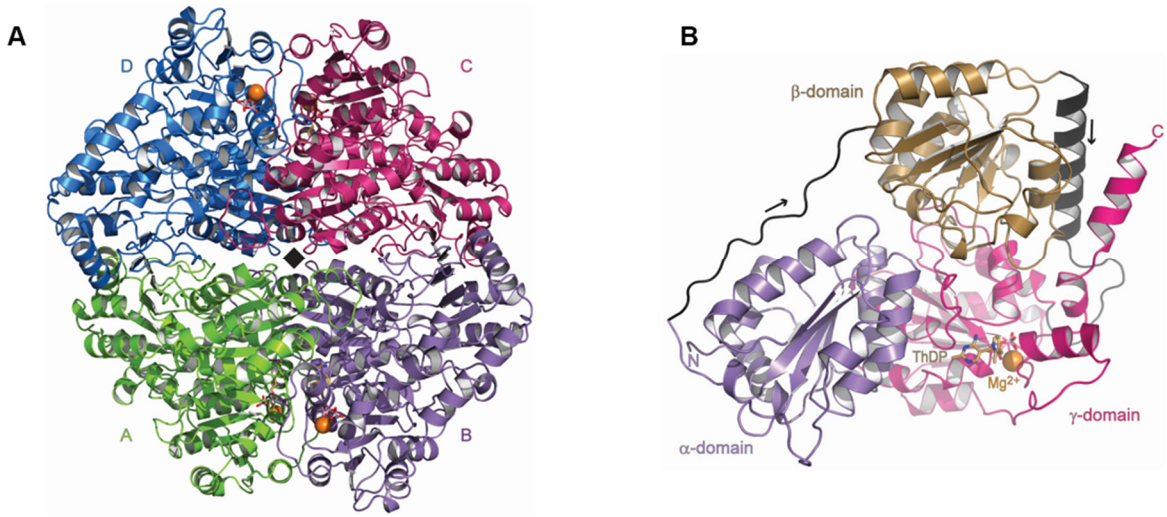

Figure 4.2: X-ray crystal structure of AlsS;
A) Overall structure of tetrameric AlsS_HisNo shown is ribbon presentation. The fourfold axis is indicated by a black square. The monomers are coloured, green (A), purple (B), red (C) and blue (D). B) Shown are the three domains of one AlsS monomer; α-domain in purple, ß-domain in brown and γ-domain in red. The C-terminus is marked in the γ-domain with a C. Mg^{2+} is shown as orange spheres and TPP molecule in stick representation.

The amino acid sequence of the very C-terminal end of *B. subtilis* and *K. pneumoniae* Als is less conserved and seven residues longer in *B. subtilis*. The nine C-terminal residues (A556 to the C-terminus) of AlsS are folded into an α-helix that is not present in *K. pneumoniae*, packs back onto the ß-domain and is solvent exposed on the opposing site. This α-helix is an extension of the structurally conserved α-helix that shields the cofactors TPP and Mg^{2+} from solvent.

4.3.2 Biochemical Characterisation of AlsS

For process scale setups, it is necessary to work at higher temperatures (60 °C or above), as at these temperatures problems with contaminations and/or side reactions descending from crude extract's host enzymes are negligible. Industry is interested in high product yields and at high titres, therefore long enzymatic half-lives as well as high activities at these temperatures are required. As a result, AlsS was characterised concerning its temperature optimum and its half-life at 50 °C and 60 °C as well as its solvent stability.

To determine the catalytic activity of AlsS towards pyruvate a coupled assay with lactate dehydrogenase (LDH) was used (Chapter 3). In a first reaction AlsS has limited time to produce acetolactate and the remaining pyruvate is converted to lactate by LDH and NADH depletion. The catalytic activity of LDH can be measured photometrically at 340 nm and the amount of consumed pyruvate by AlsS can be calculated.

4.3.2.1 Determination of pH Optima

AlsS was most active at a pH range of 5.5 to 6.5 with a clear optimum at pH 6.0. At this pH optimum, it exhibits maximum activity, which is 6x higher than at pH 7.0. At pH 4.0 no activity was observed. At pH 5.0 to pH 6.0 a distinct increase in activity could be observed. From pH 7.0 to pH 8.0 there is an activity plateau and from pH 9.0 to pH 11.0 the activity decreases. At pH 11 no activity could be detected at all (Figure 4.3A). The AlsS pH profile is consistent with previous studies [18, 37]. The pH optimum at 6.0 is prerequisite for subsequent decarboxylation of acetolactate by action of an acetolactate decarboxylase or by a low pH in 2,3 butanediol pathway [10].

4.3.2.2 Determination of Temperature Optima and Half-Life at 50 °C and 60 °C

The AlsS temperature optimum was at 50 °C and pH 7.0. This activity was with 24 (±4) U/mg almost 3x higher compared to AlsS activity at 20 °C, 30 °C and 65°C (Figure 4.3).
Furthermore, the half-life of AlsS at 50 °C and 60 °C was determined. Considering that AlsS originates from a mesophilic organism a half-life at 50 °C of 81 h and at 60 °C of 16 h is surprising. To our knowledge, this is the first time that thermostability of AlsS is reported.

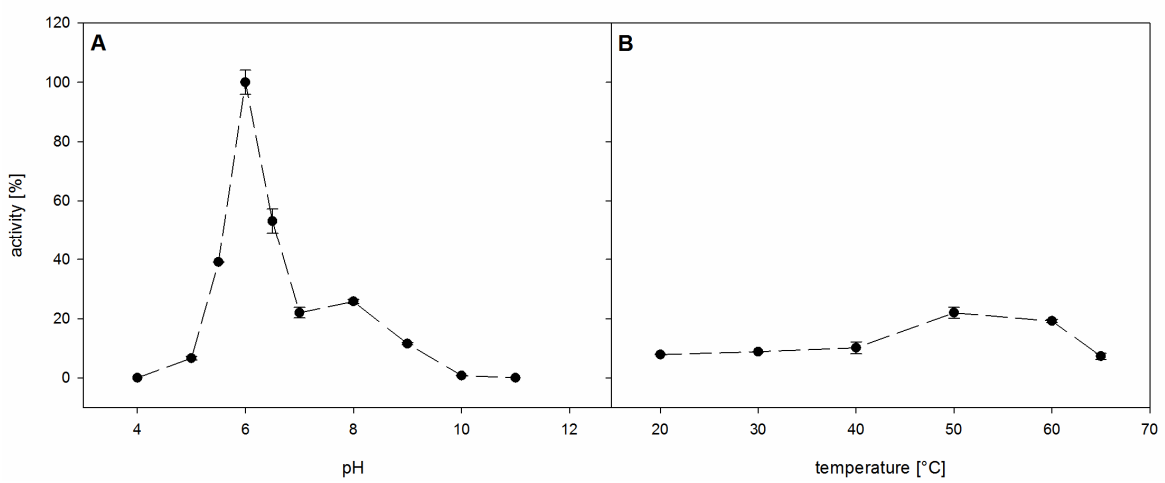

Figure 4.3: Determination of pH stability and temperature optimum of AlsS.
A) 50 mM sodium acetate buffer was used for pH 4 to 5.5, 50 mM sodium phosphate buffer for pH 6 to 6.5, 50 mM Tris buffer for pH 7 – 9 and 50 mM Caps buffer for pH 10 and 11. B) Enzyme assays were performed at 20 °C to 65 °C. Each activity is the mean of three replicates.

4.3.2.3 Determination of Solvent Tolerance

Production of solvents like isobutanol implicitly require end product tolerance of the applied enzyme systems. In cell based systems titres of 1 – 2 % (v/v) isobutanol induce toxic effects in the production host [13]. This disadvantage does not correlate with relevant enzyme systems. Therefore, AlsS was tested against 6 % (v/v) isobutanol, 6 % (v/v) n-butanol and 20 % (v/v)

ethanol (Figure 4.4). The enzyme retained 50 % activity in the presence of 3 % (v/v) isobutanol, 3 % (v/v) n-butanol and ~13 % (v/v) ethanol.

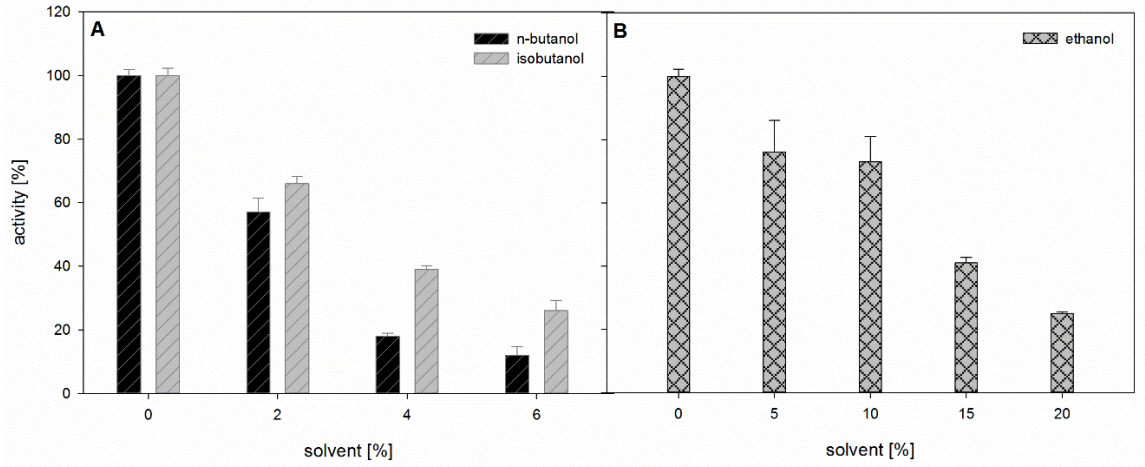

Figure 4.4: Solvent tolerance of AlsS.
A) for 0 - 6 % (v/v) n-butanol and isobutanol; B) for 0 – 20 % (v/v) ethanol.

In consequence enzymes such as AlsS are more resistant to solvent inactivation compared to cell based production systems [1, 3].

4.3.2.4 Activity Towards the Alternative Substrate KIV

Both AlsS catalysed reactions are part of the isobutanol pathway (Figure 4.1) and thus the AlsS activity towards KIV is of interest. To determine KIV specific activity, a coupled assay requiring the enzymes AlsS and alcohol dehydrogenase (Adh, horse liver) was applied. KIV is converted to isobutyraldehyde by AlsS and subsequently isobutyraldehyde is converted to isobutanol via Adh action. By supplying Adh in surplus, all produced isobutyraldehyde is directly converted to isobutanol. This reaction can be measured at 340 nm in a photometer due to the degradation of the NADH cofactor. Due to the thermostability of horse liver Adh, all KIV assays were carried out at 40 °C. Under these conditions an AlsS activity of 53 mU/mg was observed.

For industrial applications the AlsS half-life needs to be extended from 81 h at 50 °C to about two weeks. Additionally, activity improvements are necessary to provide efficient pyruvate and KIV conversion at 60 °C. To generate improved AlsS variants knowledge about active site structure function relationships were imperative.

4.3.3 Characterisation of the Structure Guided AlsS Variants

There are only a few active site centred amino acids in close proximity to the TPP cofactor or to the reaction intermediate with bound TPP (LTPP). Structure-guided variants of AlsS were

designed, targeting eight amino acid residues by single or double mutations in the TPP binding site (Figure 4.5).

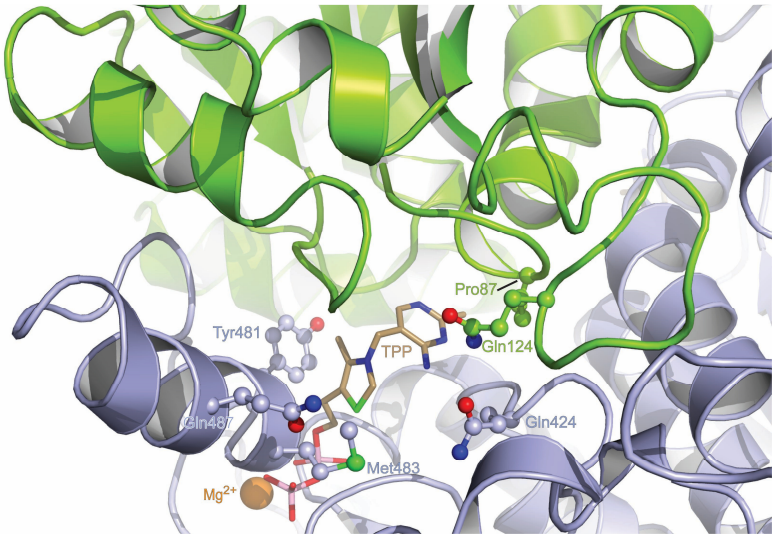

Figure 4.5: Detailed view of the catalytic site of AlsS.
Shown are amino acids Pro87, Gln124, Gln424, Tyr481, Met483, Gln487 together with TPP and $MgCl_2$.

Q124 is in hydrogen bonding distance to the LTPP moiety. Q424 points with its side chain towards the LTPP moiety and might guide the second substrate molecule in the correct position for condensation. The latter role could be supported by M483 and Q487 both residing on an α-helix and are separated by just one α-helical turn. P87 is in close proximity to Q124. On the opposite site of the C2′atom of TPP, Y481 is located and could be important for the accurate positioning of the TPP molecule.

Additionally, we have selected the amino acid residue K40, whose homologue in *K. pneumoniae* Als is thought to be involved in catalysing [14].

All AlsS variants were recombinantly expressed and purified as described for AlsS. As AlsS is a key enzyme for *in vitro* isobutanol production, enzyme variants with enhanced thermostability and activity towards the native substrate pyruvate as well as the alternative substrate KIV were selected.

Initially, factors such as thermostability and activity towards pyruvate at 50 °C and 60 °C were examined. Furthermore, we screened for AlsS mutants with enhanced activity towards KIV at 40 °C (Table 4.3). All experiments were conducted in Hepes buffer pH 7, which was most compatible with other enzyme systems involved in our cell-free isobutanol cascade [13].

Thermostability in the Presence of the Native Substrate Pyruvate

AlsS shows optimal activity at 50 °C. To identify mutants with improved catalytic properties at elevated temperatures, we have examined the reaction with pyruvate at 50 °C and 60 °C. The mutants $AlsS^{K40I}$, $AlsS^{K40Y}$, $AlsS^{Q424S}$ and $AlsS^{Q424S\_Q487S}$ showed higher half-lives at 50 °C.

AlsS^{K40Y} was found to be the variant with the highest increase in half-life at 50 °C compared to the wild-type. Furthermore, AlsS^{Q424S} was the best performing mutant with a half-life of 104 h and an activity of 27 U/mg at 50 °C.
In contrast to the wild-type enzyme, the mutants AlsS^{K40H} AlsS^{T84V}, AlsS^{Q124S}, AlsS^{M483N} and AlsS^{Y481A} showed a decrease in the reaction rates and half-lives. Under the reaction conditions at 50 °C and 60 °C as well as lower temperatures no catalytic activity was observed for AlsS^{M483N}, which indicated that this mutant was not catalytically viable.

In vitro isobutanol formation proceeds over an extended time frame. Therefore, it is beneficial to evolve enzyme variants that have an improved half-life at elevated temperatures. However, variants do not necessarily provide improved activity values. Instead a slower but persistent reaction rate is preferred.

Table 4.3: Activities and half-lives of all AlsS variants at 50 °C and 60° C, measured with pyruvate as substrate. In addition, specific activities of all AlsS variants towards KIV are mentioned.

Protein	A (U/mg) at 50 °C	$T_{1/2}$ (h) at 50 °C	A (U/mg) at 60 °C	$T_{1/2}$ (h) at 60 °C	A_{KIV} (U/mg) at 40°C
AlsS	24 (±4.00)	81	31 (±3.40)	16	0.053 (±0.0020)
AlsS^{K40H}	4 (±0.20)	44	3 (±0.30)	3	0.045 (±0.0080)
AlsS^{K40I}	3 (±0.10)	89	1 (±0.22)	0.7	0.059 (±0.0020)
AlsS^{K40Y}	7 (±0.60)	110	7 (±0.4)	7	0.031 (±0.0020)
AlsS^{T84V}	1 (±0.08)	2.5	1 (±0.17)	/	0.021 (±0.0020)
AlsS^{P87A}	18 (±2.54)	33	3 (±0.22)	0.6	0.020 (±0.0030)
AlsS^{Q124S}	6 (±0.50)	42	5 (±0.10)	1	0.014 (±0.0003)
AlsS^{Q424S}	27 (±5.00)	104	19 (±1.50)	8	0.028 (±0.0020)
AlsS^{Q424S_Q487S}	2 (±2.00)	94	/	/	0.016 (±0.0010)
AlsS^{Y481A}	1 (±0.06)	19	/	/	0.004 (±0.0010)
AlsS^{M483N}	/	/	/	/	0.009 (±0.0020)
AlsS^{Q487S}	35 (±2.00)	22	10 (±0.20)	1	0.046 (±0.0030)

Activity Towards the Alternative Substrate KIV

Both reactions catalysed by AlsS are part of the isobutanol pathway (Figure 4.1). Therefore, achieving high activities towards the substrates, i.e. pyruvate and KIV, was a development target. These factors are required for a consolidated biocatalytic cascade towards isobutanol. Thus, information about the residues for the decarboxylation of KIV is required.

Atsumi *et al.* (2009) reported 5.5 U/mg for the Kdc type activity of a His-tagged AlsS [2]. We could not confirm these results even under equivalent experimental conditions (37 °C to 40 °C). Instead, we observed a 1,000 times lower activity, i.e. in the range from 9 to 53 mU/mg.

In our study, the lowest K_M of $AlsS^{Q487S}$ (154 (±21) mM) compared to the AlsS (300 (±35) mM) did not result in a higher activity (Table 4.3) [2].

Nevertheless, the variant $AlsS^{K401}$ shows a slightly improved activity of 59 mU/mg towards KIV.

4.3.4 AlsS Structure Function Relationships

$AlsS^{T84V}$ Variant

Interestingly, in the AlsS_HisNo structure in two monomers we observed elongated electron density pointing to the C2′ atom of the TPP thiazole ring**.** We interprete the electron density as PEG molecule originating from the crystallization solution. The terminal hydroxyl group of the PEG molecule is in a distance of 3.1 Å to the TPP thiazole ring. There are no further direct contacts to the protein backbone, but indirect contact via water molecules exists (Figure 4.6).

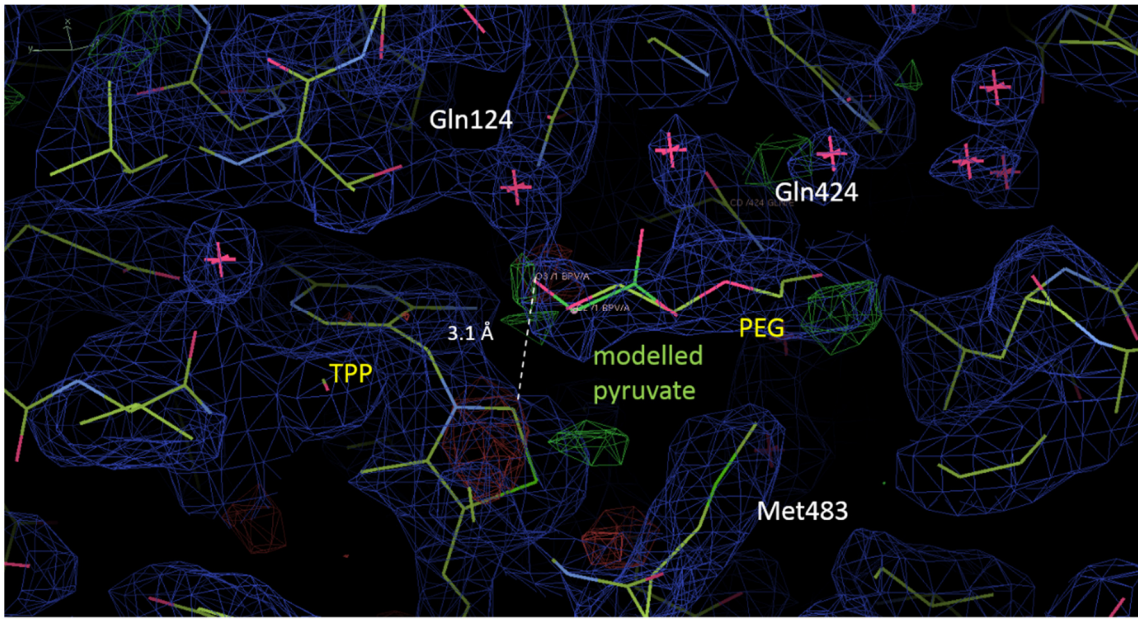

Figure 4.6: Electron density of amino acids located in the AlsS active site.
Shown are amino acids Gln124, Gln424 and Met483 with their electron density together with TPP and a PEG molecule. Additionally, the distance between the PEG molecule and the TPP thiazole ring is shown.

It is assumed, that removal of a hydrogen bridge results in reorientation of the TPP and the catalytically active residues. Further we suggested, that $AlsS^{T84}$ is in contact with the C2′ atom of the TPP thiazole ring over a hydrogen bond. To follow up on this hypothesis, we designed the $AlsS^{T84V}$ mutant. Evaluation of the catalytic properties indicated that this mutant showed

only marginal activity of 1 (±0.08) U/mg at 50 °C with a half-life of 2.5 h (Table 4.3). At 60 °C no activity was observed. This catalytic data are consistent with our hypothesis.

AlsS^{Q424S} Variant

Q424 might guide the second pyruvate in the active centre, which may affect both activity and thermostability of the enzyme. Subsequently, we constructed the mutants AlsS^{Q424S} and AlsS^{Q424S_Q487S}. Interestingly, these AlsS variants showed a red colour, which persisted from protein expression over cell disruption and even purification. For initial characterisation of this intriguing effect we recorded the absorption spectrum between 350 – 600 nm and compared it to the wild-type enzyme's spectrum. Surprisingly, we detected an absorbance profile between 440 – 550 nm with a maximum at 500 nm consistent with the red colour of AlsS^{Q424S} variants. No equivalent absorbance was observed in wild-type AlsS (Figure 4.7).

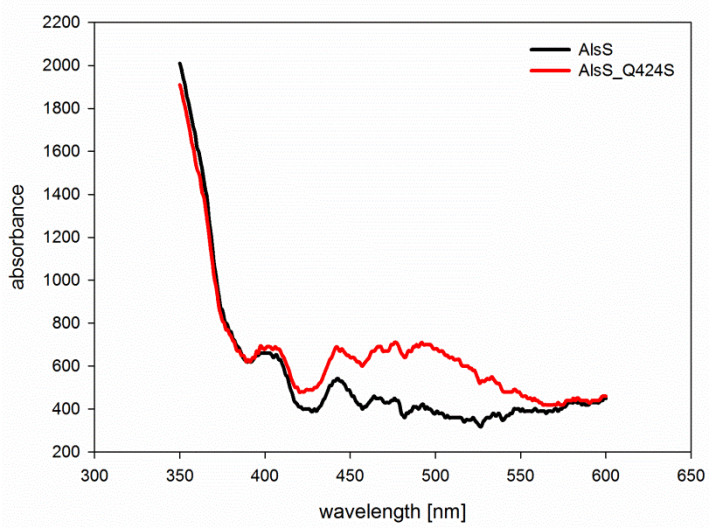

Figure 4.7: Absorbance spectra of the proteins wild-type AlsS and AlsS^{Q424S}.

During AlsS^{Q424S} gelfiltration (HighLoad Superdex S200), we could detect the elution of two distinct proteins by monitoring the elution profile at 500 nm (Figure 4.8). The two proteins were collected in two fractions, fraction I (62 – 66 ml) and fraction II (70 - 75 ml).

To verify if both fractions contain functional AlsS^{Q424S}, an activity test with pyruvate was applied. Both fractions could reduce pyruvate with an identical reaction rate suggesting that AlsS^{Q424S} may be present in two conformational states. These distinct conformational states may induce the observed red colour of the protein.

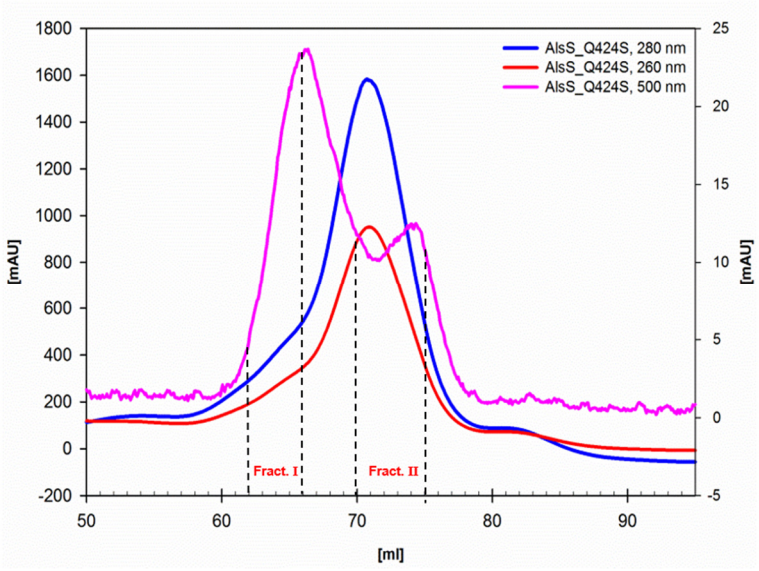

Figure 4.8: Gelfiltration of AlsS^{Q424S}.
Elution profiles were taken at 260 nm (red), 280 nm (blue) and 500 nm (purple).

While the calculated pI of AlsS^{Q424S} variant is identical with the pI of the wild-type enzyme (pI 5.45), we experimentally observed different pI values for each conformational state (Figure 4.9). Wild-type AlsS has one predominant band at a pI of 6.2. In contrast, AlsS^{Q424S} fraction I contributes two clearly distinguishable proteins focused at a pI of 5.9 and 5.2. Fraction II consists of various small proteins focused around pI 5.3. This is consistent with our hypothesis that AlsS^{Q424S} adopts two conformational states.

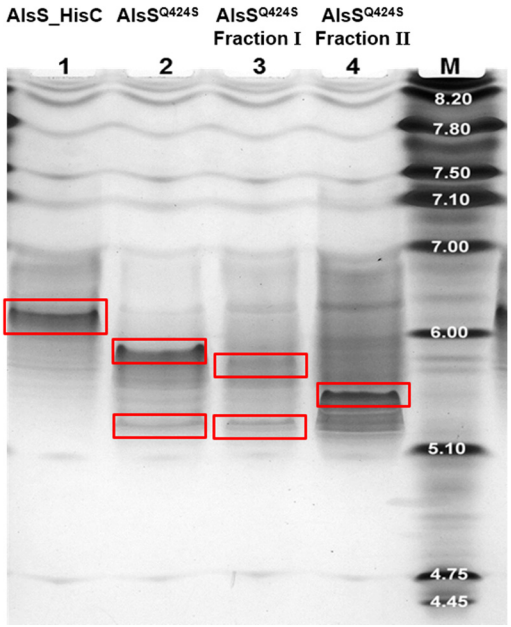

Figure 4.9: Isoelectric focusing (IEF) of AlsS and AlsS^{Q424S}.
An IEF gel with a pH range from 3 to 7 from Novex® was used. Loading scheme is: AlsS (1), AlsS^{Q424S} purified by hand column (Ni^{2+}-NTA) (2), fraction I of AlsS^{Q424S} (3) and fraction II of AlsS^{Q424S} (4) purified by affinity (Ni^{2+}-NTA)- and size exclusion chromatography. Standard was broad range pI 4.45 – 9.6 marker from Biorad.

To test whether the red colour is not a result from incorporated substances, like metals, AlsS^{Q424S} was dialysed against two litres of water and two litres 50 mM EDTA at 4 °C overnight. This procedure did not affect the red colour of the protein (Figure 4.10) indicating that it could be due to the alteration in protein conformation or folding.

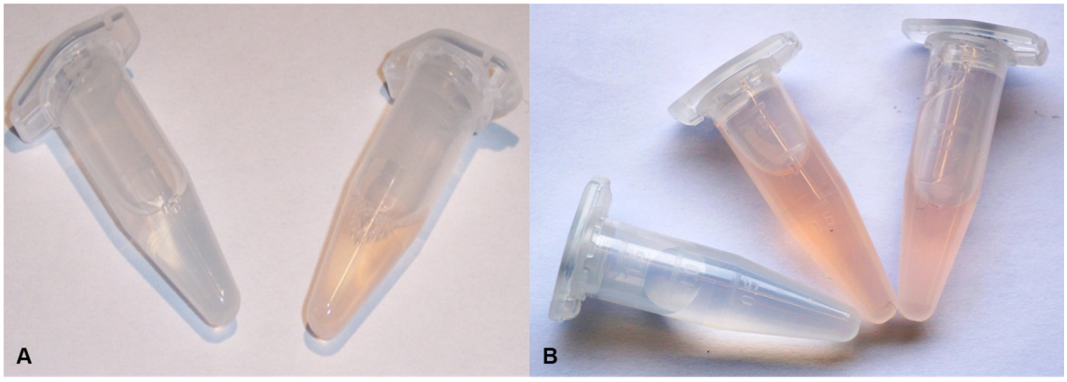

Figure 4.10: Pictures of AlsS and AlsS^{Q424S}.
A) AlsS (left) and AlsS^{Q424S} (right) after purification. B) AlsS^{Q424S} after dialyse overnight at 4 °C against two litres of water (middle) and two litres of 50 mM EDTA (right), compared to water (left).

4.4 CONCLUSIONS

Due to its hydrophobic properties and higher caloric value isobutanol is an excellent next generation building block for renewable fuel and chemical processes. Acetolactate synthase from *B. subtilis* generates two intermediates involved in isobutanol synthesis, i.e. acetolactate and isobutyraldehyde. Therefore, AlsS has application in industrial isobutanol synthesis approaches and allows to minimize the number of required enzyme systems.

Initially, AlsS activity for both substrates was determined, revealing that activity towards KIV is only a side reaction with low catalytic activity of 53 mU/mg. Subsequently, pH-, temperature-, and solvent- tolerance of AlsS were determined. AlsS has a pH optima at 6 and exhibits maximum activity at 50 °C. In addition, AlsS tolerates higher solvent concentrations than microbial hosts. In the presence of either 3 % (v/v) isobutanol, 3 % (v/v) n-butanol or ~13 % (v/v) ethanol AlsS still exhibits 50 % activity. Therefore, AlsS is suitable for isobutanol production, but activity towards KIV had to be improved.

For the first time, we solved the crystal structure of AlsS in presence of the cofactors TPP and $MgCl_2$ at a resolution of 2.34 Å. AlsS is a homo-tetramer formed by dimers of dimers analogous to the reported structure of *K. pneumoniae* Als. However, there are major structural differences in *B. subtilis* and *K. pneumoniae* Als.

The structural data were the basis for generation of structure guided AlsS variants. In our study, eight amino acid residues, located in the active site of AlsS, were exchanged by single or double mutations targeting the TPP binding site. The resulting variants, i.e. AlsS$^{K40H/I/Y}$, AlsS^{T84V},

AlsS^{P87A}, AlsS^{Q124S}, AlsS^{Q424S}, AlsS^{Q424S_Q487S}, AlsS^{Y481A}, AlsS^{M483N} and AlsS^{Q487S}, were screened for activity towards pyruvate and KIV as well as for their thermostability at 50 °C and 60 °C. We were able to identify amino acid residues involved in catalysis and a variant with a slightly improved activity towards KIV.

Interestingly, two of the AlsS mutants (AlsS^{Q424S} and AlsS^{Q424S_Q487S}) displayed a red colour, while the AlsS wild-type is colourless. Dialysis of AlsS^{Q424S} against buffer did not result in a colour change, indicating that the colour feature is not a result of reversible metal binding to AlsS. To further elucidate the colour phenomena of AlsS^{Q424S} we conducted IEF in combination with activity assays. The data indicated that AlsS^{Q424S} can switch between two conformational states.

4.5 REFERENCES

1. **Atsumi S, Hanai T, Liao JC.** 2008. Non-fermentative pathways for synthesis of branched-chain higher alcohols as biofuels. Nature **451:**86-89.
2. **Atsumi S, Li Z, Liao JC.** 2009. Acetolactate synthase from Bacillus subtilis serves as a 2-ketoisovalerate decarboxylase for isobutanol biosynthesis in Escherichia coli. Appl Environ Microbiol **75:**6306-6311.
3. **Atsumi S, Wu TY, Eckl EM, Hawkins SD, Buelter T, Liao JC.** 2010. Engineering the isobutanol biosynthetic pathway in Escherichia coli by comparison of three aldehyde reductase/alcohol dehydrogenase genes. Appl Microbiol Biotechnol **85:**651-657.
4. **Cann AF, Liao JC.** 2008. Production of 2-methyl-1-butanol in engineered Escherichia coli. Applied microbiology and biotechnology **81:**89-98.
5. **Shen CR, Liao JC.** 2008. Metabolic engineering of Escherichia coli for 1-butanol and 1-propanol production via the keto-acid pathways. Metab Eng **10:**312-320.
6. **Connor MR, Liao JC.** 2009. Microbial production of advanced transportation fuels in non-natural hosts. Current opinion in biotechnology **20:**307-315.
7. **Savrasova EA, Kivero AD, Shakulov RS, Stoynova NV.** 2011. Use of the valine biosynthetic pathway to convert glucose into isobutanol. Journal of industrial microbiology & biotechnology **38:**1287-1294.
8. **Baez A, Cho KM, Liao JC.** 2011. High-flux isobutanol production using engineered Escherichia coli: a bioreactor study with in situ product removal. Appl Microbiol Biotechnol **90:**1681-1690.
9. **GESTIS.** 2011. Substance Database.
10. **Renna MC, Najimudin N, Winik LR, Zahler SA.** 1993. Regulation of the Bacillus subtilis alsS, alsD, and alsR genes involved in post-exponential-phase production of acetoin. Journal of bacteriology **175:**3863-3875.
11. **Maestri O, Joset F.** 2000. Regulation by external pH and stationary growth phase of the acetolactate synthase from Synechocystis PCC6803. Molecular microbiology **37:**828-838.
12. **Li S, Wen J, Jia X.** 2011. Engineering Bacillus subtilis for isobutanol production by heterologous Ehrlich pathway construction and the biosynthetic 2-ketoisovalerate precursor pathway overexpression. Applied microbiology and biotechnology **91:**577-589.
13. **Guterl JK, Garbe D, Carsten J, Steffler F, Sommer B, Reisse S, Philipp A, Haack M, Rühmann B, Koltermann A, Kettling U, Brück T, Sieber V.** 2012. Cell-free metabolic engineering: production of chemicals by minimized reaction cascades. ChemSusChem **5:**2165-2172.
14. **Pang SS, Duggleby RG, Schowen RL, Guddat LW.** 2004. The crystal structures of Klebsiella pneumoniae acetolactate synthase with enzyme-bound cofactor and with an unusual intermediate. The Journal of biological chemistry **279:**2242-2253.
15. **Pang SS, Duggleby RG, Guddat LW.** 2002. Crystal structure of yeast acetohydroxyacid synthase: a target for herbicidal inhibitors. Journal of molecular biology **317:**249-262.
16. **Wang JG, Lee PKM, Dong YH, Pang SS, Duggleby RG, Li ZM, Guddat LW.** 2009. Crystal structures of two novel sulfonylurea herbicides in complex with Arabidopsis thaliana acetohydroxyacid synthase. FEBS Journal **276:**1282-1290.
17. **McCourt JA, Duggleby RG.** 2006. Acetohydroxyacid synthase and its role in the biosynthetic pathway for branched-chain amino acids. Amino Acids **31:**173-210.
18. **Gedi V, Yoon MY.** 2012. Bacterial acetohydroxyacid synthase and its inhibitors--a summary of their structure, biological activity and current status. FEBS J **279:**946-963.
19. **Sailen B.** 2002. Megaprimer PCR, p. 189-196, methods in Molecular Biology.
20. **Kabsch W.** 2010. XDS. Acta Crystallogr D Biol Crystallogr **66:**125-132.

21. **Krug M, Weiss MS, Heinemann U, Mueller U.** 2012. XDSAPP: a graphical user interface for the convenient processing of diffraction data using XDS. Journal of Applied Crystallography **45:**0-0.

22. **McCoy AJ, Grosse-Kunstleve RW, Adams PD, Winn MD, Storoni LC, Read RJ.** 2007. Phaser crystallographic software. J Appl Crystallogr **40:**658-674.

23. **Cowtan K.** 2007. Fitting molecular fragments into electron density. Acta Crystallographica Section D: Biological Crystallography **64:**83-89.

24. **Afonine PV, Grosse-Kunstleve RW, Echols N, Headd JJ, Moriarty NW, Mustyakimov M, Terwilliger TC, Urzhumtsev A, Zwart PH, Adams PD.** 2012. Towards automated crystallographic structure refinement with phenix.refine. Acta crystallographica. Section D, Biological crystallography **68:**352-367.

25. **Emsley P, Lohkamp B, Scott WG, Cowtan K.** 2010. Features and development of Coot. Acta Crystallogr D Biol Crystallogr **66:**486-501.

26. **Laskowski RA, McArthur MW, Moss DS, Thornton JM.** 1993. PROCHECK: a program to check the stereochemical quality of protein structures. J Appl Crystallog **26:**283-291.

27. **Chen VB, Arendall WB, III, Headd JJ, Keedy DA, Immormino RM, Kapral GJ, Murray LW, Richardson JS, Richardson DC.** 2010. MolProbity: all-atom structure validation for macromolecular crystallography. Acta Crystallogr D Biol Crystallogr **66:**12-21.

28. **DeLano W.** The PyMOL Molecular Graphics System on World Wide Web. 2002. There is no corresponding record for this reference.

29. **Chovancova E, Pavelka A, Benes P, Strnad O, Brezovsky J, Kozlikova B, Gora A, Sustr V, Klvana M, Medek P, Biedermannova L, Sochor J, Damborsky J.** 2012. CAVER 3.0: A Tool for the Analysis of Transport Pathways in Dynamic Protein Structures. PLoS computational biology **8:**e1002708.

30. **Schrimpf G.** 2002. Gentechnische Methoden: Eine Sammlung von Arbeitsanleitungen für das molekularbiologische Labor vol. 3. Spektrum Akademischer Verlag.

31. **Pace CN, Vajdos F, Fee L, Grimsley G, Gray T.** 1995. How to measure and predict the molar absorption coefficient of a protein. Protein science : a publication of the Protein Society **4:**2411-2423.

32. **Gasteiger E, Hoogland C, Gattiker A, Duvaud Se, Wilkins M, Appel R, Bairoch A.** 2005. Protein Identification and Analysis Tools on the ExPASy Server, p. 571-607. *In* Walker J (ed.), The Proteomics Protocols Handbook. Humana Press.

33. **Stoll VS, Blanchard JS.** 2009. Buffers: Principles and Practice1. Methods in enzymology **463:**43-56.

34. **Wolterink-van Loo S, van Eerde A, Siemerink M, Akerboom J, Dijkstra B, van der Oost J.** 2007. Biochemical and structural exploration of the catalytic capacity of Sulfolobus KDG aldolases. Biochem. J **403:**421-430.

35. **Muller YA, Schulz GE.** 1993. Structure of the thiamine- and flavin-dependent enzyme pyruvate oxidase. Science **259:**965-967.

36. **Pang SS, Duggleby RG, Guddat LW.** 2002. Crystal structure of yeast acetohydroxyacid synthase: a target for herbicidal inhibitors. J Mol Biol **317:**249-262.

37. **Holtzclaw WD, Chapman LF.** 1975. Degradative acetolactate synthase of Bacillus subtilis: purification and properties. J Bacteriol **121:**917-922.

Chapter 5

Characterisation of a highly thermostable ß-hydroxybutyryl CoA dehydrogenase from *Clostridium acetobutylicum* ATCC 824

Higher energy content and hydrophobicity makes bio-based n-butanol a preferred building block for chemical and biofuel manufacturing. Butanol is obtained by Clostridium sp. based ABE fermentation process. While the ABE process is well understood, the enzyme systems involved have not been elucidated in detail. The key enzyme ß-hydroxybutyryl CoA dehydrogenase from Clostridium acetobutylicum ATCC 824 (Hbd) was purified and characterised. Surprisingly, Hbd shows extremely high temperature (T > 60 °C), pH (4 - 11) and solvent (n-butanol, isobutanol, ethanol) stability. Hbd catalyses acetoacetyl-CoA hydration to ß-hydroxybutyryl-CoA up to pH 9.5, where the reaction is reversed. Substrate (acacCoA, ß-hbCoA) and cofactor (NADH, NAD^+, NADPH and $NADP^+$) specificities were determined. We identified NAD^+ as an uncompetitive inhibitor. Identification of process relevant enzymes such as Hbd is key to optimise butanol production via cellular or cell-free enzymatic systems.

5.1 INTRODUCTION

Butanol is a next generation renewable building block for the chemical and fuel sector due to its high energy content and hydrophobicity. Conventionally, bio-based n-butanol is produced via the *Clostridium acetobutylicum* based acetone (A), butanol (B) and ethanol (E) fermentation process [1, 2]. However, the conventional ABE process suffers from marginal economic viability, low product titres due to end-product toxicities above 1 – 2 % (v/v) [3] and the requirement to separate the different solvents via fractionated distillation.

To increase mass efficiency of the process recombinant n-butanol-production has been realised in *E. coli* [4], *B. subtilis* [5] and *S. cerevisiae* [3] by cloning genetic elements for n-butanol biosynthesis into these microorganisms. However, to date this approach could hardly improve product yield. To obtain a mass and energy efficient n-butanol production process, it has been suggested to produce n-butanol using cell-free enzyme cascades [6]. This approach would potentially allow for much higher product yields and simplify downstream processing as we have recently shown for ethanol and isobutanol [7]. Key to a successful implementation of cell-free n-butanol production is the selection of process relevant enzyme complements with enhanced process stability and favourable catalytic properties.

However, while the physiology and genetics for ABE-biosynthesis is well understood, the concerted properties of the 14 enzyme systems involved in converting glucose to ABE have not been studies in detail.

A central enzyme in n-butanol biosynthesis is ß-hydroxybutyryl CoA dehydrogenase (Hbd; E.C. 1.1.1.157). Hbd catalyses the reversible reduction of acetoacetyl-CoA (acacCoA) to ß-hydroxybutyryl-CoA (ß-hbCoA) involving the cofactor NADH (Figure 5.1) [4, 8, 9].

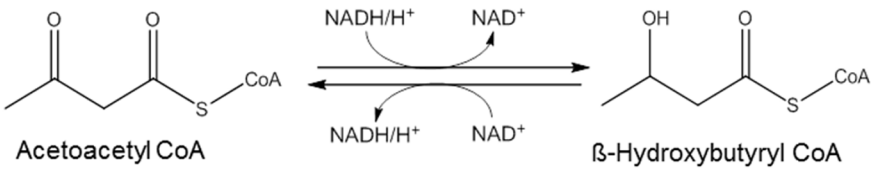

Figure 5.1: Reaction catalysed by Hbd from *C. acetobutylicum* ATCC 824.

In our quest to select process relevant Hbd variants for n-butanol production, we applied genome mining tools to *C. acetobutylicum* ATCC 824 [10], which was one of the first strains used on an optimized ABE process.

At present, only uncertain catalytic data for *C. acetobutylicum* ATCC 824 Hbd (*Ca*Hbd) (catalytic activity = 0.03 U/mg to 11.6 U/mg), derived from crude cell extracts, are available [4, 8, 11]. By contrast, some properties of the purified *C. kluyveri* Hbd [12] and *C. beijerinckii* (former "*C. butylicum*") NRRL B593 Hbd [13] have been described. While for *C. beijerinckii*

Hbd pH dependence and kinetic constants for acacCoA, ß-hbCoA, NADH, NAD^+ and NADPH utilisation are reported [13], data for *C. kluyveri* Hbd only state a dependence of NADPH as cofactor. Data for recombinant *C. saccharobutylicum* (former *C. acetobutylicum*) Hbd only reported an activity with NADH as cofactor. On amino acid level *C. saccharobutylicum* and *C. beijerinckii* exhibit 79 % and 78 % sequence identity compared with *C. acetobutylicum*, respectively, whereas *C. kluyveri* only possesses 69 % identity.

More recently, the characterisation of Hbd type FadB2 (ß-hydroxybutyryl-CoA dehydrogenase) from *Mycobacterium tuberculosis* was reported [9]. Conventionally, FadB (ß-hydroxyacyl-CoA dehydrogenase (E.C. 1.1.1.35)) catalyses the third step in ß-oxidation of fatty acid degradation and therefore preferentially catalyses the oxidation of ß-hbCoA to acacCoA. For the FadB2 isoenzyme cofactor specificities for NADH, NAD^+, NADPH and pH effects on catalysis have been described [9].

Although the amino acid sequence identity (43 %) between FadB2 and *Ca*Hbd is quite low, both enzymes are capable to perform the same reaction. However, in contrast to Hbd the reaction of FadB2 favours the conversion of ß-hbCoA to acacCoA, involved in fatty acid catabolism of the ß-oxidation pathway.

Structurally, the hbd enzyme family has been poorly characterised.

To elucidate the full catalytic potential of elusive *Ca*Hbd, this study focuses on comprehensive characterisation of solvent, temperature and pH stability as well as substrate and cofactor specificities. The resulting data justify the utilisation of the purified *Ca*Hbd for construction of improved n-butanol production processes.

5.2 MATERIALS AND METHODS

5.2.1 Devices, Chemicals, Strains and Plasmids

Tables with all used devices (Table 9.1), chemicals (Table 9.2), strains (9.1.1) and plasmids (9.1.2) are attached in Chapter 9.

5.2.2 Structural Modelling of *Ca*Hbd and Molecular Dynamics Simulations

Structural Modelling of *Ca*Hbd

We have used HHpred server [14] and the Yasara bioinformatics suite to model the *Ca*Hbd structure. Modelling was conducted according to manufacturer's protocols and official guidelines.

Temperature and pH Dependent Molecular Dynamics Simulations

Molecular dynamics (MD) simulations employed the Yasara software suite using the AMBER99 force field [15]. The system was composed of the HHpred modelled *Ca*Hbd structure, immersed in a rectangular TIP3P water box with a 10 Å buffer. Sodium chloride adjusted to a 0.1 molar concentration balanced the electrostatic charge associated with the protein. Periodic boundary conditions were applied, while the Particle-mesh Ewald algorithm was used for the calculation of long range electrostatic interactions. The time step for intramolecular forces was chosen to be 1.25 fs. The cut-off for non-bonded van der Waals interactions was 10 Å. For temperature and pH dependent simulations, 1300 steepest decent minimizing were coupled to simulated annealing steps preceding the productive 1 ns MD run. Data resulting from the MD simulations were primarily analysed by Yasara. Using these MD boundaries temperature dependent protein unfolding simulations were carried out at 85 °C using the modelled *Ca*Hbd structure with omitted substrate. In analogy structural changes occurring at pH 5, 7 and 10 were determined using the modelled *Ca*Hbd structure in the presence of the substrate acacCoA.

5.2.3 Cloning

The *Cahbd* gene (GeneBank No. AE001437.1) was cloned into the *E. coli*-compatible vector pCBR_HisC [7] using *Bfua*I and *Bsa*I restriction sites. For amplification of *Cahbd* the upstream primer 5′-CAGCAAGGTCTCTCATATGAAAAAGGTATGTGTTATAGGT (*Bfua*I restriction site underlined) and the downstream primer 5′-TTTTGAATAATCGTAGAAACCTTTTCCTGATT-TTCTTCC were used.

5.2.4 Heterologous Expression and Enzyme Purification for Enzymatic Assays

Enzyme expression was performed using *E. coli* BL21(DE3) as host strain. *Ca*Hbd was expressed in LB media supplemented with 50 µg/ml kanamycin. After inoculation cells were grown to OD_{600} = 0.5 – 0.7 at 37 °C and subsequently induced with 1 mM isopropyl-ß-D-thiogalactopyranoside (IPTG). For further cultivation, the temperature was lowered to 25 °C for 20 h. Cell lysates were prepared with Emulsiflex-B15, cell debris was removed by centrifugation (21,000 g, 4 °C, 20 min). Protein purification was performed using Ni^{2+}-NTA resin. Desalting of the proteins was performed with PD-10 columns (GE Healthcare, Munich, Germany). Protein concentration was measured at 280 nm with unfolded protein in 8 M Urea [16]. The necessary extinction coefficient was calculated by the ExPASY ProtParam tool [17].

5.2.5 Enzyme Assays

Activity of *Ca*Hbd was measured at 340 nm via monitoring the depletion or formation of NADH and NADPH, respectively. The assays were performed in a microtiter plate format using a monochromator equipped plate reader. The reaction mixture excluding the protein was incubated at the measured temperature. Hence, the pH-values of all buffers were adjusted to the desired temperature according to Stoll [18]. All controls and each enzymatic reaction were performed in triplicate.

For the thermal-stability-assays, *Ca*Hbd was stored over several days at 40 °C, 50 °C, 60 °C, 70 °C and 80 °C in a water bath. Subsequently, the assays were performed in reaction mixtures containing 50 mM Hepes (pH 7 at current temperature), 0.3 mM acacCoA and 0.3 mM NADH. Reaction mixtures for the determination of temperature optima were prepared accordingly. Up to 65 °C activities were determined at its current temperature. Measurements above 65 °C were done by incubating *Ca*Hbd in a heating block for 15 min followed by activity determinations at 50 °C.

For solvent-stability-assays, reaction mixtures contained 50 mM Hepes (pH 7 at 50 °C), 0.3 mM acacCoA, 0.3 mM NADH and n-butanol (0 – 10 % (v/v)), ethanol (0 – 20 % (v/v)) or isobutanol (0 – 10 % (v/v)). All assays were performed at 50 °C.

During the determination of pH-optima, a sodium acetate buffer was applied for the pH-range 4 - 6, Tris buffer for pH 7 - 9 and Caps buffer for pH 10 – 11 at 50 °C. The reaction mixtures contained 50 mM of current buffer, 0.3 mM acacCoA and 0.3 mM NADH or 0.6 mM ß-hbCoA and 0.3 mM NAD^+/$NADP^+$.

5.2.6 Kinetics of *Ca*Hbd

*Ca*Hbd was added with a final concentration of 0.75 µg/ml to the reaction mixture, which contained 50 mM Hepes (pH 7 at 50 °C) and 50 mM Caps (pH 10 at 50 °C), respectively. In case of the K_M determination for NADPH the *Ca*Hbd concentration was increased to 9.4 µg/ml. CoA substrates and cofactor amounts applied were 0.4 mM acacCoA, 0.8 mM ß-hbCoA, 0.3 mM NADH and 0.3 mM NAD^+, respectively. For the inhibition studies, different amounts of NAD^+ were added to the reaction mixture. The kinetic parameters K_M, v_{max} and k_{cat} for each substrate and cofactor were determined by varying their concentrations and fitting the data to the Michaelis-Menten equation by using Sigma Plot 12.5.

5.2.7 Circular Dichroism Measurements

CD spectra were obtained with a JASCO spectropolarimeter, model J-715. A quartz cuvette exhibiting a light path lengths of 0.1 cm and for temperature regulation a thermocouple (JASCO) was used. *Ca*Hbd was dissolved in 50 mM NaPi buffer (pH 7 at 20 °C) at a

concentration of 0.21 mg/ml. All obtained spectra were corrected for buffer contributions and the final spectrum represents the average of 16 scans.
Also the *Ca*Hbd temperature dependence was analysed at 225 nm. During these experiments the temperature was increased by a ramp of 0.75 °C/min using a Peltier thermocouple.

5.3 RESULTS AND DISCUSSION

5.3.1 Structural Characterisation of *Ca*Hbd

At present, no crystal structure of a microbial Hbd involved in butanol biosynthesis is available. Based on primary sequence *Ca*Hbd shows 44 % identity to a probable Hbd from *E. coli* K12 (pdb ID: 3MOG), for which a crystal structure is reported. However, the *E. coli* protein is involved in fatty acid catabolism and not in n-butanol formation. Additionally, the two proteins show only minor convergence in secondary structure features. To identify a suitable structural scaffold for *Ca*Hbd we applied multiple sequence profile alignments with the *Ca*Hbd template using the HHpred server, which employs profile Hidden Markov Models [14]. The selected protein scaffolds for sequence alignment and structure modelling gave e-values of 9×10^{-55} - 3.6×10^{-55}, with *Homo sapiens* Hbd showing the highest secondary structural similarity. Interestingly, the *Homo sapiens* Hbd catalyses the same reaction as *Ca*Hbd [19]. Using the alignment data and structure prediction tools of the HHpred server, we were able to create a high quality *Ca*Hbd model. Subsequently, we applied the MUSTANG algorithm [15] of the Yasara bioinformatics suite to carry out an almost complete tertiary structural alignment of *Ca*Hbd with the *Homo sapiens* Hbd scaffold (pdb ID: 1F0Y). The tertiary structure alignment between the two enzymes resulted in an RMSD (root mean square deviation) value of 0.324 Å over 277 aligned amino acid residues with an overall 45.49 % primary sequence identity. In the resulting high quality *Ca*Hbd model, substrate and cofactor positions were adopted from structural data of human 3-hydroxyacyl CoA dehydrogenase (Figure 5.2). The structure of *Ca*Hbd represents a typical α/ß fold enzyme, which is dominated by α-helical bundles that are linked by several unordered loops (Figure 5.2A). Much like other NADH/NADPH dependent dehydrogenases *Ca*Hbd features an extended ß-sheet domain, which contains the Rossmann fold topology crucial for cofactor binding (Figure 5.2A and B) [20]. *Ca*Hbd features opposing binding sites for each the acacCoA substrate and NADH cofactor, respectively. The cofactor NADH is oriented perpendicular to the acacCoA substrate, which potentially aids electron transfer during acacCoA reduction (Figure 5.2B). *Ca*Hbd is a globular protein with minimized solvent accessibility (Figure 5.2C).

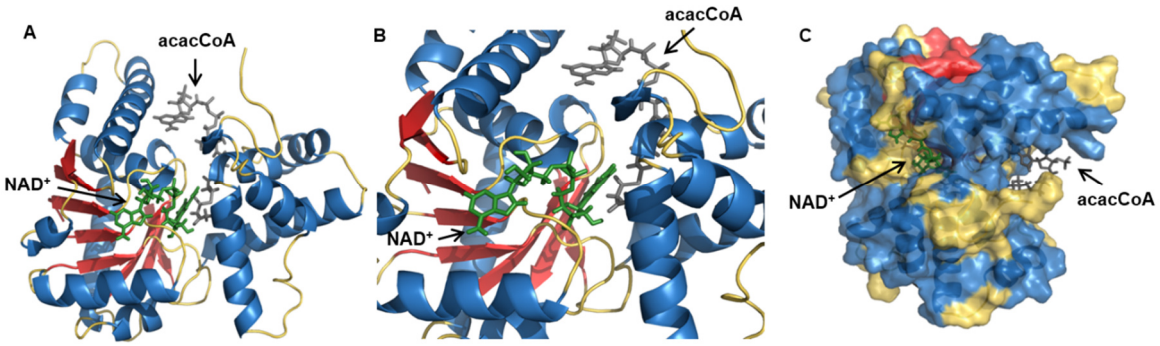

Figure 5.2: Modelled *Ca*Hbd structure.
(A) Structural overview with the substrate acacCoA and NAD+ as cofactor, (B) active site and (C) surface of *Ca*Hbd. The Rossmann fold is marked as ß-sheets. The figures were prepared using PyMOL [21].

Both NADH and acacCoA are situated in binding pockets, which are only partially shielded against the solvent, which may influence their stability under extreme pH and temperature conditions. To further elucidate these effects we have applied biochemical methods and state of the art molecular dynamics simulations to compliment experimental observations.

5.3.2 Biochemical Characterisation of *Ca*Hbd

5.3.2.1 Determination of pH Optima

To compare the pH effects of *Ca*- and *C. beijerinckii* Hbd for the native acacCoA reduction and the reversible ß-hbCoA oxidation we examined both reactions over a broad range of pH-values, using an established NADH assay [8, 13].
The pH effects of the *Ca*Hbd reaction with acacCoA and ß-hbCoA as substrates were studied at 50 °C (Figure 5.3).

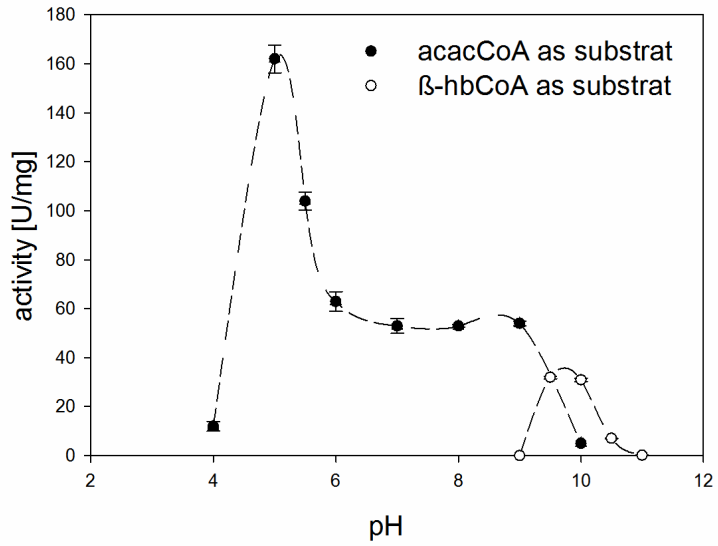

Figure 5.3: Effect of pH on the *Ca*Hbd catalysed reactions.
50 mM sodium acetate buffer was used for pH 4 - 6, 50 mM Tris buffer for pH 7 - 9 and 50 mM Caps buffer for pH 10 – 11 at 50 °C. Each activity is the mean of three repilciates.

The conventional reduction of acacCoA to ß-hbCoA occurs over a wide pH range between 4 - 10 with a pH_{opt} at 5. By contrast, the reverse reaction, oxidation of ß-hbCoA to acacCoA with NAD^+ as cofactor is catalysed only within a small pH-range of 9.5 to 10.5 with a maximum at 10 (Figure 5.3). The pH dependence of Hbd reaction can be correlated with the physiology of microbial solventogenesis. In the primary fermentation phase (acidogenesis) clostridia produce acids (i.e. acetate, butyrate) thereby lowering media's pH. Subsequently, the external pH of the medium shifts below 5 triggering clostridial metabolism to switch on solvent production [22-26]. Therefore, synergies between the pH profile of Hbd and the microbial physiology are essential for solvent production.

This notion is further corroborated by the fact that pH profiles of acacCoA and ß-hbCoA conversion are almost identical between the Hbd enzymes from *C. acetobutylicum* and *C. beijerinckii*, respectively.

To further clarify the pH effects on the reactivity of *Ca*Hbd we have used MD simulations to elucidate potential energy minimized structural changes of the enzyme at pH 5 and 10, respectively. The structural overlay of pH dependent *Ca*Hbd conformations (Figure 5.4A) indicates only minor overall distortions in the enzyme structure. The calculated structural changes at pH 5 compared to pH 10 can be quantified by an RMSD value of 1.68 Å.

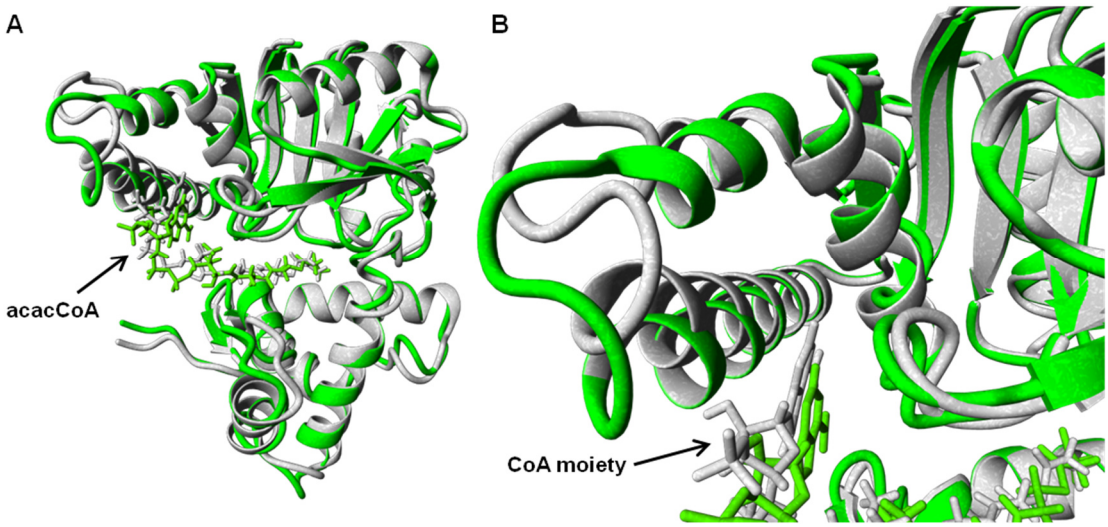

Figure 5.4: MD simulated *Ca*Hbd structures at different pH values.
A) *Ca*Hbd structural overlay at pH 5 (white) and pH 10 (green). B) Enlarged structural features resulting in substrate reorientation. The enlarged helical domains are potentially involved in substrate binding and catalysis.

However, two outer α-helical domains, linked by a short loop (Figure 5.4B), are responsible for substrate binding and are slightly twisted at pH 10. This structural change results in a significant reorientation of the CoA moiety of the substrate. This substrate repositioning in the

active site may contribute to the preference for ß-hbCoA oxidation observed at pH 10. Hence, the MD simulations support biochemical data on pH dependent reaction reversal.

5.3.2.2 Determination of Temperature Optima and Half-life

For a stable n-butanol production process the application of highly stable enzyme systems to achieve relevant production rates are required [7]. Therefore, we closely examined the thermostability of *Ca*Hbd.

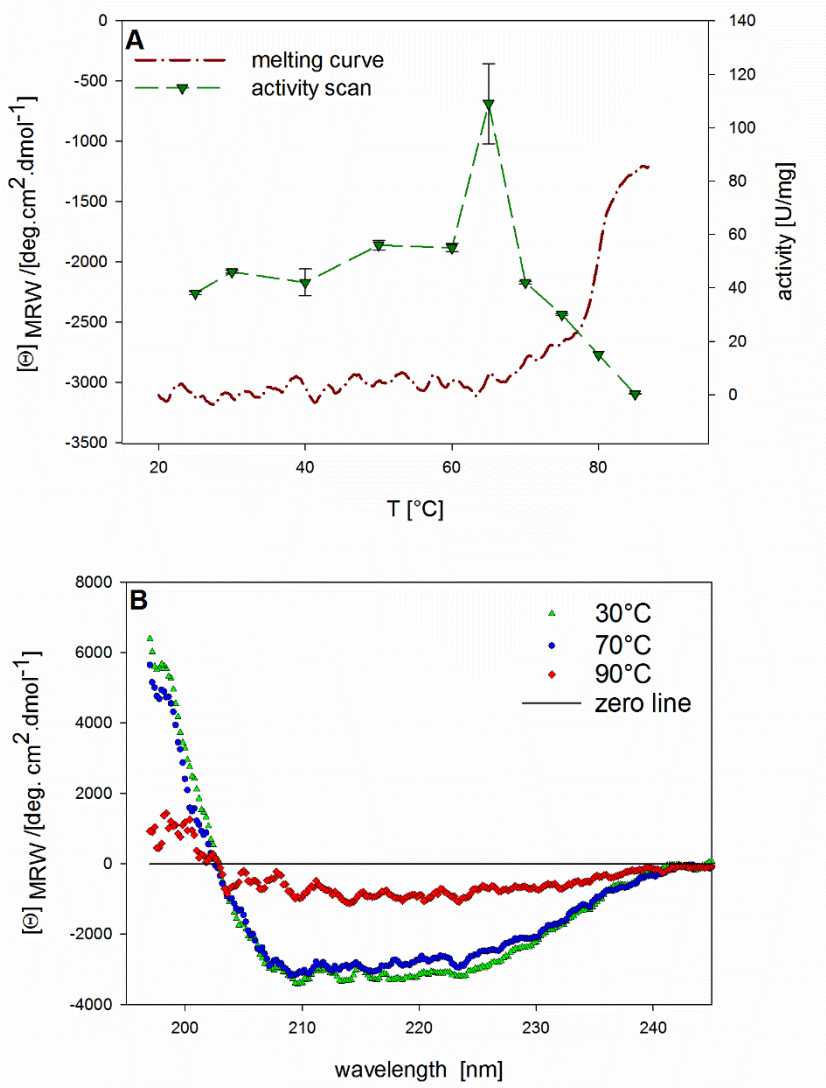

Figure 5.5: Determination of temperature optimum and thermostability of *Ca*Hbd.
Enzyme assays were performed in a range from 25 °C to 85 °C. A) Temperature wavelength scan from 10 °C to 90 °C (heating rate: 0.75 °C / min) at 225 nm was obtained via CD spectrometer as well as determination of temperature optimum of *Ca*Hbd by activity assays. B) Superimposed CD-spectra of the temperature wavelength scan of *Ca*Hbd at 30 °C, 70 °C and 90 °C. Every 20 °C a complete wavelength scan was carried out. Values of CD spectroscopy are presented in mean residue ellipticity ($[\Theta]_{MRW}$).

A temperature dependent profile for the reaction of *Ca*Hbd with acacCoA and NADH as co-substrate is shown in Figure 5.5A. The temperature rise from 25 °C to 60 °C resulted in a 1.5 fold increase of activity (Figure 5.5A). At T_{opt} (65 °C) an activity of 109 (±15) U/mg was

observed. Above 65 °C *Ca*Hbd activity gradually decreased. The concurrent CD measurements supported the activity profile, since protein unfolding was not observed up to 65 °C (Figure 5.5A and B). Above 65 °C structural unfolding was detected with a terminal unfolding point at 85 °C. Based on this data a T_m of 79 °C was calculated.

Relevant activities for *Ca*Hbd over extended time frames (t ≤ 380 h) could be determined at 40 °C, 50 °C, 60 °C, 70 °C and 80 °C, respectively (Table 5.1), indicating that *Ca*Hbd is a highly thermostable enzyme. Interestingly, no definitive half-life could be determined for *Ca*Hbd in the temperature range of 40 °C to 60 °C even after 380 h (~16 days). In this time frame enzyme activity still remained in the range of 62 % (40 °C and 50 °C) to 67 % (60 °C) with respect to the starting values.

Table 5.1: Half-life activity of *Ca*Hbd at 40 °C, 50 °C, 60 °C, 70 °C and 80 °C, respectively. The remaining activity in per cent after 380 h is specified in the 3rd column.

T [°C]	Half-life [h]	A_{0h}/A_{380h} [%]
40	/	62
50	/	62
60	/	67
70	42	/
80	0.9	/

By contrast, at 70 °C the *Ca*Hbd half-life activity could be observed after 42 h. Further, at 80 °C the half-life was reached in less than 1 h, indicating irreversible protein unfolding which was confirmed by CD measurements (Figure 5.5A). To our knowledge this is the first account of *Ca*Hbd being an extremely thermostable enzyme.

To further elucidate the structural features providing the pronounced *Ca*Hbd thermostability we applied MD simulations to virtually expose *Ca*Hbd to 80 °C over a defined time period. Comparing the time dependent structural models indicate a significant decrease of solvent exposed outer α-helical domains (t_0 = 51.8 % → t_{final} = 34.8 %) and their conversion to unfolded turns (t_0= 8.2 % → t_{final} = 19.1 %) and coil topologies (t_0 = 21.6 % → t_{final}= 29.1 %). These structural changes resulted in an increase of the calculated accessible surface area (t_0 = 13120.42 Å → t_{final} = 13172.4 Å), consistent with partial unfolding of solvent exposed protein structures. In contrast, buried protein structures, such as the extended ß-sheet domain, harbouring the catalytically relevant Rossmann fold and were protected from unfolding (t_0 = 16.7 % → t_{final} = 15.2 %). The preservation of buried structures of the enzyme active site provides extended catalytic activity of *Ca*Hbd at elevated temperatures. Therefore, MD simulations corroborate biochemical and biophysical data on thermostability of *Ca*Hbd.

From a process-engineering perspective the extended thermostability of *Ca*Hbd would provide extended operation capacity and reduced enzyme costs in an optimally balanced, cell-free n-butanol production process.

5.3.2.3 Determination of Catalytic Properties

To elucidate the catalytic properties of *Ca*Hbd the kinetic constants, substrate and cofactor specificities were determined. Here, we particularly focused on defining the catalytic limits of the pH dependent, reversible acacCoA reduction. For the first time this study reports a comprehensive substrate and cofactor dependence of a *Ca*Hbd involved in n-butanol biosynthesis.

Substrate specificities

When measured at its respective pH optimum, the *Ca*Hbd catalysed acacCoA reduction (162 (±6) U/mg) is 5 times faster than the ß-hbCoA oxidation (31 U/mg; Figure 5.5). Interestingly, assay data obtained at equal concentrations of ß-hbCoA and NAD^+, indicated that only 50 % of the substrate was converted during the reaction. Since commercial ß-hbCoA is a racemic mixture, this data suggests that only a single enantiomer is an active reactant. It has previously been reported that *E. coli* Hbd is selective for the (S)-stereoisomer [11]. It is therefore, reasonable that also *Ca*Hbd is specific for the (S)-enantiomer of ß-hbCoA.
The kinetic data shown in Table 5.2 summarises *Ca*Hbd properties for specific reactions with acacCoA, ß-hbCoA, NADH, NAD^+ and NADPH, respectively.

Table 5.2: Kinetic parameters of *Ca*Hbd. The standard deviation is stated in parentheses.

	V_{max} [U/mg]	K_M [mM]	k_{cat} [s^{-1}]	k_{cat}/K_M [M^{-1} s^{-1}]
Acetoacetyl-CoA	75.7 (±2.7)	0.11 (±0.01)	38.6 (±1.3)	3.5 (±0.2) x 10^5
ß-Hydroxybutyryl-CoA	53.3 (±1.2)	0.29 (±0.01)	27.1 (±0.6)	9.4 (±0.1) x 10^4
NADH	61.5 (±2.9)	0.14 (±0.02)	31.4 (±1.4)	2.3 (±0.2) x 10^5
NAD^+	55.1 (±1.9)	0.27 (±0.02)	28.1 (±0.9)	1.0 (±0.4) x 10^5
NADPH	3.31 (±0.27)	0.45 (±0.07)	1.7 (±0.1)	3.8 (±0.4) x 10^3

In line with the previous observation K_M value of the *Ca*Hbd reaction with its native substrate acacCoA (K_M = 0.11 (±0.01) mM) was one third of the value observed with ß-hbCoA (K_M = 0.29 (±0.01) mM), which indicates a higher binding capacity of acacCoA to the enzymes active site. Additionally, we have examined *Ca*Hbd cofactor specificities.

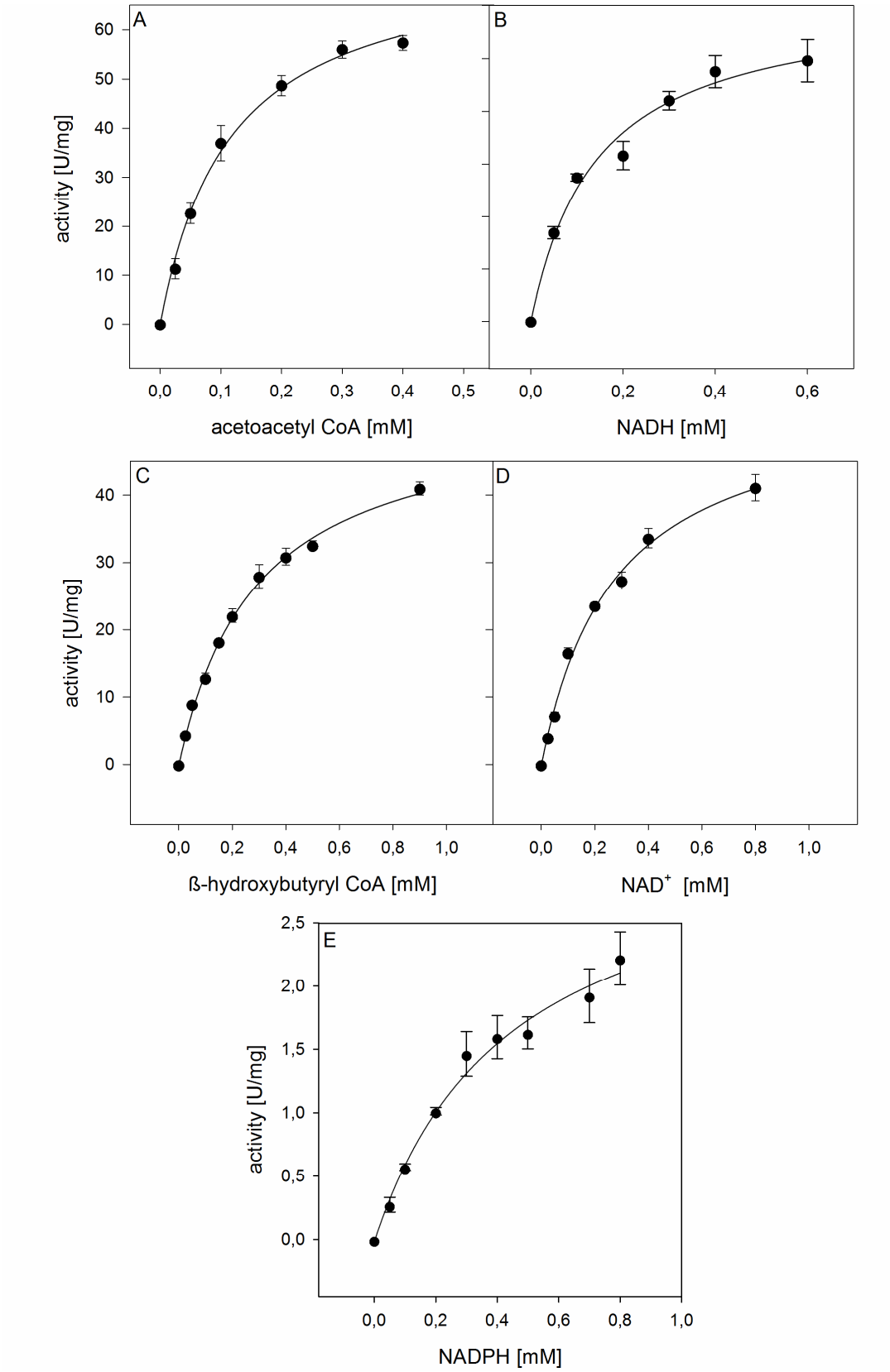

Figure 5.6: Kinetic data for *Ca*Hbd characterisation.
Substrate based reactions: (A) acetoacetyl CoA concentration dependency, (B) ß-hydroxybutyryl CoA concentration dependency; Cofactor based reactions: (C) NADH, (D) NAD^+ and (E) NADPH conditions at 50 °C. The experimental results were fitted to the Michaelis-Menten equation. Each activity is the mean of three replicates.

Again *Ca*Hbd shows a greater binding capacity to the reductant NADH (K_M = 0.14 (±0.02) mM) compared to the oxidant NAD^+ (K_M = 0.27 (±0.02) mM), which indicates that the native enzyme significantly favours the reduction of acacCoA. Therefore, the reaction of acacCoA towards ß-hbCoA is both kinetically and thermodynamically (ΔG^0= - 3,76 kcal/mol [27]) favoured, which drives the overall reaction towards n-butanol production instead of fatty acid catabolism as observed for FadB2 [9]. We collected our kinetic data series at pH 7, which is just above the pH optimum (pH_{opt} 5) of *Ca*Hbd. The main reasoning for this experimental set-up was the enhanced stability of NADH at neutral pH and the downstream opportunity to create a n-butanol targeted enzyme cascade, which takes pH requirements of other enzyme systems into account.

By contrast, in reports on the catalytic properties of *C. beijerinckii* Hbd kinetics at the pH optimum for acacCoA reduction (pH 5.5) and ß-hbCoA oxidation (pH 9), respectively, were measured. Additionally, reactions for *C. beijerinckii* Hbd were recorded at 26 °C, compared to 50 °C applied in this study. Therefore, a direct comparison of kinetic data for *Ca*Hbd and *C. beijerinckii* Hbd is limited. Nevertheless, the specificity constant for acacCoA reduction was about 1,000 fold higher in *C. beijerinckii* Hbd (k_{cat}/K_M = 1.3 × 10^8 $M^{-1}s^{-1}$) compared to *CaHbd* (k_{cat}/K_M = 3.5 × 10^5 $M^{-1}s^{-1}$), while the respective K_M value was 10 fold lower in *C. beijerinckii* Hbd (K_M = 0.014 mM) compared to *Ca*Hbd (K_M = 0.11 mM), respectively. This data set indicates that *C. beijerinckii* Hbd has an improved catalytic efficiency and substrate binding compared to *Ca*Hbd under the respective experimental conditions.

Cofactor specificities

To obtain a comprehensive data set on the cofactor dependence for *Ca*Hbd, we have examined the reaction with NADH, NAD^+, NADPH and $NADP^+$ (Table 5.2 and Figure 5.6).

Initial experiments indicate that *Ca*Hbd has a clear preference towards NADH as cofactor, since corresponding reactions with NADPH resulted in a 18 fold decrease in activity. This trend was mirrored in the catalytic efficiency constants (k_{cat}/K_M) for the NADH- (k_{cat}/K_M = 2.3 (±0.2) x 10^5 $M^{-1}s^{-1}$) and NADPH-linked reaction (k_{cat}/K_M = 3.8 (±0.4) x 10^3 $M^{-1}s^{-1}$), respectively. This suggests that NADH is the physiological co-substrate of *Ca*Hbd. When the reverse (oxidative) reaction with ß-hbCoA was examined, NAD^+ (k_{cat}/K_M = 1.0 (±0.4) x 10^5 $M^{-1}s^{-1}$) was preferred over $NADP^+$, whose activity was so low (catalytic activity = 0.005 (±0.001) U/mg) that no catalytic constants could be determined. A direct activity comparison indicates that NAD^+ (catalytic activity = 55.1 (±1.9) U/mg) reacts 11,000 times faster than $NADP^+$.

The same cofactor preference was observed for FadB2 from *Mycobacterium tuberculosis* [9]. While the cofactor preference of *Ca*Hbd mirrors that of *C. beijerinckii* Hbd, literature reports

for *C. saccharobutylicum* Hbd a very selective preference only for NADH as cofactor [28]. On the contrary, *C. kluyveri* Hbd only accepts NADPH as its cofactor [12].

*Ca*Hbd Cofactor and Substrate Inhibition

Kim and Copeland reported the characterisation of *Rhizobium* sp. strain CC 1192 acetyl-CoA acetyltransferase using a coupled enzyme reaction with commercial 3-hydroxyacyl CoA dehydrogenase [29]. Their study eludes that accumulation of NAD^+ concentrations greater than 0.5 mM in the reaction may lead to Hbd inhibition.

In this study, we quantified this inhibitory effect for the first time. The effect of product (NAD^+) inhibition on the NADH dependent acacCoA reduction to ß-hbCoA was considered using steady-state kinetic data (Figure 5.7).

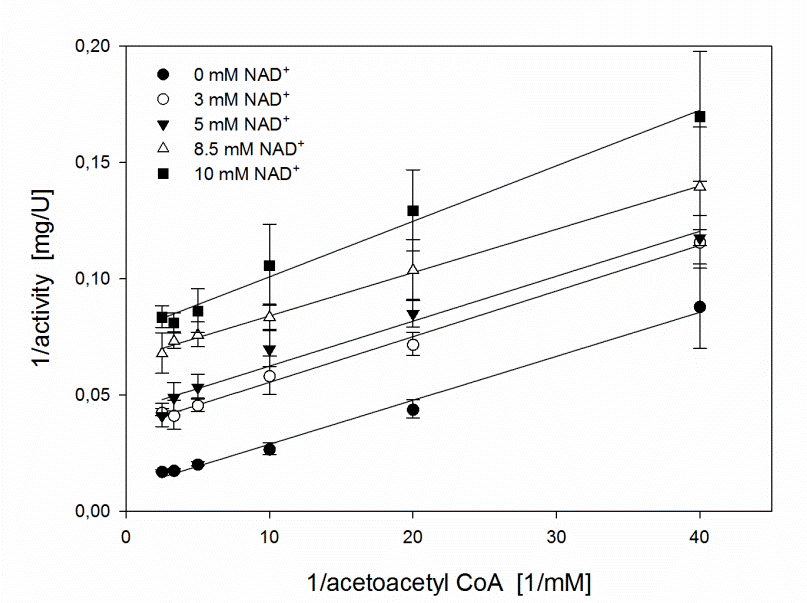

Figure 5.7: Steady state kinetic characterisation of *Ca*Hbd.
Double-reciprocal plots monitoring NAD^+ product inhibition with respect to NADH. Each activity is the mean of three repilcates.

For each of the examined NAD^+ concentrations (0 – 10 mM NAD^+) the K_M and v_{max} values of the respective reactions decreased continuously. In the absence of NAD^+, K_M and v_{max} values in the order of 0.11 (±0.01) mM and 75.7 (±2.70) U/mg were observed (Table 5.2). By contrast, addition of 10 mM NAD^+ respective K_M and v_{max} values were reduced to 0.03 (±0.005) mM and 13.04 (±0.39) U/mg, respectively.

The double-reciprocal plot of v_0 plotted versus the concentration of acacCoA results in a set of parallel lines (Figure 5.7), which allows deduction of a K_i value of 2.0 mM for NAD^+ addition. Kinetic data indicates that NAD^+ acts as an uncompetitive inhibitor, suggesting that *Ca*Hbd contains two distinct binding sites, for acacCoA/ß-hbCoA and the cofactor pair

NADH/NAD^+, respectively. Therefore, the kinetic data set for NAD^+ inhibition is consistent with current structural model of *Ca*Hbd (Figure 5.2).

Colby and Chen reported that C. *beijerinckii* Hbd is inhibited by acacCoA at concentrations as low as 20 µM [13]. Their study showed that the substrate inhibition can be relieved by addition of NADH concentrations in excess of 20 µM. In this study a similar effect could be observed. However, for *Ca*Hbd a slight decrease in activity could also be determined when NADH was supplied at limiting concentrations (data not shown).

5.3.2.4 Determination of Solvent Tolerance

In order to construct efficient n-butanol production systems, enzymes with high solvent tolerance are required. This study examined the solvent tolerance of the Hbd enzyme family for the first time. Consequently, *Ca*Hbd was tested for its stability towards the process relevant alcohols ethanol, n-butanol and isobutanol [7]. *Ca*Hbd retained 50 % activity in the presence of 20 % (v/v) ethanol, 9 % (v/v) n-butanol and 10 % (v/v) isobutanol (Figure 5.8). The significant solvent tolerance of *Ca*Hbd is of particular process relevance for both cell and cell-free n-butanol production methods.

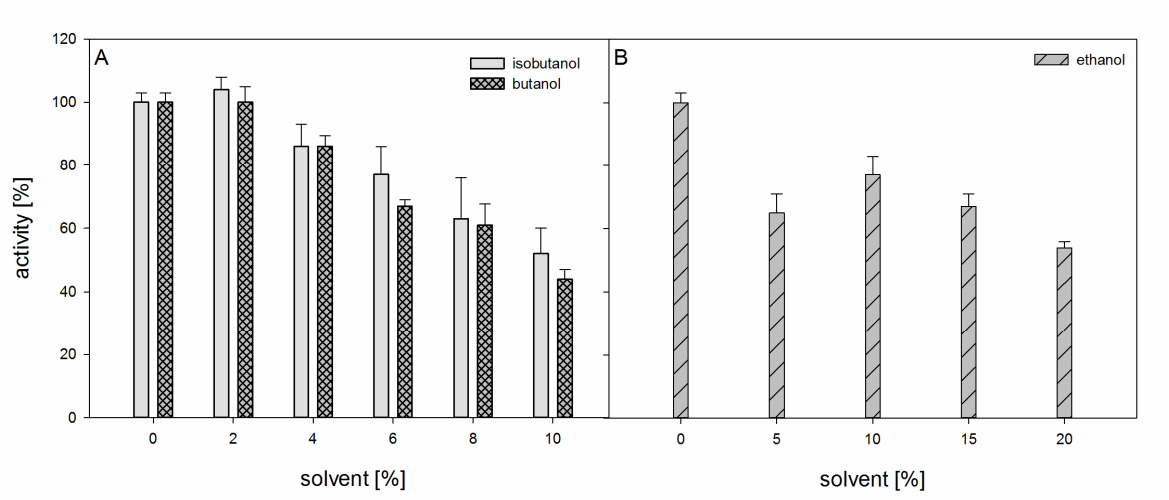

Figure 5.8: Solvent tolerance of *Ca*Hbd.
(A) for 0 - 10 % (v/v) n-butanol and isobutanol; (B) for 0 – 20 % (v/v) ethanol.

C. acetobutylicum ATCC 824 can produce 7.9 g/l n-butanol, whereas *C. acetobutylicum* NRRL B591 only produces 2.6 g/l n-butanol [30]. Thus *C. acetobutylicum* ATCC 824 belongs to the best n-butanol production strains, but its growth is inhibited by 50 % at 0.9 % (v/v) n-butanol. By a stepwise enrichment procedure a more n-butanol-tolerant mutant was found, which growth is halved by 1.9 % (v/v) n-butanol [30]. Hbd from *C. acetobutylicum* ATCC 824 remains 44 % of its native activity at even 10 % (v/v) n-butanol and 50 °C. Furthermore, at n-butanol concentrations above 10 % (v/v) (20 °C) a biphasic butanol/water system is formed spontaneously. Within the biphasic system *Ca*Hbd's activity could easily increase again,

because most n-butanol is removed from the water phase and subsequently accumulated in the upper organic phase. Therefore, decreased influence of the product's toxicity as observed for *Ca*Hbd, is an outstanding process advantage particularly when cell-free enzyme cascades are applied for n-butanol production [31].

5.4 CONCLUSIONS

Butanol is a next generation building block for renewable chemical and biofuel processes due to its enhanced energy content and hydrophobicity compared to first generation fuels such as ethanol. Current, cell-based n-butanol production systems are not mass efficient due to side products (ethanol and acetone). Additionally, these cell based systems are limited in their productivity due to end-product toxicities. An alternative to cell-based production approaches are cell-free enzyme cascades which potentially can convert monomeric sugars into n-butanol with much higher yields. Subsequently, these features allow for simplified, energy efficient product recovery [7]. However, both robust cell and cell-free production systems require upstream identification of process relevant enzyme systems, which preferentially show enhanced solvent and thermostability as well as good catalytic features. Although the physiology of cell based n-butanol production has been investigated in detail, the enzyme systems involved in n-butanol production have only been marginally characterised both structurally and biochemically. This study focused on identification and correlation of biochemical and structural features of the *Ca*Hbd, a key enzyme in n-butanol biosynthesis. We have applied state of the art structural modelling procedures to create a high quality model of *Ca*Hbd. To our knowledge this is the first structural model of the microbial Hbd family, involved in n-butanol biosynthesis. The enzyme structure shows a globular overall structure with maximal packing of secondary structure. As with all NADH dependent dehydrogenases, Hbd harbours a Rossmann binding domain, which is embedded into an extended ß-barrel fold. The substrate binding site located in a linked α-helical domain, which is placed opposite the cofactor binding site. Subsequently, we attempted to correlate *Ca*Hbd biochemical properties to its structural features. This is the account of catalytic features of a purified, recombinant *Ca*Hbd capable of the reversible, pH dependent reduction of acacCoA over a pH range of 5 - 9. The reverse reaction with ß-hbCoA occurs only at pH 9 - 11 and is 5 times slower than the reaction with acacCoA. This suggests that *Ca*Hbd preferentially acts in n-butanol synthesis direction and is not part of the ß-oxidation catabolism of the fatty acid, where ß-hbCoA is a key intermediate. The catalytic constants indicate that the enzyme shows a clear preference to NADH/NAD^+ as a cofactor, while only residual activity with NADPH could be observed. Interestingly, we could identify NAD^+ as a non-competitive inhibitor of the *Ca*Hbd reaction with acacCoA. This indicates that in butanol biosynthesis acacCoA

conversion to ß-hbCoA is tightly controlled. Therefore, in any cell-free n-butanol biosynthesis approach the substrate flux from the master intermediate acetyl-CoA over acacCoA to ß-hbCoA requires definitive cofactor balancing to enable efficient conversion of respective CoA intermediates towards n-butanol as the end product. The kinetic data for NAD^+ inhibition indicates that the enzyme has distinct binding sites for cofactor and substrate, respectively. This data was consistent with the structural features of our *Ca*Hbd model. Next to comprehensive characterisation of *Ca*Hbd substrate and cofactor specificities, we have characterised the thermo- and solvent stability of the enzyme family for the first time. Interestingly, *Ca*Hbd is extremely thermostable with an apparent T_m of 79 °C and an activity half of 1 h at 80 °C. Further, *Ca*Hbd is surprisingly solvent stable. At n-butanol concentrations up to 10 % (v/v) 45 % activity are remaining over extended time periods. Together features such as thermo- and solvent stability are extremely important for enzyme systems to be selected for targeted cell and cell-free n-butanol production systems. Therefore, *Ca*Hbd is an excellent candidate for creating improved biotechnological n-butanol production processes. Additionally, at 10 % (v/v) n-butanol forms a biphasic system with water, which would allow simple gravimetric separation of the butanol product from the aqueous reaction phase. The pronounced thermo- and solvent stability of *Ca*Hbd is routed in its compact, globular protein structure, which we could demonstrate using our *Ca*Hbd model.

5.5 REFERENCES

1. **Dürre P.** 1998. New insights and novel developments in clostridial acetone/butanol/isopropanol fermentation. Applied microbiology and biotechnology **49:**639-648.
2. **Jones DT, Woods DR.** 1986. Acetone-butanol fermentation revisited. Microbiological reviews **50:**484-524.
3. **Steen EJ, Chan R, Prasad N, Myers S, Petzold CJ, Redding A, Ouellet M, Keasling JD.** 2008. Metabolic engineering of Saccharomyces cerevisiae for the production of n-butanol. Microbial cell factories **7:**36.
4. **Inui M, Suda M, Kimura S, Yasuda K, Suzuki H, Toda H, Yamamoto S, Okino S, Suzuki N, Yukawa H.** 2008. Expression of Clostridium acetobutylicum butanol synthetic genes in Escherichia coli. Applied microbiology and biotechnology **77:**1305-1316.
5. **Nielsen DR, Leonard E, Yoon SH, Tseng HC, Yuan C, Prather KL.** 2009. Engineering alternative butanol production platforms in heterologous bacteria. Metabolic engineering **11:**262-273.
6. **Zhang YH.** 2010. Production of biocommodities and bioelectricity by cell-free synthetic enzymatic pathway biotransformations: challenges and opportunities. Biotechnol Bioeng **105:**663-677.
7. **Guterl JK, Garbe D, Carsten J, Steffler F, Sommer B, Reisse S, Philipp A, Haack M, Rühmann B, Koltermann A, Kettling U, Brück T, Sieber V.** 2012. Cell-free metabolic engineering: production of chemicals by minimized reaction cascades. ChemSusChem **5:**2165-2172.
8. **Boynton ZL, Bennet GN, Rudolph FB.** 1996. Cloning, sequencing, and expression of clustered genes encoding beta-hydroxybutyryl-coenzyme A (CoA) dehydrogenase, crotonase, and butyryl-CoA dehydrogenase from Clostridium acetobutylicum ATCC 824. Journal of bacteriology **178:**3015-3024.
9. **Taylor RC, Brown AK, Singh A, Bhatt A, Besra GS.** 2010. Characterisation of a beta-hydroxybutyryl-CoA dehydrogenase from Mycobacterium tuberculosis. Microbiology **156:**1975-1982.
10. **Nolling J, Breton G, Omelchenko MV, Makarova KS, Zeng Q, Gibson R, Lee HM, Dubois J, Qiu D, Hitti J, Wolf YI, Tatusov RL, Sabathe F, Doucette-Stamm L, Soucaille P, Daly MJ, Bennett GN, Koonin EV, Smith DR.** 2001. Genome sequence and comparative analysis of the solvent-producing bacterium Clostridium acetobutylicum. Journal of bacteriology **183:**4823-4838.
11. **Lee SH, Park SJ, Lee SY, Hong SH.** 2008. Biosynthesis of enantiopure (S)-3-hydroxybutyric acid in metabolically engineered Escherichia coli. Applied microbiology and biotechnology **79:**633-641.
12. **Madan VK, Hillmer P, Gottschalk G.** 1973. Purification and properties of NADP-dependent L(+)-3-hydroxybutyryl-CoA dehydrogenase from Clostridium kluyveri. European journal of biochemistry / FEBS **32:**51-56.
13. **Colby GD, Chen JS.** 1992. Purification and properties of 3-hydroxybutyryl-coenzyme A dehydrogenase from Clostridium beijerinckii ("Clostridium butylicum") NRRL B593. Applied and environmental microbiology **58:**3297-3302.
14. **Soding J, Biegert A, Lupas AN.** 2005. The HHpred interactive server for protein homology detection and structure prediction. Nucleic acids research **33:**W244-248.
15. **Konagurthu AS, Whisstock JC, Stuckey PJ, Lesk AM.** 2006. MUSTANG: a multiple structural alignment algorithm. Proteins **64:**559-574.
16. **Connor MR, Liao JC.** 2009. Microbial production of advanced transportation fuels in non-natural hosts. Current opinion in biotechnology **20:**307-315.

17. **Gasteiger E, Hoogland C, Gattiker A, Duvaud Se, Wilkins M, Appel R, Bairoch A.** 2005. Protein Identification and Analysis Tools on the ExPASy Server, p. 571-607. *In* Walker J (ed.), The Proteomics Protocols Handbook. Humana Press.

18. **Stoll VS, Blanchard JS.** 2009. Buffers: Principles and Practice1. Methods in enzymology **463:**43-56.

19. **Barycki JJ, O'Brien LK, Strauss AW, Banaszak LJ.** 2000. Sequestration of the active site by interdomain shifting. Crystallographic and spectroscopic evidence for distinct conformations of L-3-hydroxyacyl-CoA dehydrogenase. The Journal of biological chemistry **275:**27186-27196.

20. **Nardini M, Dijkstra BW.** 1999. Alpha/beta hydrolase fold enzymes: the family keeps growing. Current opinion in structural biology **9:**732-737.

21. **DeLano W.** The PyMOL Molecular Graphics System on World Wide Web. 2002. There is no corresponding record for this reference.

22. **Thorn GJ, King JR, Jabbari S.** 2013. pH-induced gene regulation of solvent production by Clostridium acetobutylicum in continuous culture: parameter estimation and sporulation modelling. Mathematical biosciences **241:**149-166.

23. **Papoutsakis ET.** 2008. Engineering solventogenic clostridia. Current opinion in biotechnology **19:**420-429.

24. **Bahl H, Andersch W, Braun K, Gottschalk G.** 1982. Effect of pH and butyrate concentration on the production of acetone and butanol by Clostridium acetobutylicum grown in continuous culture. European journal of applied microbiology and biotechnology **14:**17-20.

25. **Bahl H, Andersch W, Gottschalk G.** 1982. Continuous production of acetone and butanol by Clostridium acetobutylicum in a two-stage phosphate limited chemostat. European journal of applied microbiology and biotechnology **15:**201-205.

26. **Janssen H, Doring C, Ehrenreich A, Voigt B, Hecker M, Bahl H, Fischer RJ.** 2010. A proteomic and transcriptional view of acidogenic and solventogenic steady-state cells of Clostridium acetobutylicum in a chemostat culture. Applied microbiology and biotechnology **87:**2209-2226.

27. **Jankowski MD, Henry CS, Broadbelt LJ, Hatzimanikatis V.** 2008. Group contribution method for thermodynamic analysis of complex metabolic networks. Biophys J **95:**1487-1499.

28. **Youngleson JS, Jones DT, Woods DR.** 1989. Homology between hydroxybutyryl and hydroxyacyl coenzyme A dehydrogenase enzymes from Clostridium acetobutylicum fermentation and vertebrate fatty acid beta-oxidation pathways. Journal of bacteriology **171:**6800-6807.

29. **Kim SA, Copeland L.** 1997. Acetyl Coenzyme A Acetyltransferase of Rhizobium sp. (Cicer) Strain CC 1192. Applied and environmental microbiology **63:**3432-3437.

30. **Lin YL, Blaschek HP.** 1983. Butanol Production by a Butanol-Tolerant Strain of Clostridium acetobutylicum in Extruded Corn Broth. Applied and environmental microbiology **45:**966-973.

31. **Guterl J-K, Sieber V.** 2013. Biosynthesis "debugged": Novel bioproduction strategies. Engineering in Life Sciences **13:**4-18.

Chapter 6

Crotonyl-CoA to Butyryl-CoA Conversion

6.1 INTRODUCTION

Climate change and growing energy demand induce the development of renewable processes [1, 2]. One of the most advanced process options is the conversion of biomass to bioethanol. However, its low energy density and high hygroscopicity makes it a poor gasoline replacement [3]. Butanol is a designated next generation renewable building block due to its improved energy density and its unlimited admix ability with fossil fuels [3].

The renewable n-butanol production is based on the fermentative conversion of biomass hydrolysates via clostridia species. Starting from the universal glycolytic intermediate pyruvate, the native, coenzyme A dependent n-butanol biosynthesis pathway of *C. acetobutylicum*, involves seven enzymatic steps. Primarily, the pyruvate dehydrogenase complex transforms pyruvate into acetyl-CoA. Then thiolase (acetyl-CoA acetyltransferase) condenses two molecules of acetyl-CoA to one molecule of acetoacetyl-CoA. Subsequently, acetoacetyl-CoA has to go through four steps of NADH-dependent reduction and one dehydration reaction to yield n-butanol (Figure 1.3; Chapter 1) [4].

A key intermediate in n-butanol biosynthesis is crotonyl-CoA, which is conventionally converted to butyryl-CoA by clostridial butyryl-CoA dehydrogenase (Bcd) (EC 1.3.8.1) (Figure 6.1).

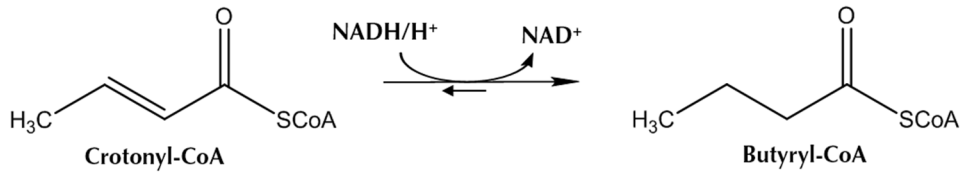

Figure 6.1: Reaction catalysed by clostridial butyryl-CoA dehydrogenase.

Recombinant Bcd from *C. acetobutylicum* ATCC 824 (*Ca*Bcd) is active under semi- and anaerobic conditions [5, 6]. Co-expression of the electron-transfer-proteins *Ca*EtfA and *Ca*EtfB was found to be essential for clostridial Bcd activity [6]. This limits Bcd applicability in cell-free n-butanol biosynthesis.

A high-titre production of n-butanol might be only possible, when a high driving force exists. In clostridial n-butanol biosynthesis pathway NADH and reduced ferredoxin (Bcd-EtfAB complex) is used as reducing power.

If NADH can serve as sole cofactor in the n-butanol biosynthesis pathway the accumulating NADH could be used as a driving force, as NAD^+ is needed for conversion of pyruvate to acetyl-CoA [7].

An alternative biocatalyst to Bcd is trans-2-enoyl-CoA reductases (Ter) (EC 1.3.1.44) [8, 9]. Ter from *Treponema denticola* (*Td*Ter) [10, 11], does not require an FAD^+ cofactor and prefers NADH over NADPH as cofactor. Another key factor, which enhances *Td*Ter suitability for *in vitro* n-butanol biosynthesis is its high substrate specificity for crotonyl-CoA [9, 12].
Moreover, the reverse reaction, oxidizing butyryl-CoA, is not observed [7, 9, 12]. The reduction reaction of *Td*Ters is favoured by the large equilibrium constant that can be explained by the difference in redox potentials. The NAD^+/NADH pair possesses a much lower redox potential (-320 mV) than the crotonyl-CoA/butyryl-CoA pair (-125 mV), keeping butyryl-CoA in the reduced state [12].
The irreversibility of the *Td*Ter catalysed reaction, may also serve as a driving force to channel the carbon flux towards n-butanol [7]. *Td*Ter's biochemically and structurally good characterisation fosters its optimisation and adaptability for *in vitro* n-butanol biosynthesis. [9, 12, 13].
*Td*Ter was crystallized with (pdb-ID: 4FBG) [12] and without bound NAD^+ cofactor (pdb-ID: 4GGP) [13]. The structure comprises a substrate-binding and a cofactor-binding domain (Figure 6.2).

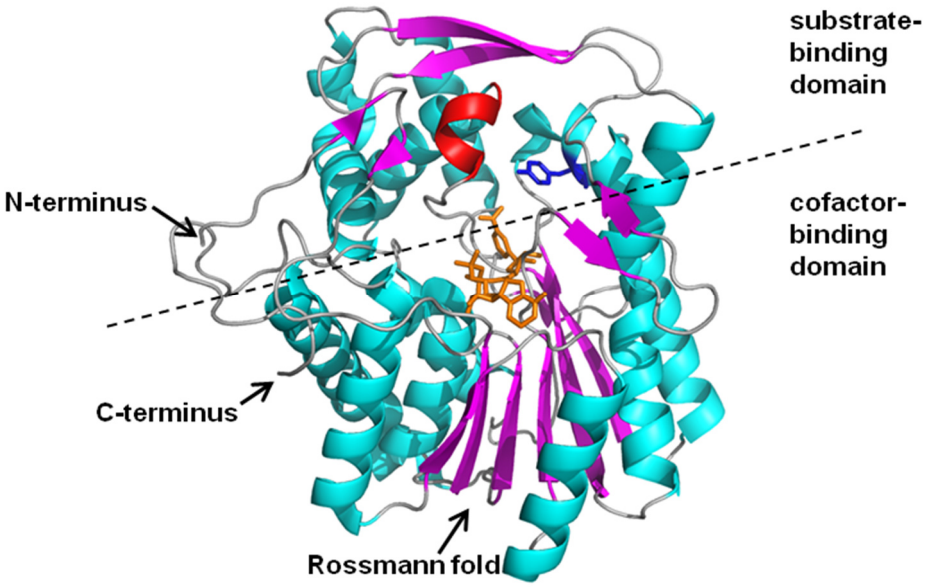

Figure 6.2: Overall structure of *Td*Ter-NAD^+ complex.
Bound NAD^+ is shown with a stick model in orange, α-helices are coloured in cyan, ß-strains in violet and loops in grey. The substrate-binding loop is coloured in red and putatively catalytic Y240 in blue (pdb-ID: 4FBG). The figure was prepared using PyMOL [14].

The cofactor-binding domain assumes a typical Rossmann fold consisting of six-stranded parallel ß-sheets. The catalytic active site is located at the interface between the two domains and can be located by the putatively catalytic tyrosine Y240 [12, 13].

This study generally focuses on cell-free n-butanol production by reconstruction of the clostridial n-butanol biosynthesis pathway. Therefore, all involved enzymes starting from pyruvate were established in our lab and further analysed for their applicability in cell-free n-butanol biosynthesis reaction setup.
In this section current state of knowledge concerning *Ca*Bcd-*Ca*EtfAB-complex and *Td*Ter will be summarized. The *Ca*Bcd-*Ca*EtfAB-complex, *Td*Ter as well as Bcd from *Geobacillus thermodenitrificans* (*Gth*Bcd) will be screened for their applicability in cell-free n-butanol production.

6.2 MATERIALS AND METHODS

6.2.1 Devices, Chemicals, Strains and Plasmids

Tables with all used devices (Table 9.1), chemicals (Table 9.2), strains (9.1.1) and plasmids (9.1.2) are attached in Chapter 9.

6.2.2 Cloning – Plasmid Construction

The sequences for all named primers as well as all obtained plasmids in the following section are listed in Chapter 9.

6.2.2.1 Bcd Complex from *C. acetobutylicum* ATCC 824

pCBR_Cabcd_HisC, pCBR_Cabcd_HisNo

The open reading frame of *bcd* from *C. acetobutylicum* ATCC 824 was amplified by PCR with the plasmid Dü-pDRIVE_CRT+BCD as template, applying the primers 5′ bcdII_pCBR and 3′ bcdII_pCBR. The *Cabcd* gene was cloned into the vector pCBR_HisC and pCBR_HisNo pre-digested with *Bfua*I and *Bsa*I.

pCBR_CaetfA_HisC, pCBR_CaetfA_HisNo, pCBR_CaetfB_HisN, pCBR_CaetfB_HisC, pCBR_CaetfB_HisNo

The genes *CaetfA* and *CaetfB* were obtained by PCR with Dü-pDRIVE_etfA+etfB+Hbd as template applying the primers 5′ EtfA_pCBR and 3′ EtfA_pCBR for *CaetfA* and 5′ EtfB_pCBR and 3′ EtfB_pCBR for *CaetfB*. Subsequently, *CaetfA* was cloned in the vectors pCBR_HisC and pCBR_HisNo and *CaetfB* gene was cloned in all three pCBR-vectors pre-digested with *Bfua*I and *Bsa*I.

6.2.2.2 Ter from *T. denticola*

pCBR_Tdter_HisC, pCBR_Tdter_HisNo

The *E. coli* codon optimised *Tdter* gene was synthesised by Geneart (Regensburg, Germany) using the published gene sequence of *Tdter* as template (GenBank accession No. AE017248). *Tdter* was ligated into the vectors pCBR_HisC and pCBR_HisNo pre-digested with *Bfua*I and *Bsa*I.

6.2.2.3 Bcd from *G. thermodenitrificans*

pCBR_Gthbcd_HisN, pCBR_Gthbcd_HisC, pCBR_Gthbcd_HisNo

After optimising the published amino acid sequence (NCBI reference-sequence YP_001125561.1) for *E. coli* usage *Gthbcd* gene was synthesised by Geneart (Regensburg, Germany). The open reading frame of *Gthbcd* was amplified by PCR with the plasmid pMA_Gthbcd as template, applying the primers 5′ bcdI_pCBR and 3′ bcdI_pCBR. *Gthbcd* was cloned into the vectors pCBR_HisN, pCBR_HisC and pCBR_HisNo pre-digested with *Bfua*I and *Bsa*I.

6.2.3 Heterologous Protein Expression

Enzyme expression was performed in *E. coli* BL21(DE3) as host strain. *Ca*Bcd, *Ca*EtfA, *Ca*EtfB, *Td*Ter and *Gth*Bcd were expressed in LB medium supplemented with 50 µg/ml kanamycin. After inoculation, cells were grown to an OD_{600} = 0.5 – 0.7 at 37 °C and subsequently induced with 1 mM IPTG. For further cultivation temperature was kept at 37 °C for 4 h. For *Gth*Bcd expression temperature was decreased to 18 °C after induction and incubated for further 21 h. Afterwards the cells were harvested by centrifugation (4,500 g, 4 °C, 30 min). The cell pellets were stored at -20 °C.

6.2.4 Purification of *Td*Ter

The cell pellet was resuspended in 50 mM Hepes pH 8.0, 20 mM imidazole. Cell lysate was prepared with an Emulsiflex-B15 and cell debris removed by centrifugation (25,000 g, 4 °C, 20 min). A Ni^{2+}-NTA column (column volume (cv) ~ 4 ml; Thermo Scientific, Schwerte, Germany) was equilibrated with 50 mM Hepes pH 8.0, 20 mM imidazole. The His_6 tagged enzyme was loaded on the column and washed with 3 cv of equilibration buffer. The tagged enzyme was eluted with 50 mM Hepes pH 8.0 and 500 mM imidazole.

Desalting of the protein was achieved via a PD-10 column (GE Healthcare, Freiburg, Germany). The purified protein was stored as liquid stock with 10 % (v/v) glycerol at -80 °C. Protein concentration of the unfolded protein dissolved in 8 M urea was measured at 280 nm

[15]. The corresponding extinction coefficient was calculated by ExPASY's ProtParam tool [16].

6.2.5 Photometrical Assay for Bcd and Ter Activity

Protein activity was measured at 340 nm by monitoring the depletion of NADH. The assays were performed in a microtiter plate format using a monochromator equipped plate reader. Reaction mixture contained 50 mM Hepes buffer, 0.3 mM crotonyl-CoA and 0.3 mM NADH. The reaction mixture excluding the protein was incubated at the desired temperature. Hence, the pH-value of the Hepes buffer was adjusted to the assay temperature according to Stoll [17]. Each enzymatic reaction was performed in triplicate.

6.3 RESULTS AND DISCUSSION

6.3.1 Expression of *Ca*Bcd-*Ca*EtfAB-Complex

In an initial approach to produce *in vitro* n-butanol, parts of the native clostridial pathway were constructed. As clostridial enzymes are known to be quite thermostable they are suitable for technical applications, where high reaction temperatures and long enzymatic half-lives are required. In our pathway design the oxygen sensitivity of the *Ca*Bcd-*Ca*EtfAB-complex was crucial for success and was subsequently evaluated.

The genes *Cabcd*, *CaetfA* and *CaetfB* were cloned in different pCBR expression vectors (see 6.2.2.1). All three proteins were expressed in *E. coli* BL21(DE3) and after cell disruption samples were analysed on a 12 % SDS-page.

*Ca*Bcd could be expressed in moderate amounts, whereby only a small fraction was soluble. The protein band on the SDS-page was consistent with the calculated weight of 41 kDa (Figure 6.3A).

*Ca*EtfA could be expressed in small amounts. On the SDS-gel it was identified at approximately 36 kDa. However, most of the protein was insoluble (Figure 6.3B).

*Ca*EtfB was equally distributed between soluble and insoluble fraction. Figure 6.3C shows *Ca*EtfB as a small band at approximately 27 kDa.

In summary *Ca*Bcd, *Ca*EtfA and *Ca*EtfB fused to a His_6-tag could be expressed in small amounts as soluble proteins.

Reconstitution of enzyme activities indicated that the reaction was not efficient under aerobic and semi-aerobic conditions.

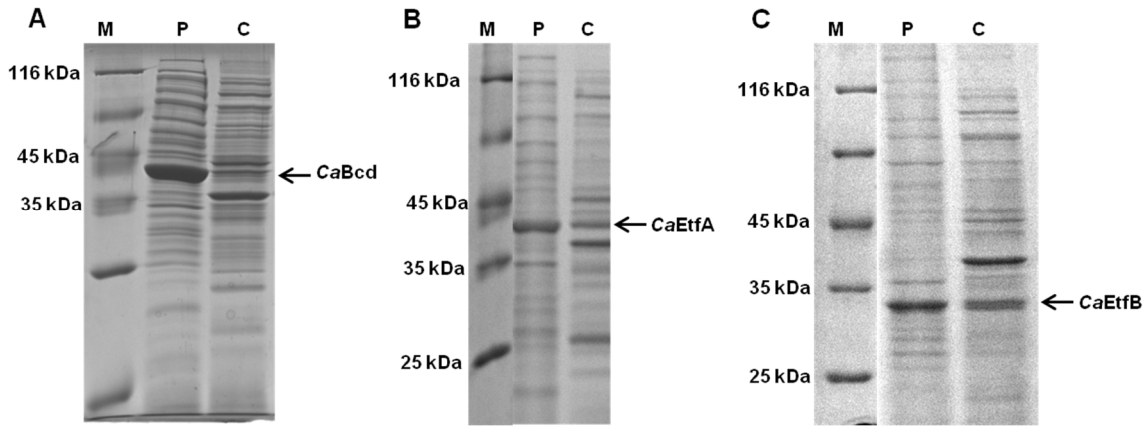

Figure 6.3: 12% SDS-pages showing the expression of (A) *Ca*Bcd, (B) *Ca*EtfA and (C) *Ca*EtfB.
M: unstained protein ladder; P: cell pellet; C: crude extract;

No more work was invested to improve expression of *Ca*Bcd, *Ca*EtfA and *Ca*EtfB.
Instead literature was screened for alternative enzyme activities, which could work under aerobe conditions. Here we could identify *Td*Ter as a potential candidate.

6.3.2 Expression and Catalytic Properties of *Td*Ter

Ter catalyses the conversion of crotonyl-CoA to butyryl-CoA. Ter from *T. denticola* was evaluated for its capability to aerobically convert crotonyl-CoA to butyryl-CoA, a key step in our *in vitro* n-butanol biosynthesis. *Td*Ter uses NADH as its sole cofactor and exhibits a high specificity for crotonyl-CoA as its substrate, while the oxidation of butyryl-CoA is inefficient [7, 9, 12].

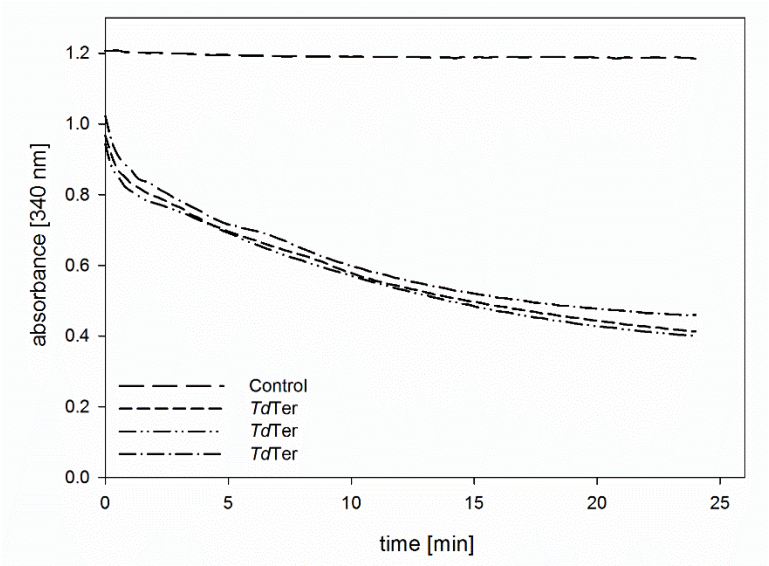

Figure 6.4: Photometrical *Td*Ter activity assay, measured at 340 nm (50 °C).
Assay mixture included 50 mM Hepes pH 7, 0.3 mM crotonyl-CoA, 0.3 mM NADH. Concentration of *Td*Ter was $1.8*10^{-3}$ mg/ml. Three replicates of one measurement as well as the control without protein are shown.

The *Tdter* gene was amplified by PCR, cloned into pCBR expression vectors (see 6.2.2.2) and transformed into *E. coli* BL21(DE3) resulting in a soluble and active protein.

Activity of *Td*Ter was detected using a photometrical assay, measuring the depletion of NADH at 340 nm, as described by Hoffmeister *et al.* (2005) [8]. It is reported that initial *Td*Ter reactivity is very fast. Therefore, stop-flow analytics would be required to determine the initial rate of *Td*Ter activity.

Characterisation of *Td*Ter

Determination of the initial rate with a plate reader is due to its mechanical setup hardly possible as the reaction is almost over until the measurement can be started. This observation is shown in Figure 6.4 as the gap between the control (straight line at 1.2) and the *Td*Ter activity lines, which start at approximately 1.0 absorbance units.
However, we tried to estimate *Td*Ter activity. Therefore, reciprocal calculations applying linear equation were used to extrapolate an activity of 30 (±2.5) U/mg.
The decrease in enzymatic activity can be explained by the effect of butyryl-CoA inhibition. Additionally, it was reported, that NAD^+ acts as a competitive inhibitor for NADH binding and a mixed inhibitor with respect to crotonyl-CoA. By contrast, butyryl-CoA serves as a mixed inhibitor of both substrates [13].
Nevertheless, two very different *Td*Ter activities have been reported. Tucci *et al.* (2007) observed an *Td*Ter activity with crotonyl-CoA as substrate and NADH as cofactor of 43 (±4.8) U/mg at 30 °C [9]. This value is consistent with the activity in this study of 30 (±2.5) U/mg at 50 °C. By contrast Hu *et al.* (2013) described an eleven times higher activity of 455.8 (±9.6) U/mg at 25 °C [12], using the same substrates. The authors attributed this high difference in activity to variations in purification methods of the enzymes [12]. In our study, we applied the same one-step affinity chromatography protocol as reported by Tucci *et al.* (2007). This could explain, why our measured values perfectly fit to the ones reported by Tucci *et al.* (2007) [9].
Biochemical studies indicated that *Td*Ter prefers NADH (455.8 (±9.6) U/mg) over NADPH (15.3 (±1.7) U/mg) and uses an ordered bi-bi reaction mechanism initiated through binding of the redox cofactor [12, 13].

***Td*Ter Substrate Selectivity**

Further, *Td*Ter showed higher catalytic efficiency on C_6 (hexenoyl-CoA) and C_{12} (dodecenoyl-CoA) substrates compared to the C_4 substrate (crotonyl-CoA), which is essential in production of diesel (C_{12}-C_{20}) equivalents [13].

*Td*Ter Thermostability

For a stable cell-free n-butanol production process the application of highly stable enzyme systems to achieve relevant production rates is required [1]. As mentioned before, it was hardly possible to determine the activity of *Td*Ter. Nevertheless, determination of *Td*Ter activity after incubation at 50 °C for 17.5 h with a photometrical activity assay estimated an activity of 0.25 (±0.02) U/mg (Figure 6.5), indicating a 116 times decrease in activity. Moreover, *Td*Ter is almost completely inhibited after 10 min. This could be attributed to NAD^+ and butyryl-CoA binding (Figure 6.5).

As data indicated *Td*Ter not to be thermostable, an alternative enzyme system would be more suitable. In this context, we identified Bcd from *Geobacillus thermodenitrificans* (*Gth*Bcd) originating from a thermophilic organism as a possible alternative.

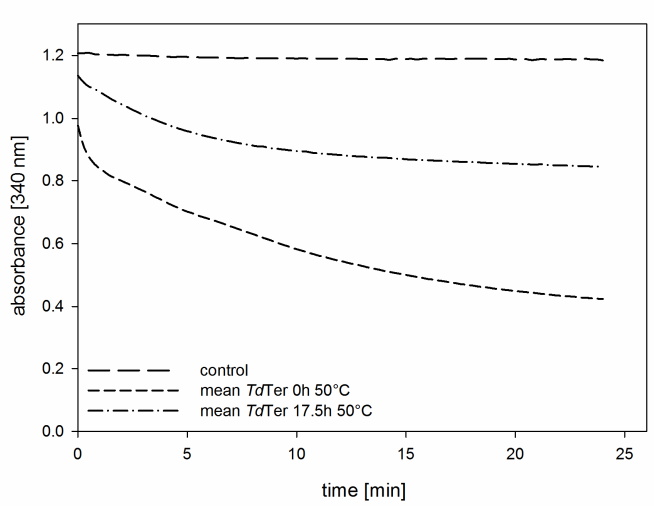

Figure 6.5: Comparison of *Td*Ter activity measurements after 0 and 17.5 h incubation at 50 °C. Shown are the mean values of three replicates of *Td*Ter incubated at 50 °C for 0 h (Figure 6.4) and 17.5 h. The assay mixture contained 50 mM Hepes pH 7, 0.3 mM crotonyl-CoA and 0.3 mM NADH. Concentration of *Td*Ter for the thermostability assays was $60*10^{-3}$ mg/ml.

6.3.3 Expression and Catalytic Properties of *Gth*Bcd

The genus *Geobacillus* is known for its easy adaptability to a wide range of environmental niches. Therefore, it had attracted industrial interest for potential applications in biotechnological processes as source of thermostable enzymes [18].

The complete genome of *G. thermodenitrificans* NG80-2, which grows up to 73 °C (T_{opt} = 65 °C) was published in 2006 and comparative genomic analysis revealed the Bcd sequence of *G. thermodenitrificans* [19].

In our study, the gene *Gthbcd* was cloned in three different pCBR expression vectors (see 6.2.2.3). All three proteins were expressed in *E. coli* BL21(DE3) and after cell disruption samples of all cell extracts were analysed on a 12 % SDS-gel. *Gth*Bcd could be expressed in

moderate amounts and largely as a soluble protein. The recombinant protein gave a band at approximately 43 kDa (Figure 6.6).

The crude extract of *Gth*Bcd was incubated for 20 min at 60 °C in a heating block. Subsequently, the sample was centrifuged (5 min, 25,000 g) and the supernatant was loaded on the SDS-gel (see Figure 6.6, H^2). The faint band at 43 kDa indicated, that most of the protein is precipitated during the 20 min incubation at 60 °C suggesting that *Gth*Bcd is not as thermostable.

However, our experimental set-up is not entirely conclusive. *Gth*Bcd can be co-precipitated with *E. coli* proteins. It is possible that *E. coli* protein just aggregate and pull *Gth*Bcd with them.

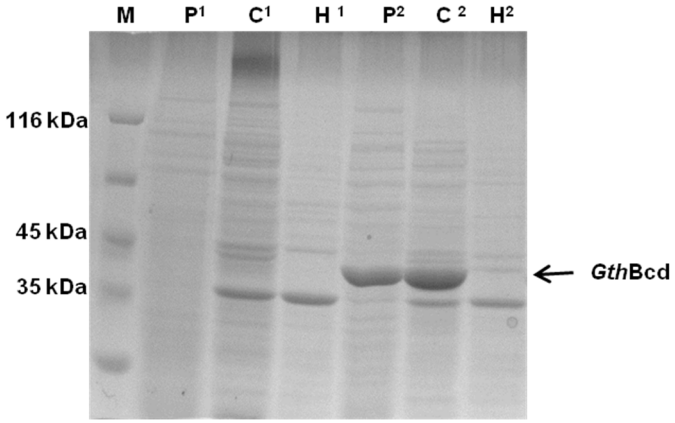

Figure 6.6: 12% SDS-page of *Gth*Bcd expression (2) compared with cell background (1) originating from *E. coli*.
M: unstained protein ladder; P: cell pellet; C: crude extract; H: crude extract incubated at 60 °C for 20 min;

Activity of *Gth*Bcd

Furthermore, no activity of *Gth*Bcd could be obtained in an aerobic photometrical assay where NADH depletion at 340 nm was determined.

Homology Sequence of *Gth*Bcd

Alignment of the amino acid sequences revealed that *Gth*Bcd possesses a higher similarity to *Ca*Bcd (53 %) than *Td*Ter (36 %). Interestingly, no significant similarity was found between *Ca*Bcd and *Td*Ter, although they are catalysing the same reaction.

It is assumed that *Gth*Bcd due to its similarity to *Ca*Bcd might also need two electron-transfer proteins and can only be active in an anaerobic or semi-aerobic environment. Up to now no publication describes *Gth*Bcd to be an active butyryl-CoA dehydrogenase. Therefore, *Gth*Bcd was classified as not suitable for aerobic, cell-free n-butanol production.

6.4 CONCLUSIONS

Butanol is a next generation building block for renewable biofuel and chemical synthesis due to its enhanced energy content and its high hydrophobicity. Cell-based n-butanol production systems suffer from limited mass efficiency caused by side products, i.e. acetone and ethanol, and end-product toxicity.

A promising alternative to cell-based n-butanol production approaches are cell-free enzyme cascades which can convert monomeric sugars into n-butanol with potentially much higher yields.

A key intermediate in n-butanol biosynthetic pathway is crotonyl-CoA, which is conventionally reduced to butyryl-CoA by clostridial butyryl-CoA dehydrogenases.

In this study, two different butyryl-CoA dehydrogenases from *C. acetobutylicum* ATCC 824 and from *G. thermodenitrificans* were considered, as well as a trans-2-enoyl-CoA reductase from *T. denticola*.

*Ca*Bcd requires two electron-transfer proteins, i.e. *Ca*EtfA and *Ca*EtfB, for activity. Additionally, the resulting protein complex can only operate in anaerobic or semi-aerobic conditions. It transpired that for industrial applicability oxygen tolerance of the applied enzymes is required. Therefore, *Ca*Bcd was classified as not suitable for our n-butanol production. Nevertheless, it could be shown that *Ca*Bcd, *Ca*EtfA and *Ca*EtfB could be solubly expressed with a terminal His_6-tag.

*Td*Ter is a biochemically and structurally well characterised enzyme, which combines several advantages compared to clostridial Bcds. *Td*Ter shows high activity and specificity towards crotonyl-CoA as substrate, accepts NADH as sole cofactor and does not catalyse the oxidation of butyryl-CoA, resulting in an irreversibility of the reaction. In our assays an activity of 30 U/mg could be predicted. However, *Td*Ter is strongly inhibited by NAD^+ as well as by butyryl-CoA and this observation prevented exact photometrical activity measurements. Additionally, *Td*Ter possesses a relatively low thermostability.

A Bcd variant from the thermophilic organism *G. thermodenitrificans* was evaluated. However, *Gth*Bcd showed no activity in the photometrical assay assuming that *Gth*Bcd also needs electron-transfer proteins as *Ca*Bcd. Furthermore, data suggests, that *Gth*Bcd additionally requires an anaerobic or semi-aerobic environment like *Ca*Bcd. In summary, it turned out that *Gth*Bcd is no suitable candidate for aerobic n-butanol production.

6.5 REFERENCES

1. **Guterl JK, Garbe D, Carsten J, Steffler F, Sommer B, Reisse S, Philipp A, Haack M, Rühmann B, Koltermann A, Kettling U, Brück T, Sieber V.** 2012. Cell-free metabolic engineering: production of chemicals by minimized reaction cascades. ChemSusChem **5:**2165-2172.
2. **Himmel ME, Ding SY, Johnson DK, Adney WS, Nimlos MR, Brady JW, Foust TD.** 2007. Biomass recalcitrance: engineering plants and enzymes for biofuels production. Science **315:**804-807.
3. **Dürre P.** 2007. Biobutanol: an attractive biofuel. Biotechnology journal **2:**1525-1534.
4. **Yan Y, Liao JC.** 2009. Engineering metabolic systems for production of advanced fuels. J Ind Microbiol Biotechnol **36:**471-479.
5. **Atsumi S, Cann AF, Connor MR, Shen CR, Smith KM, Brynildsen MP, Chou KJ, Hanai T, Liao JC.** 2008. Metabolic engineering of Escherichia coli for 1-butanol production. Metab Eng **10:**305-311.
6. **Inui M, Suda M, Kimura S, Yasuda K, Suzuki H, Toda H, Yamamoto S, Okino S, Suzuki N, Yukawa H.** 2008. Expression of Clostridium acetobutylicum butanol synthetic genes in Escherichia coli. Appl Microbiol Biotechnol **77:**1305-1316.
7. **Shen CR, Lan EI, Dekishima Y, Baez A, Cho KM, Liao JC.** 2011. Driving forces enable high-titer anaerobic 1-butanol synthesis in Escherichia coli. Appl Environ Microbiol **77:**2905-2915.
8. **Hoffmeister M, Piotrowski M, Nowitzki U, Martin W.** 2005. Mitochondrial trans-2-enoyl-CoA reductase of wax ester fermentation from Euglena gracilis defines a new family of enzymes involved in lipid synthesis. The Journal of biological chemistry **280:**4329-4338.
9. **Tucci S, Martin W.** 2007. A novel prokaryotic trans-2-enoyl-CoA reductase from the spirochete Treponema denticola. FEBS Lett **581:**1561-1566.
10. **Loesche WJ.** 1988. The role of spirochetes in periodontal disease. Adv Dent Res **2:**275-283.
11. **Loesche WJ, Grossman NS.** 2001. Periodontal disease as a specific, albeit chronic, infection: diagnosis and treatment. Clin Microbiol Rev **14:**727-752, table of contents.
12. **Hu K, Zhao M, Zhang T, Zha M, Zhong C, Jiang Y, Ding J.** 2013. Structures of trans-2-enoyl-CoA reductases from Clostridium acetobutylicum and Treponema denticola: insights into the substrate specificity and the catalytic mechanism. Biochem J **449:**79-89.
13. **Bond-Watts BB, Weeks AM, Chang MC.** 2012. Biochemical and structural characterisation of the trans-enoyl-CoA reductase from Treponema denticola. Biochemistry **51:**6827-6837.
14. **DeLano W.** The PyMOL Molecular Graphics System on World Wide Web. 2002. There is no corresponding record for this reference.
15. **Pace CN, Vajdos F, Fee L, Grimsley G, Gray T.** 1995. How to measure and predict the molar absorption coefficient of a protein. Protein science : a publication of the Protein Society **4:**2411-2423.
16. **Gasteiger E, Hoogland C, Gattiker A, Duvaud Se, Wilkins M, Appel R, Bairoch A.** 2005. Protein Identification and Analysis Tools on the ExPASy Server, p. 571-607. *In* Walker J (ed.), The Proteomics Protocols Handbook. Humana Press.
17. **Stoll VS, Blanchard JS.** 2009. Buffers: Principles and Practice1. Methods in enzymology **463:**43-56.
18. **McMullan G, Christie JM, Rahman TJ, Banat IM, Ternan NG, Marchant R.** 2004. Habitat, applications and genomics of the aerobic, thermophilic genus Geobacillus. Biochem Soc Trans **32:**214-217.
19. **Feng L, Wang W, Cheng J, Ren Y, Zhao G, Gao C, Tang Y, Liu X, Han W, Peng X, Liu R, Wang L.** 2007. Genome and proteome of long-chain alkane degrading Geobacillus thermodenitrificans NG80-2 isolated from a deep-subsurface oil reservoir. Proc Natl Acad Sci U S A **104:**5602-5607.

Chapter 7

Catalytic Modules in Non-natural Butanol Biosynthesis: Conversion of the key intermediate crotylalcohol to n-butanol via a designed enzyme cascade

Conventionally, bio-butanol is produced via the anaerobe ABE fermentation that employs Clostridia species as cellular production systems. Alternatively, tailor-made, cell-free enzyme cascades are emerging as alternative production systems, which hold the promise of rapid adaptability to harsh process conditions and improved n-butanol yields. However, the molecular complexity of natural n-butanol biosynthesis currently prohibits realization of a robust cell-free n-butanol production process. Recently, simplified, non-natural n-butanol production pathways have been predicted by computational methods. However, enzyme systems that allow consecutive conversion of predicated intermediates to n-butanol have not been identified. A key biosynthetic module in computationally predicted n-butanol production is the conversion of crotylalcohol to n-butanol. We have designed a non-natural enzyme cascade that allows a three step conversion of crotylalcohol to n-butanol using just two enzymes. The involved enzyme systems horse liver alcohol dehydrogenase and 2-enoate reductase from Bacillus subtilis show pronounced substrate promiscuity, which allows the consolidated conversion of crotylalcohol to n-butanol. Further, the designed enzyme cascade allows production of n-butanol using only the NAD^+/NADH redox couple as a unified electron shuttle, which significantly reduces the molecular complexity of the cell-free reaction cascade. This is the first study that could experimentally validate a reaction module of a computationally predicted n-butanol production pathway. The development of designed, cell-free reaction cascades will pave the way towards mass- and cost-efficient n-butanol production at an industrial scale.

7.1 INTRODUCTION

Climate change and dwindling fossil resources drive industrial developments of renewable, biomass based processes for fuels, chemicals and commodity products [1, 2]. Industrial alcohols such as bio-ethanol are key in the development of renewable processes, as they are versatile platform chemicals for fuel and commodity production. However, due to its low energy density and low hydrophobicity bio-ethanol is no ideal replacement for fossil fuels [3]. An emerging bio-fuel alternative is n-butanol, which due to its unlimited miscibility with fossil fuels and its higher energy density is poised to be a key next generation renewable building block [3]. Conventionally, n-butanol is produced via the anaerobe *Clostridium acetobutylicum* based acetone (A), butanol (B) and ethanol (E) fermentation process. However, the conventional cell based ABE process suffers from marginal economic viability and low product titres due to end-product toxicity above 1 - 2 % (v/v) and accumulation of undesired metabolic products [4]. An emerging alternative is the development of non-natural, cell-free enzyme cascades that selectively convert sugars into platform chemicals such as n-butanol [5]. Cell free enzymatic processes can potentially result in higher product yields as there is no requirement to maintain viable cellular functions and the rapid adaptability of component enzymes to harsh industrial reaction conditions [2]. Therefore, cell-free production systems enable the targeted, mass efficient production of chemical products.

Starting from the universal glycolytic intermediate pyruvate, the native, coenzyme A dependent n-butanol biosynthesis pathway of *C. acetobutylicum*, involves seven enzymatic steps that require different cofactor systems to yield n-butanol [6] (Figure 7.1). Recently, consolidated, computational models of non-natural n-butanol biosynthesis from pyruvate have been proposed (Figure 7.1), which could guide experimental reaction engineering towards a consolidated cell-free process [5, 7-9]. In our quest to construct a consolidated, tailor-made, cell-free n-butanol production system we have evaluated several biosynthetic modules that have been predicted in the conversion of pyruvate to n-butanol [6-8]. A key intermediate in the predicted n-butanol production cascade is crotonaldehyde [6-8]. However, at present no enzyme system capable of catalysing the conversion of crotonaldehyde to butyraldehyde has been identified.

This study reports a non-natural, three step enzyme cascade, which allows the conversion of crotylalcohol to crotonaldehyde, which is then further, elaborated via butyraldehyde to n-butanol. Interestingly, we could achieve this three step reaction with only two enzyme systems utilizing their respective substrate promiscuity.

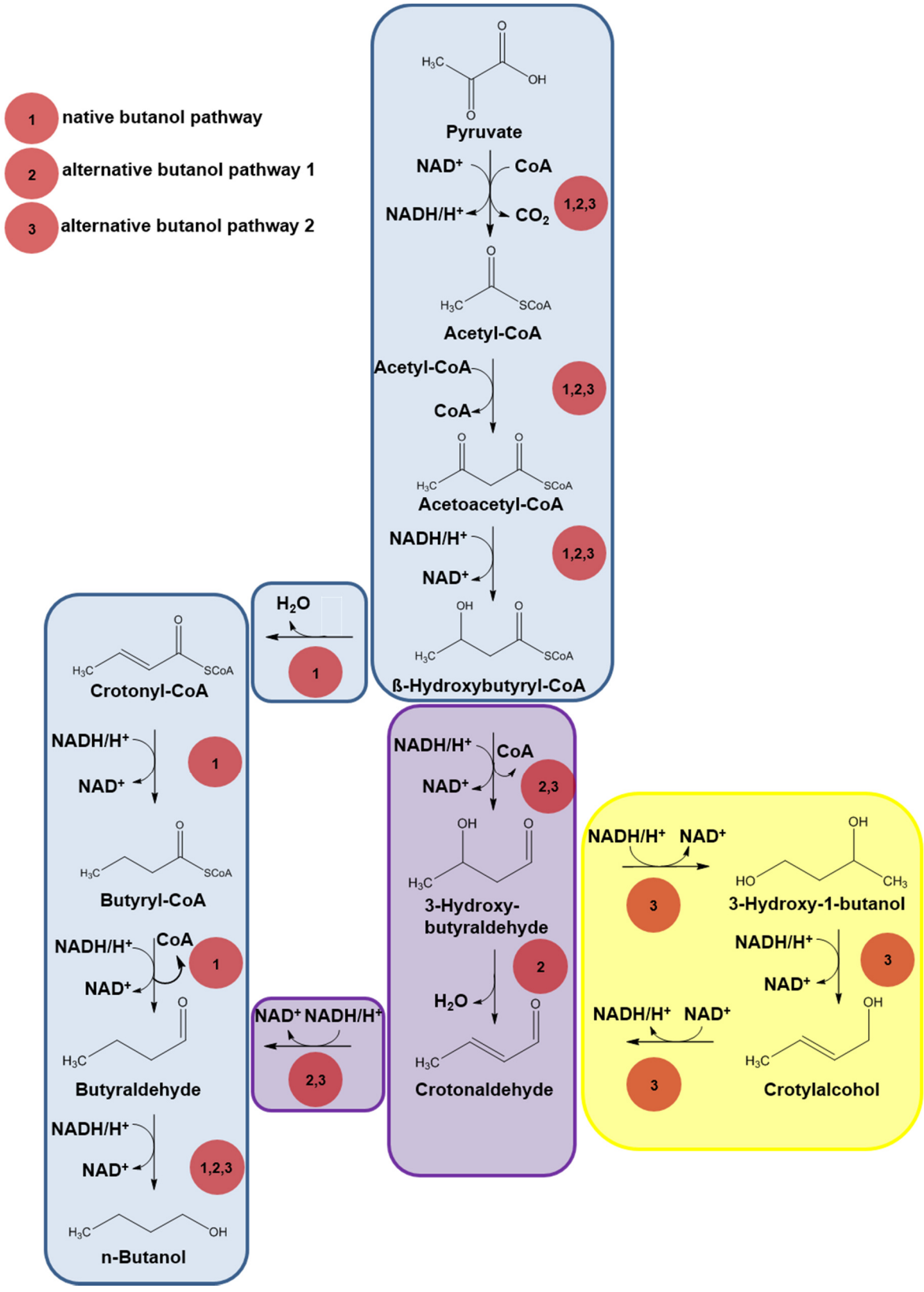

Figure 7.1: Enzyme-catalysed reactions comprising the native (in blue and numbered 1) and two alternative (in purple numbered 2 and yellow numbered 3) pathways for synthesising of n-butanol from pyruvate.

Each reaction module was established individually prior to combining enzymatic reactions to allow consolidated aerobic conversion of crotylalcohol to n-butanol.

For the first time we could identify an enzyme system that catalyses the dedicated conversion of crotonaldehyde to butyraldehyde. Further, this is the first report on the experimental validation of computationally predicated biosynthetic modules involved in non-natural n-butanol biosynthesis. The data will contribute to the development of mass efficient n-butanol production systems, which are prerequisite for an advanced bio-butanol process design.

7.2 MATERIALS AND METHODS

7.2.1 Devices, Chemicals, Strains and Plasmids

Tables with all used devices (Table 9.1), chemicals (Table 9.2), strains (9.1.1) and plasmids (9.1.2) are attached in Chapter 9.

7.2.2 Isolation of Genomic DNA

Isolation of the genomic DNA from *B. subtilis* was conducted using the genomic DNA isolation kit from Thermo Scientific, according to the manufacturer's instructions.

7.2.3 Cloning of *yqjM*

B. subtilis yqjM gene was cloned into the vector pET28a pre-digested with *Nco*I and *Xho*I. The open reading frame of *B. subtilis yqjM* was amplified by PCR, applying the primers 5' YqjM_pET28a (GCG CCA TGG CCA GAA AAT TAT TTA CAC CTA TTA) and 3' YqjM_pET28a (ATA TCT CGA GCC AGC CTC TTT CGT ATT GAA CAG GG). The restriction sites contained in the primer's sequences are underlined.

7.2.4 Heterologous Expression and Purification of YqjM

Enzyme expression was performed using *E. coli* HMS174(DE3) as host strain. YqjM was expressed in TB medium supplemented with 50 µg/ml kanamycin. After inoculation, cells were grown to an OD_{600} = 0.5 – 0.7 at 37 °C and subsequently induced with 1 mM IPTG. For further cultivation temperature was kept at 25 °C for 20 h. Subsequently, the cells were harvested (4,500 g, 4 °C, 30 min).

The cell pellet was resuspended in 50 mM Hepes pH 8.0, 20 mM imidazole. Cell lysate was prepared with Emulsiflex-B15 and cell debris removed by centrifugation (25,000 g, 4 °C, 20 min). A Ni^{2+}-NTA column (column volume (cv) ~ 4 ml; Thermo Scientific, Schwerte, Germany) was equilibrated with 50 mM Hepes pH 8.0, 20 mM imidazole. His_6 tagged enzyme was loaded on the column and washed with 3 cv of equilibration buffer. The tagged enzyme

was eluted with 50 mM Hepes pH 8.0 and 500 mM imidazole. The protein containing fractions were well visible, because of the yellow protein colour. Desalting of the protein was performed with PD-10 columns (GE Healthcare). The protein was stored as liquid stock with 10 % (v/v) glycerol at - 80 °C. Protein concentration of the unfolded protein dissolved in 8 M urea was measured at 280 nm [10]. The corresponding extinction coefficient was calculated by ExPASY's ProtParam tool [11].

7.2.5 GC-FID Analysis

Reaction mixtures for analysis of YqjM activity with gas chromatography (GC) contained 50 mM Hepes buffer pH 7, 20 mM crotonaldehyde, 20 mM NADH and 0.05 mM FMN. Reaction mixtures of the Adh assays contained 50 mM Hepes buffer pH 7, 20 mM crotylalcohol and 20 mM NAD^+. Additionally, the pH-value of the Hepes buffer was adjusted to 40 °C according to Stoll [12]. For coupled YqjM and Adh assay, reaction mixtures consisted of 50 mM Hepes buffer pH 7, 20 mM crotylalcohol, 20 mM NADH and 20 mM NAD^+. YqjM was added to a final mass of 0.34 mg and Adh to 0.28 mg, respectively.

All substrates and products could be quantified by a Trace GC Ultra, equipped with a Headspace Tri Plus auto sampler, an agitator and a flame ionization detector (FID). The GC analysis was performed on a StabiWax column (length 30 m, internal diameter 0.25 mm, film thickness 0.25 µm (Macherey-Nagel, Düren, Germany), with helium (1.2 ml min^{-1}) as carrier gas. Injector and detector temperature were 200 °C, whereas the oven temperature programme was 50 °C for 2 min, raised to 200 °C with a ramp of 10 °C min^{-1}, the end temperature was held for 1 min. The samples (500 µl in a 10 ml gas-tight headspace vial) were incubated at 40 °C for 15 min. For the analysis 700 µl of the headspace were injected (headspace syringe 100 °C) in the split mode with a flow of 10 ml min^{-1}. For quantification of the crotylalcohol and crotonaldehyde concentrations, the FID response in each sample was related to control measurements of known concentrations (20 mM). The concentrations of butyraldehyde and n-butanol in each sample were determined by correlating the GC-FID response to control samples (butanol: 10 mM; butyraldehyde: 10 mM) of a separate GC run.

7.2.6 HPLC-DAD Analysis

Crotonyl-CoA and butyryl-CoA were quantified by an Agilent HPLC 1100 system, equipped with an auto sampler, column oven and a diode-array detector. CoA-substrate detection was performed at 260 nm. The isocratic separation was done on a Luna 3U C 18(2) 100A column equipped with a precolumn security guard cartridge C18 4 x 2 mm at 25 °C (Phenomenex, Aschaffenburg, Germany). As mobile phase a mixture of buffer A (10 mM potassium-phosphate buffer, pH 6.5) and buffer B (10 mM potassium-phosphate buffer containing 40 %

methanol, pH 6.5) at a flow rate of 0.4 ml min^{-1} was used. In the first ten minutes buffer B was continuously increased from 30 % to 80 %. This 80 % to 20 % (buffer B to A) mixture was hold for 5 min, followed by a 15 min instant decrease of buffer B to 30 %. This mixture (30 / 70 % (v/v) buffer B/A) was hold for further 10 min.

Reaction mixtures contained 50 mM Hepes buffer pH 7, 0.1 mM crotonyl-CoA, 0.1 mM NADH and 0.05 mM FAD^+ and FMN, respectively. *Td*Ter was added with a final concentration of 0.4 mg/ml and YqjM with 0.34 mg/ml. The injected sample volume was 10 µl.

7.3 RESULTS AND DISCUSSION

Crotylalcohol and crotonaldehyde are key building blocks in a computational reaction cascade that predicts conversion of pyruvate to n-butanol [7]. In the predicated reaction cascade an oxidation of crotylalcohol and a subsequent reduction of crotonaldehyde yield butyraldehyde. This is further reduced to yield n-butanol as the end-product. Enzymatic conversion of crotylalcohol to crotonaldehyde and butyraldehyde to n-butanol has been reported utilizing microbial and mammalian alcohol dehydrogenases [13-15]. By contrast, no enzyme systems for the dedicated conversion of crotonaldehyde to butyraldehyde have been identified yet. To experimentally establishing the desired reaction cascade, we first screened for enzyme systems that could individually catalyse each step involved in the conversion of crotylalcohol to n-butanol (Figure 7.2). As the reactivity of alcohol dehydrogenases towards crotylalcohol and butyraldehyde is established, we primarily screened for enzymes which could accept both substrates. The identification of a single Adh capable of catalysing two reactions would allow for construction of a consolidated reaction cascade. Further, we selected a 2-enoate reductase, which could accept the substrate crotonaldehyde and catalyse its conversion to butyraldehyde. Ultimately, the selected enzyme reactions were combined to allow a consolidated conversion of crotylalcohol to n-butanol (Figure 7.2).

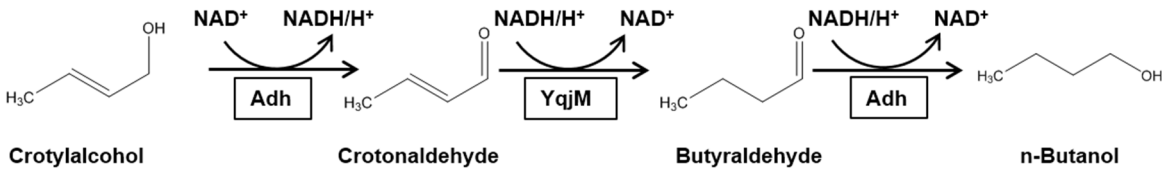

Figure 7.2: Non-natural enzyme cascade for conversion of crotylalcohol to n-butanol.
Adh: commercial horse liver alcohol dehydrogenase, YqjM: recombinant 2-enoate reductase from *B. subtilis*.

7.3.1 Conversion of Crotylalcohol to Crotonaldehyde

Literature data indicated that horse liver alcohol dehydrogenase (Adh) is an ideal candidate for the oxidation/reduction of C4 compounds due to its relatively high activity towards butyraldehyde [14]. As this reaction is relevant for downstream catalytic steps, we have evaluated, if Adh also shows activity towards the primary substrate, crotylalcohol (Figure 7.2). Therefore, Adh was incubated in 50 mM Hepes buffer (pH 7, 40 °C) with the cofactor NAD^+ and crotylalcohol as the sole substrate for one hour. As Adh is a mesophilic enzyme a reaction temperature of 40 °C was chosen to prevent denaturation over the assay period [16]. Adh was able to effectively catalysing the conversion of crotylalcohol to crotonaldehyde (Figure 7.3).

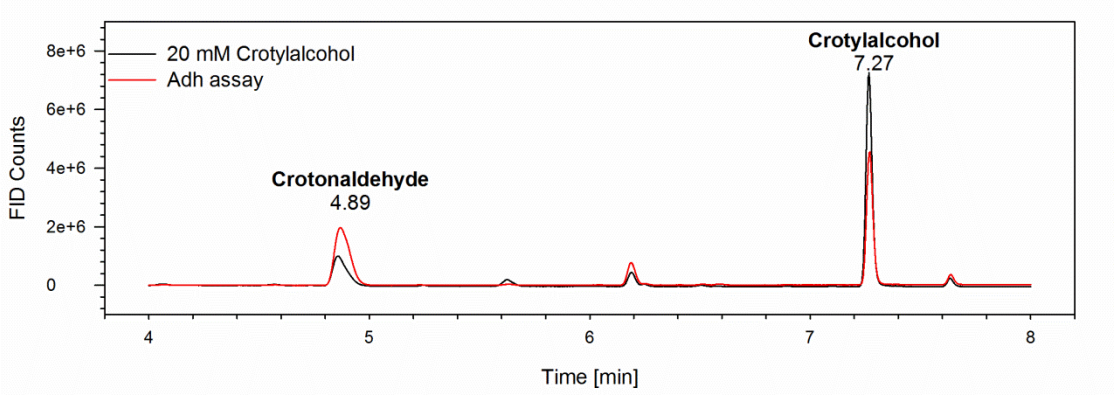

Figure 7.3: Reactivity of horse liver Adh towards crotylalcohol via GC-FID measurements: Adh assay with crotylalcohol as substrate (in red) and 20 mM crotylalcohol as control (black); The assay was conducted in 50 mM Hepes buffer (pH 7), 20 mM crotylalcohol and 20 mM NAD^+ at 40 °C. Crotylalcohol has a retention time of 7.27 min. A butanol contamination from the crotylalcohol stock resulted in a peak at 6.2 min.

However, GC data indicated that the reaction was not quantitative, as only one third of the substrate was converted to crotonaldehyde. Since the conversion of crotylalcohol to crotonaldehyde is thermodynamically unfavourable (ΔG_0 = -5.78 kcal/mol; [17]), it is reasonable that the reaction reached an equilibrium. To allow efficient conversion of crotylalcohol to n-butanol, it is therefore imperative that one of the subsequent enzymatic steps is capable of quantitatively converting either crotonaldehyde or butyraldehyde. This is the first report of a characterised Adh accepting both crotylalcohol and butyraldehyde as substrates. The substrate promiscuity of Adh is the basis for construction of a consolidated reaction cascade towards n-butanol.

7.3.2 Conversion of Crotonaldehyde to Butyraldehyde by YqjM

At present no enzyme system for the dedicated conversion of crotonaldehyde to butyraldehyde has been identified. This is partially due to the transient reactivity of crotonaldehyde in aqueous reaction systems. Since the enzyme family of 2-enoate reductases

accepts a wide range of α-, ß-unsaturated aldehydes and ketones [18, 19], we have applied an *in vitro* screening effort to identify an enzyme capable of converting crotonaldehyde to butyraldehyde. In these screening efforts we identified the NADH dependent 2-enoate reductase YqjM derived from *B. subtilis* (EC 1.3.1.31) as a key candidate.

YqjM belongs to the family of Old Yellow Enzymes (OYE) (EC 1.6.99.1) [18]. OYEs were the first enzyme family reported to feature a catalytically active flavin (FMN) moiety as part of the active site. In biological redox reactions enzyme-bound flavin serves as a temporary sink of electrons, which are further passed on to an electron-accepting protein or substrate species.

Interestingly, YqjM displays pronounced substrate promiscuity, accepting a range of chemically different substrates including quinones, α-, ß-unsaturated aldehydes and ketones [18, 19]. Additionally, it has been demonstrated that YqjM acts as a detoxification enzyme in the antioxidant defence system [18], suggesting that YqjM has multiple physiological substrates. Further, YqjM is promiscuous in its cofactor choice as it can utilize both NADH and NADPH in molar amounts [19]. This feature is of particular importance in the construction of a consolidated reaction cascade, since NADH can be used as the sole redox mediator (Figure 7.1 and Figure 7.2), which significantly reduces the molecular complexity of the entire system. The observed substrate promiscuity of YqjM is further corroborated through its open catalytic domain [20].

In this study, we have utilized YqjM's substrate promiscuity for the targeted reduction of crotonaldehyde to butyraldehyde.

Characterisation of Recombinant YqjM

The *yqjM* gene was isolated from *B. subtilis* genomic DNA by PCR and cloned into a standard expression vector pET28a. Subsequently, YqjM was expressed in *E. coli* HMS174(DE3) with a C-terminal His_6-Tag. After cell disruption YqjM was found to be equally distributed between the soluble and insoluble fractions. The molecular weight (Mr = 38 kDa) of recombinant YqjM was consistent with the literature [12]. Prior to *in vitro* application, soluble YqjM was purified to homogeneity by application of Ni^{2+}-NTA affinity chromatography.

Reactivity of YqjM Towards Crotonaldehyde

The activity of 2-enoate reductases could be determined spectrometrically by measuring the decrease in NADH absorbance at 340 nm. However, for reactions of YqjM in aerobe media, this spectrophotometric measurement is complicated by a side-reaction with molecular oxygen, which leads to the non-productive depletion of the NADH pool [18, 21] (Figure 7.4).

In this study, no reliable data on YqjM activities could be collected using spectrophotometric measurements. Therefore, we applied a validated GC based methodology to accomplish quantitative measurements of YqjM activity towards crotonaldehyde.

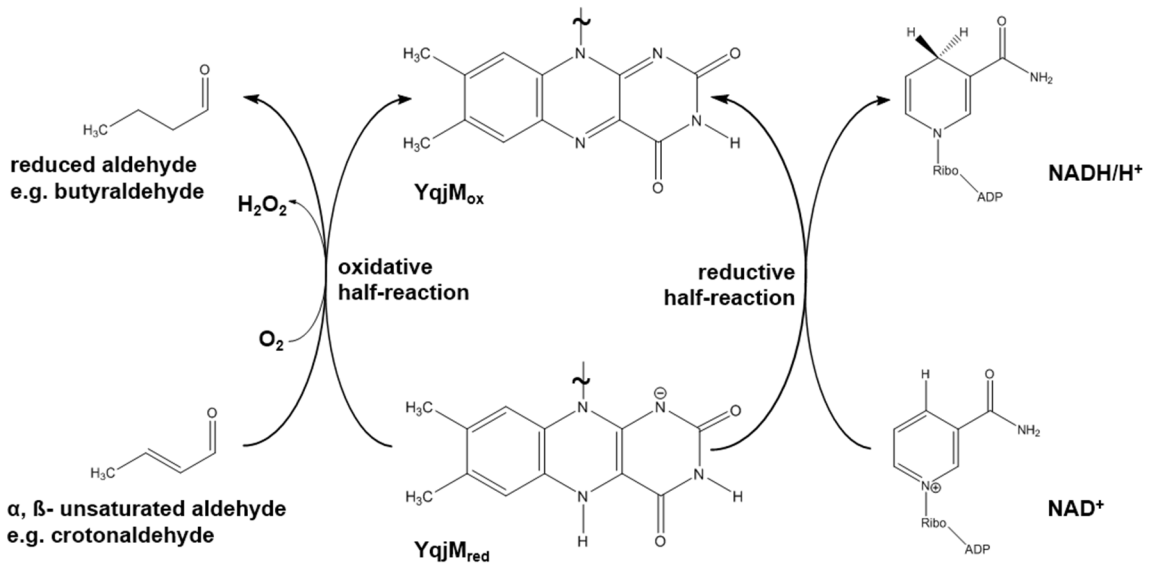

Figure 7.4: The catalytic cycle of YqjM. Inherited from [22].

In analogy to the Adh reaction, YqjM activity was determined at 40 °C (t = 1 h) in a Hepes buffer system (pH 7) containing FMN and NADH as cofactors and crotonaldehyde as the sole substrate.

The resulting GC measurements revealed that recombinant YqjM-His_6 variant was indeed catalytically active and able to convert crotonaldehyde to butyraldehyde (Figure 7.5).

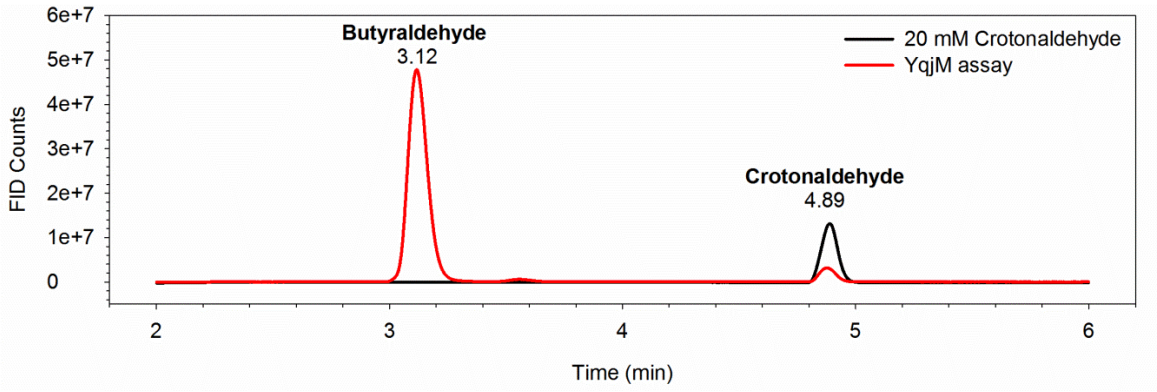

Figure 7.5: Conversion of crotonaldehyde to butyraldehyde with recombinant YqjM:
GC measurements: YqjM assay with the crotonaldehyde substrate (in red) and 20 mM butyraldehyde as control (in black); the assay was conducted in 50 mM Hepes buffer (pH 7) with 20 mM crotonaldehyde, 20 mM NADH and 0.05 mM FAD^+ at 40 °C.

In contrast, to our data, literature describes the YqjM-His_6 variant as catalytically inactive [21]. However, this literature evidence is based on spectrophotometric data, which are inconclusive due to the parallel reaction of YqjM with molecular oxygen present in the reaction [21]. That the YqjM-His_6 variant (catalytic activity = 1 U/mg) may be less active than the wt enzyme can be deduced by structural analysis of YqjM (pdb-ID.: 1Z48). Structurally intact YqjM is a homo-tetramer (Figure 7.6).

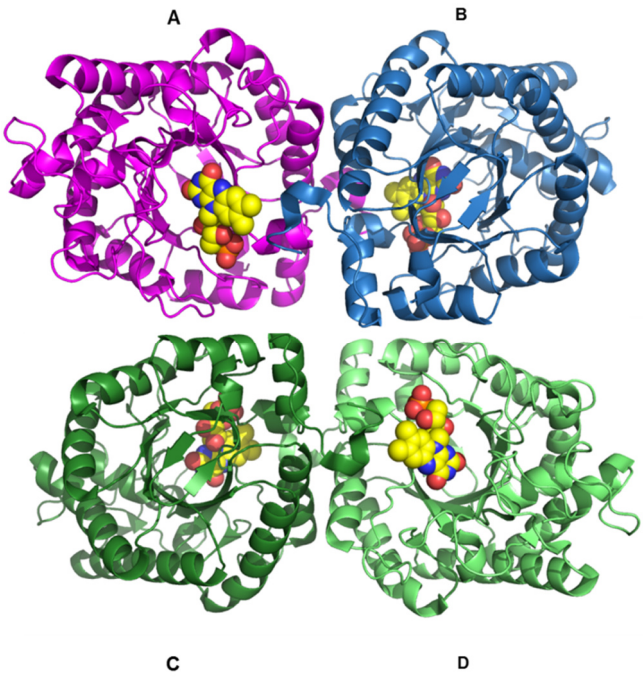

Figure 7.6: Ribbon diagram of YqjM represented in orthogonal mode.
Each subunit is coloured differently. FMN is shown as spheres. Inherited from [20] and prepared using PyMOL [23].

Apparently, a close interaction of the C-terminus of each YqjM monomer with its neighbouring subunit results in formation of basic AB dimers, which are required to maintain structural integrity and catalytic viability. Introduction of the C-terminal His_6-tag in YqjM impairs the formation of the AB dimer and interferes with substrate binding, ultimately constraining catalysis [20, 21].

To our knowledge, this is the first report describing the targeted enzymatic conversion of crotonaldehyde to butyraldehyde.

7.3.3 Consolidated Conversion of Crotylalcohol to Butanol in Presence of NADH/NAD^+ as the Sole Redox Couple

This study aims to create an enzyme cascade for the conversion of crotylalcohol to n-butanol. It was demonstrated that horse liver Adh is able to catalyse the reduction of crotylalcohol to crotonaldehyde and butyraldehyde to n-butanol (7.3.1). Further, we identified YqjM to catalyse the intermediate reaction involving the conversion of crotonaldehyde to butyraldehyde (7.3.2). Therefore, combining horse liver Adh and YqjM allows for consolidated conversion of crotylalcohol to n-butanol using NADH/NAD^+ as the sole redox couple, which significantly reduced the molecular complexity of the reaction system.
The consolidated conversion of crotylalcohol to n-butanol was initially carried out overnight (15 h) at 40 °C using a Hepes buffer system (pH 7) containing YqjM and Adh as well as the

cofactors FMN (required by YqjM), NAD^+ and NADH. All reaction intermediates and products were quantified using an established GC methodology (Figure 7.7).

The GC data indicated that in the reaction system horse liver Adh could only partially convert crotylalcohol to crotonaldehyde (c = 7.8 mM, corresponding to 39 %). YqjM was capable to convert crotonaldehyde to butyraldehyde (c = 15 mM, corresponding to 76 %), while horse liver Adh was able to convert a significant amount of butyraldehyde to the end product n-butanol (c = 10.3 mM).

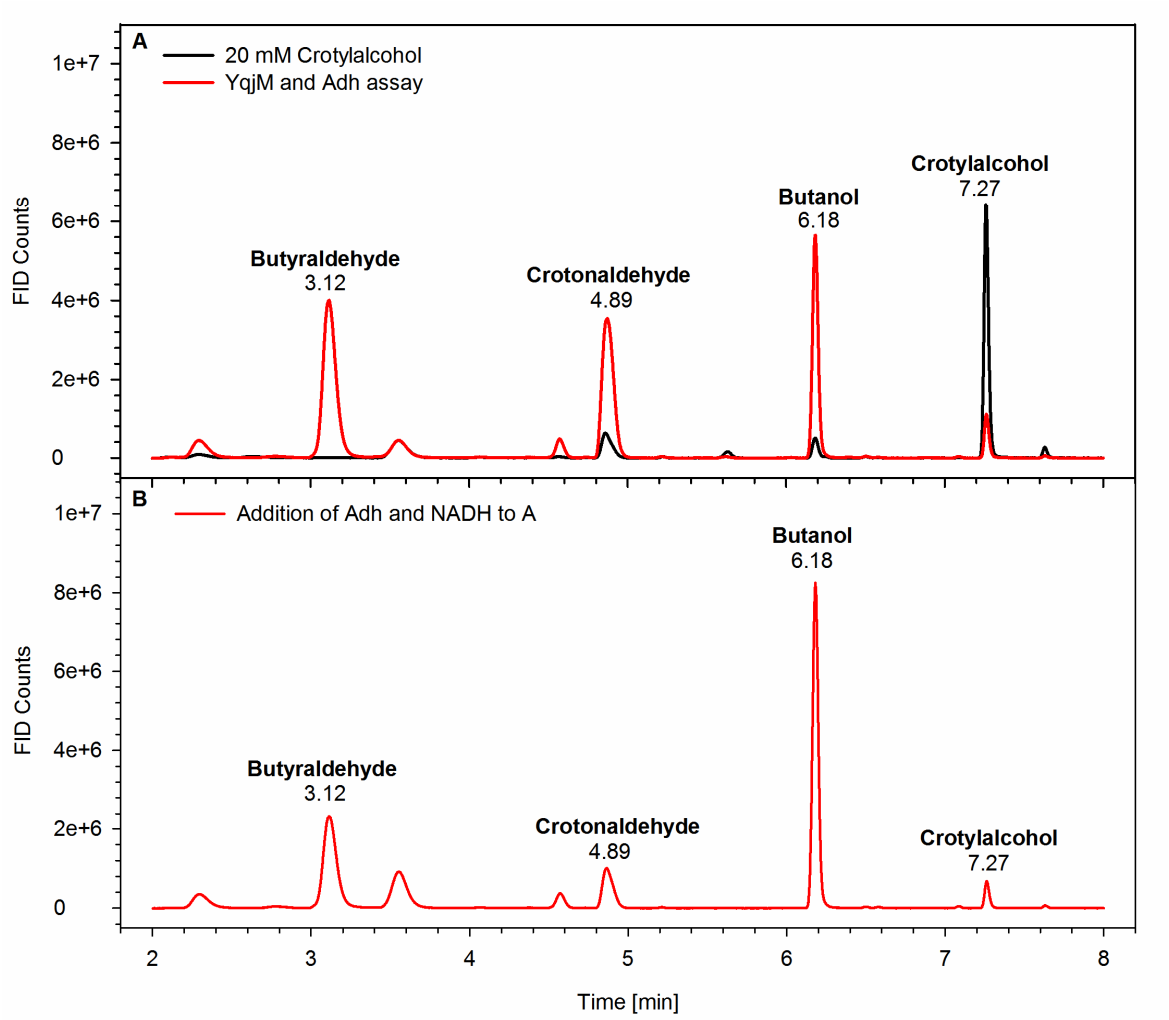

Figure 7.7: Chromatograms of GC measurements;
(A) Result of YqjM and Adh assay with crotylalcohol as substrate (in red) and 20 mM crotylalcohol as control (in black); (B) To assay (A) Adh and NADH were again added and incubated at 40 °C for another hour. Crotylalcohol has a retention time of 7.27 min, n-butanol of 6.18 min, crotonaldehyde of 4.89 min and butyraldehyde of 3.1 min.

Over the entire reaction cascade approximately 51.5 % of the initial crotylalcohol could be converted to n-butanol. This is the first proof of concept that the non-natural tailor-made enzyme cascade in this study could carry out the chemical conversions predicted by computational methods [7].

In an attempt to further optimize the reaction cascade, we added fresh Adh and NADH after the overnight incubation period. This was reasonable as Adh and NADH have limited stability at elevated temperatures [2, 16]. Due to the reaction stoichiometry for NADH utilization (Figure 7.2) and the non-productive reaction of YqjM with O_2, it was expected that the system`s NADH pool was rapidly depleted [21].

After addition of Adh and NADH, the reaction was allowed to continue for an additional hour. The addition of Adh and NADH resulted in a 25 % increase in n-butanol (c = 14.5 mM, corresponding to 72.5 %) yield. Therefore, titration of NADH during the reaction may significantly increase the n-butanol product yield thereby counteracting the effects of molecular oxygen (Figure 7.7B). Similar observations have been made in the cell-free production of isobutanol [2].

This is the first evidence that the synergistic action of YqjM and Adh allow concerted conversion of crotylalcohol to n-butanol. There are significant efforts to establish consolidated biosynthetic pathways in cellular and cell-free production systems [5, 7, 8, 14]. Computational models of alternative pathways can guide experimental approaches to validate alternative, non-natural reaction systems. For the first time we could realise an enzyme cascade that carries out an essential reaction module in non-natural aerobic n-butanol biosynthesis predicated by computational models [7].

7.3.4 Conversion of Crotonaldehyde to Butyraldehyde by *Td*Ter

We showed that YqjM from *B. subtilis* and Adh from horse liver worked together as coupled enzymes and were hereby performing three different reactions (Figure 7.2).

Wu *et al.* (2011) published crotonyl-CoA can be reduced to butyryl-CoA by the same enzyme, which catalyses reduction of crotonaldehyde to butyraldehyde. In the native n-butanol pathway crotonyl-CoA is reduced by clostridial butyryl-CoA dehydrogenases (Bcd). Bcd is an anaerobic enzyme, which needs two electron-transfer-proteins for its activity (Chapter 6) [24]. Therefore, the aerobically working trans-2-enoyl CoA reductase from *Treponema denticola* (*Td*Ter) is often used [25].

As a consequence, we evaluated, if YqjM is also able to reduce crotonyl-CoA and *Td*Ter to reduce crotonaldehyde.

In a first approach, *Td*Ter was incubated with NADH and crotonaldehyde for one hour in a water bath at 40 °C. Afterwards the assay was analysed by GC measurements showing that no crotonaldehyde was converted to butyraldehyde. To support a possible *Td*Ter activity on crotonaldehyde, Adh was added to the reaction mixture in order to shift reaction equilibrium towards product formation. In a further assay *Td*Ter, Adh, crotylalcohol, NADH and NAD^+ were incubated together overnight at 40 °C. Despite conversion of crotylalcohol to

crotonaldehyde by Adh action, no *Td*Ter further working on the aldehyde substrate could be detected (Figure 7.8).

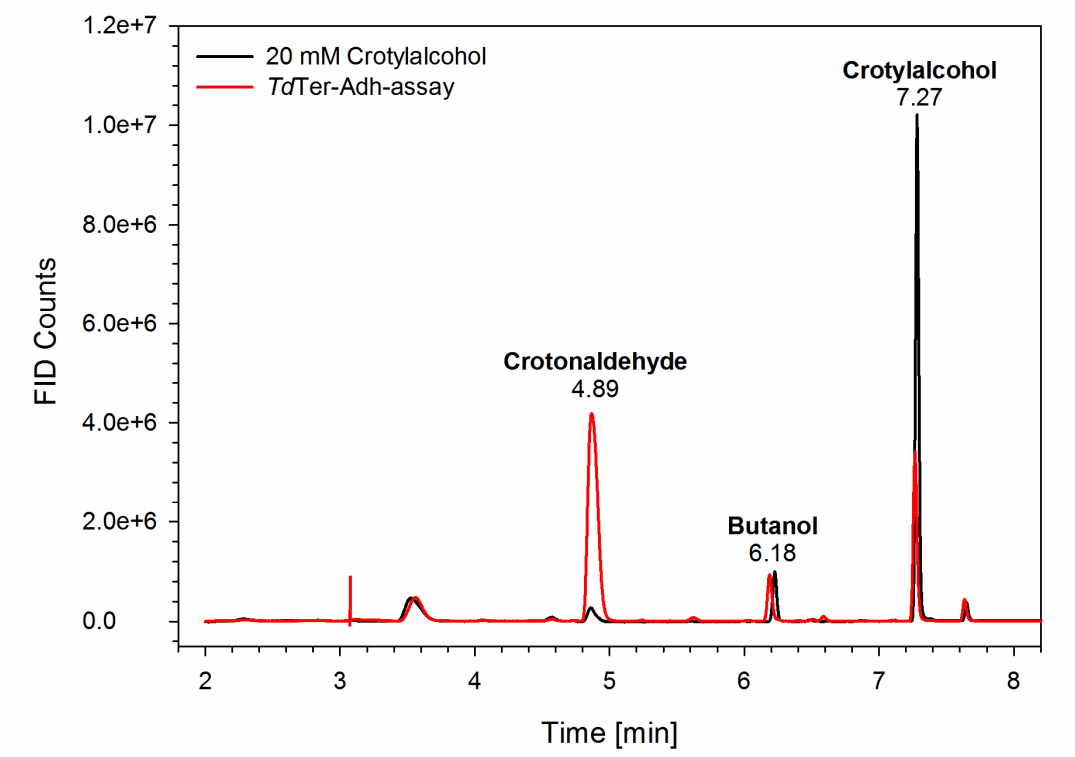

Figure 7.8: Chromatogram of GC measurement;
Result of *Td*Ter-Adh assay with crotylalcohol as substrate (in red) and 20 mM crotylalcohol as control (in black). Crotylalcohol has a retention time of 7.27 min, n-butanol of 6.18 min and crotonaldehyde of 4.89 min.

Additionally, the catalytic activity of YqjM with crotonyl-CoA as substrate was tested. Therefore, the remaining crotonyl-CoA as well as the built butyryl-CoA were measured by HPLC. Again no activity could be detected, showing, that despite the similar reaction mechanism the substrate differences are crucial, in contrast to the prediction of Wu *et al.* (2011) [7].

7.4 CONCLUSIONS

Due to its enhanced energy content and hydrophobic properties, bio-based n-butanol is a desired next generation building block for renewable chemical and fuel processes [1, 2]. While cellular n-butanol production systems suffer from limited productivity due to end-product toxicities and unproductive metabolic side reactions [3]. Recently, cell-free enzyme cascades emerge as alternative production systems that provide mass efficient production of platform chemicals and rapid adaptability to harsh process conditions [5].

Natural biosynthetic pathways involved in cellular n-butanol production are highly complex, involving multiple reaction steps and several cofactors [3]. More recently, computational

methodologies have been employed to predict non-natural reaction steps for the conversion of pyruvate to n-butanol [7]. These computationally predicted reaction modules allow for a significant reduction in molecular complexity compared to their natural counterparts. Hence, computational pathway design may guide experimental efforts to design a consolidated enzyme cascade for n-butanol production. A key reaction module in the predicted n-butanol production pathway is the conversion of crotylalcohol to n-butanol. In this study, we presented a new, non-natural enzyme cascade that allows for the consecutive conversion of crotylalcohol to n-butanol via crotonaldehyde and butyraldehyde. Horse liver Adh could be identified to catalyse both the conversion of crotylalcohol to crotonaldehyde and the final oxidation of butyraldehyde to n-butanol with good yields. Further, the 2-enoate reductase from *B. subtilis* YqjM could be identified to catalyse the intermediate conversion of crotonaldehyde to butyraldehyde.

Interestingly, both Adh and YqjM can utilize the same NAD^+/NADH redox system, which allowed to design a cell-free enzyme cascade with significant reduction of molecular complexity. Application of both Adh and YqjM allowed the consolidated three step conversion of crotylalcohol to n-butanol utilizing the pronounced substrate promiscuity of the employed enzyme systems. Reaction analysis indicated that the non-productive side reaction of YqjM with molecular oxygen derived from the reaction medium, leads to rapid depletion of the available NADH pool, thereby limiting n-butanol yields. Initial optimisation of the reaction system indicates that NADH titration during the reaction can increase conversion efficiency of crotylalcohol to n-butanol. Alternatively, the reaction may be conducted under anaerobic conditions, thereby eliminating the reaction of oxygen with YqjM.

This is the first report demonstrating that non-natural enzyme systems can be used to validate computational models of alternative n-butanol production pathways. In conclusion, computationally predicted reaction pathways can guide the experimental development of non-natural biosynthesis routes for molecular efficient, consolidated n-butanol production systems. These developments are essential for the design of molecular and cost efficient industrial processes.

7.5 REFERENCES

1. **Himmel ME, Ding SY, Johnson DK, Adney WS, Nimlos MR, Brady JW, Foust TD.** 2007. Biomass recalcitrance: engineering plants and enzymes for biofuels production. Science **315:**804-807.
2. **Guterl JK, Garbe D, Carsten J, Steffler F, Sommer B, Reisse S, Philipp A, Haack M, Rühmann B, Koltermann A, Kettling U, Brück T, Sieber V.** 2012. Cell-free metabolic engineering: production of chemicals by minimized reaction cascades. ChemSusChem **5:**2165-2172.
3. **Dürre P.** 2007. Biobutanol: an attractive biofuel. Biotechnology journal **2:**1525-1534.
4. **Steen EJ, Chan R, Prasad N, Myers S, Petzold CJ, Redding A, Ouellet M, Keasling JD.** 2008. Metabolic engineering of Saccharomyces cerevisiae for the production of n-butanol. Microb Cell Fact **7:**36.
5. **Zhang YH.** 2010. Production of biocommodities and bioelectricity by cell-free synthetic enzymatic pathway biotransformations: challenges and opportunities. Biotechnol Bioeng **105:**663-677.
6. **Yan Y, Liao JC.** 2009. Engineering metabolic systems for production of advanced fuels. J Ind Microbiol Biotechnol **36:**471-479.
7. **Wu D, Wang Q, Assary RS, Broadbelt LJ, Krilov G.** 2011. A computational approach to design and evaluate enzymatic reaction pathways: application to 1-butanol production from pyruvate. J Chem Inf Model **51:**1634-1647.
8. **Ranganathan S, Maranas CD.** 2010. Microbial 1-butanol production: Identification of non-native production routes and in silico engineering interventions. Biotechnology journal **5:**716-725.
9. **Nielsen DR, Leonard E, Yoon SH, Tseng HC, Yuan C, Prather KL.** 2009. Engineering alternative butanol production platforms in heterologous bacteria. Metab Eng **11:**262-273.
10. **Pace CN, Vajdos F, Fee L, Grimsley G, Gray T.** 1995. How to measure and predict the molar absorption coefficient of a protein. Protein science : a publication of the Protein Society **4:**2411-2423.
11. **Gasteiger E, Hoogland C, Gattiker A, Duvaud Se, Wilkins M, Appel R, Bairoch A.** 2005. Protein Identification and Analysis Tools on the ExPASy Server, p. 571-607. *In* Walker J (ed.), The Proteomics Protocols Handbook. Humana Press.
12. **Stoll VS, Blanchard JS.** 2009. Buffers: Principles and Practice1. Methods in enzymology **463:**43-56.
13. **Orbegozo T, de Vries JG, Kroutil W.** 2010. Biooxidation of primary alcohols to aldehydes through hydrogen transfer employing janibacter terrae. European Journal of Organic Chemistry **2010:**3445-3448.
14. **Light D, Dennis M, Forsythe I, Liu C-C, Green D, Kratzer D, Plapp B.** 1992. Alpha-isoenzyme of alcohol dehydrogenase from monkey liver. Cloning, expression, mechanism, coenzyme, and substrate specificity. Journal of Biological Chemistry **267:**12592-12599.
15. **Petersen DJ, Welch RW, Rudolph FB, Bennett GN.** 1991. Molecular cloning of an alcohol (butanol) dehydrogenase gene cluster from Clostridium acetobutylicum ATCC 824. Journal of bacteriology **173:**1831-1834.
16. **Brand L, Everse J, Kaplan NO.** 1962. Structural Characteristics of Dehydrogenases*. Biochemistry **1:**423-434.
17. **Jankowski MD, Henry CS, Broadbelt LJ, Hatzimanikatis V.** 2008. Group contribution method for thermodynamic analysis of complex metabolic networks. Biophys J **95:**1487-1499.
18. **Fitzpatrick TB, Amrhein N, Macheroux P.** 2003. Characterisation of YqjM, an Old Yellow Enzyme homolog from Bacillus subtilis involved in the oxidative stress response. The Journal of biological chemistry **278:**19891-19897.

19. **Stueckler C, Hall M, Ehammer H, Pointner E, Kroutil W, Macheroux P, Faber K.** 2007. Stereocomplementary bioreduction of alpha,beta-unsaturated dicarboxylic acids and dimethyl esters using enoate reductases: enzyme- and substrate-based stereocontrol. Org Lett **9:**5409-5411.

20. **Kitzing K, Fitzpatrick TB, Wilken C, Sawa J, Bourenkov GP, Macheroux P, Clausen T.** 2005. The 1.3 Å crystal structure of the flavoprotein YqjM reveals a novel class of old yellow enzymes. Journal of Biological Chemistry **280:**27904-27913.

21. **Fitzpatrick TB, Auweter S, Kitzing K, Clausen T, Amrhein N, Macheroux P.** 2004. Structural and functional impairment of an Old Yellow Enzyme homologue upon affinity tag incorporation. Protein Expr Purif **36:**280-291.

22. **Kohli RM, Massey V.** 1998. The oxidative half-reaction of Old Yellow Enzyme. The role of tyrosine 196. The Journal of biological chemistry **273:**32763-32770.

23. **DeLano W.** The PyMOL Molecular Graphics System on World Wide Web. 2002. There is no corresponding record for this reference.

24. **Inui M, Suda M, Kimura S, Yasuda K, Suzuki H, Toda H, Yamamoto S, Okino S, Suzuki N, Yukawa H.** 2008. Expression of Clostridium acetobutylicum butanol synthetic genes in Escherichia coli. Appl Microbiol Biotechnol **77:**1305-1316.

25. **Tucci S, Martin W.** 2007. A novel prokaryotic trans-2-enoyl-CoA reductase from the spirochete Treponema denticola. FEBS Lett **581:**1561-1566.

Chapter 8

Conclusions and Outlook

8.1 CONCLUSIONS

8.1.1 Production of Chemicals via Minimized Reaction Cascades

An innovative, cell-free, aerobic reaction cascade was developed in cooperation between the Technische Universität München and the industrial partner Clariant Produkte Deutschland GmbH (München, Germany).

In this cell-free approach an artificial minimized glycolytic reaction cascade was used to form the central intermediate pyruvate from glucose. Subsequently, biofuels like ethanol, isobutanol and n-butanol can potentially be synthesised cell-free and under aerobic conditions from the intermediate pyruvate. Furthermore, NADH was the sole cofactor in all catalysed reactions.

Cell-free reaction cascades exhibit several advantages compared to cell-based systems, namely the possibility to design non-natural biosynthesis pathways, no substrate flux in undesired side reactions and higher tolerance to harsh reaction conditions.

The higher tolerance of enzymes towards solvents enables production of higher solvent titres, which potentially allow simple gravimetric separation of the alcohol from the aqueous reaction phase.

8.1.1.1 Isobutanol Synthesis

Acetohydroxyacid Synthases – Preparation for Crystallisation

The decarboxylation of one molecule pyruvate and the subsequent ligation to another molecule of pyruvate, which is involved in isobutanol synthesis was one focus of this work.

This reaction is performed by two different enzyme-families. On the one hand by acetohydroxyacid synthases (AHAS) originating from the branched-chain amino acid (BCAA) biosynthetic pathway and on the other hand from acetolactate synthases (Als) originating from butane-2,3-dione biosynthesis pathway.

Structurally, AHASs are composed of one catalytic and one regulatory subunit and only the holoenzyme exhibits full catalytic activity. AHAS are not only interesting for isobutanol synthesis, but also from a structural perspective. At present, no crystal structure of a bacterial AHAS complex is available. As we were able to acquire Dr. Bernhard Loll from the FU Berlin as our cooperation partner for enzyme crystallization, we aimed to solve the crystal structure of a bacterial AHAS complex.

Therefore, we considered two different bacterial AHAS from *E. coli* (AHAS II) and from *B. stearothermophilus*. As preliminary crystallisation studies of *E. coli* AHAS II (IlvG) did not lead to a valid crystal structure, it was tried to solve it in this study. AHAS from

B. stearothermophilus (IlvBN) was selected for its thermophilic nature allowing industrial applications. In this study, most work was spent on expressing the regulatory and catalytic subunit in equal amounts. Additionally, several variants of *ilvBN* were cloned to maximize crystallization potential. An alignment between IlvB and IlvG revealed that IlvG is 13 amino acids shorter than IlvB. As IlvG was already crystallized, a 13 amino acids truncated *ilvBN* variant was cloned.

Another protein modification aimed to reduce surface entropy. Therefore, surface exposed arginines and lysines were mutated to alanines and three mutation pairs were cloned separately and in all possible combinations.

Finally, all cloned constructs were tested for enzyme expression and all relevant constructs were subsequently transferred to our cooperation partner for crystallographic studies.

AHAS Activity Assays

For industrial applicability of AHAS a highly thermostable and solvent tolerant variant is required. We conducted a literature study and identified a pyruvate decarboxylase assay for determination of AHAS activity and thermostability. Additionally, a reported GC assay for acetolactate detection was improved by using potassium permanganate instead of sulphuric acid.

Considering Structure Function Correlation of AlsS

Als from *Bacillus subtilis* (AlsS) can form acetolactate, but also catalyses the decarboxylation of 2-ketoisovalerate (KIV), another intermediate in non-natural isobutanol synthesis.

AlsS is thus interesting for industrial approaches, as it minimizes the number of required enzymes for isobutanol synthesis. Additionally, Als consists of one subunit only, simplifying enzyme expression and purification. Initially, AlsS activity towards each substrate was determined. Data indicated that activity towards KIV is only a side reaction with low catalytic activity of 53 mU/mg. Subsequently, pH-, temperature-, and solvent- tolerances, in the presence of pyruvate as substrate, were determined. AlsS has its optima at pH 6 and 50 °C, respectively. In the presence of either 3 % isobutanol, 3 % n-butanol or ~13 % ethanol AlsS still exhibits 50 % activity. Therefore, AlsS is suitable for isobutanol production, but activity towards KIV had to be improved. In a cooperation with the FU-Berlin we were able to solve the crystal structure of AlsS with the cofactors TPP and $MgCl_2$ with a resolution of 2.34 Å. The structural data were used to obtain enzyme variants with improved activities and enhanced selectivity for KIV. We substituted critical amino acids for catalysis and substrate recognition. These variants were screened for activity towards pyruvate and KIV as well as for their thermostability at 50 °C and 60 °C.

We were able to identify catalytically relevant active amino acids and a variant with a marginally improved KIV activity.

8.1.1.2 Butanol Synthesis

Butanol is a next generation building block for renewable chemical and biofuel processes due to its enhanced energy content and hydrophobicity compared to first generation fuels such as ethanol. Current, cell-based n-butanol production systems are not mass efficient due to side products like ethanol and acetone. In addition, enzyme systems involved in n-butanol production are often only marginally characterised both structurally and biochemically.

Reduction of Acetoacetyl-CoA

A part of this work focused on identification and correlation of biochemical and structural features of ß-hydroxybutyryl-CoA dehydrogenase from *Clostridium acetobutylicum* ATCC 824 (*Ca*Hbd). We have applied state of the art structural modelling procedures to create a high quality model of *Ca*Hbd. Subsequently, we have attempted to correlate *Ca*Hbd biochemical properties to its structural features. Purified, recombinant *Ca*Hbd is capable of the reversible, pH dependent reduction of acetoacetyl-CoA (acacCoA) over a pH range of 5 - 9. The reverse reaction with ß-hydroxybutyryl-CoA (ß-hbCoA) occurs only at pH 9 - 11 and is 5 times slower than the reaction with acacCoA.

The catalytic constants indicate that the enzyme shows a clear preference to NADH/NAD^+ as a cofactor, while only residual activity with NADPH could be observed. In addition, we could identify NAD^+ as a non-competitive inhibitor of the *Ca*Hbd reaction with acacCoA. This indicates that in n-butanol biosynthesis acacCoA conversion to ß-hbCoA is tightly controlled. Additionally, we have characterised the thermo- and solvent stability of *Ca*Hbd. Interestingly, *Ca*Hbd is extremely thermostable with an apparent T_m of 79 °C and an activity half of 1 h at 80 °C. Furthermore, *Ca*Hbd is surprisingly solvent stable. At n-butanol concentrations up to 10 % (v/v) 45 % activity are remaining over extended time periods.

Reduction of Crotonyl-CoA

Two different butyryl-CoA dehydrogenases from *C. acetobutylicum* ATCC 824 (*Ca*Bcd) and from *G. thermodenitrificans* (*Gth*Bcd) were considered, as well as a trans-2-enoyl-CoA reductase from *T. denticola* (*Td*Ter).

*Ca*Bcd needs two electron-transfer proteins, i.e. *Ca*EtfA and *Ca*EtfB, for its activity and an anaerobic or semi-aerobic environment. For industrial applicability oxygen tolerance of the applied enzyme systems is preferred as it simplifies process design. Therefore, *Ca*Bcd was classified as not suitable for our n-butanol production.

*Td*Ter is a biochemically and structurally well characterised enzyme as it combines several advantages compared to clostridial Bcd. *Td*Ter shows high activity and specificity towards crotonyl-CoA as substrate, needs NADH as sole cofactor and does not catalyse the oxidation of butyryl-CoA, resulting in an irreversibility of the reaction. However, *Td*Ter is strongly inhibited by NAD^+ as well as by butyryl-CoA and possesses relatively low thermostability.
Therefore, *Gth*Bcd was tested as a more thermostable Bcd. However, *Gth*Bcd showed no activity in the photometrical assay suggesting that *Gth*Bcd also requires electron-transfer proteins such as *Ca*Bcd for activity. Furthermore, it can be concluded that *Gth*Bcd may also need an anaerobic or semi-aerobic environment like *Ca*Bcd to function. In summary, it turned out that *Gth*Bcd is no suitable candidate for aerobic n-butanol production.

Non-natural n-Butanol Production Pathways

Computational methodologies have been employed to predict non-natural reaction steps for the conversion of pyruvate to n-butanol. These computationally predicted reaction modules allow for a significant reduction in molecular complexity compared to their natural counterparts. A key reaction module in a predicted n-butanol production pathway is the conversion of crotylalcohol to n-butanol. In a non-natural enzyme cascade we converted crotylalcohol to n-butanol via crotonaldehyde and butyraldehyde. Horse liver Adh could be identified to catalyse both the conversion of crotylalcohol to crotonaldehyde and the final reduction of butyraldehyde to n-butanol with good yields. Further, the 2-enoate reductase from *B. subtilis* YqjM could be identified to catalyse the conversion of crotonaldehyde to butyraldehyde.
Interestingly, both Adh and YqjM can utilize the same NAD^+/NADH redox system, which allowed to design a cell-free enzyme cascade with significant reduction of molecular complexity.

8.2 OUTLOOK

8.2.1 Production of Chemicals via a Minimized Reaction Cascade

Pyruvate, the central intermediate in our cell-free systems, may serve as a starting substrate for biosynthesis of many other compounds. Optimization of participating systems may allow improvements and extension of the production system with focus on activity, solvent tolerance and thermostability.
Further research might focus on the usage of cost efficient sugar resources derived from lignocellulose hydrolysate as process feedstock.

8.2.1.1 Isobutanol Biosynthesis

A further research perspective might be to obtain an AlsS variant with good activity towards pyruvate and KIV. In this respect, directed mutagenesis of *alsS* with *error prone* PCR might be a targeted option. A high throughput screening is possible as KIV consumption can be detected by NADH depletion in a photometrical assay. First approaches in our lab showed, that the low activity of AlsS towards KIV will pose a problem. On the one hand, a lot of enzyme is required for a detectable reaction. However, the large amounts of crude enzyme extract in the assay can distort the result. On the other hand, a reliable and effective method for cell disruption has to be developed as different amount of enzymes in the assays can also distort the result.

8.2.1.2 Butanol Synthesis

In our lab several approaches for cell-free n-butanol synthesis were conducted, but at present no reliable result was achieved and further research is still ongoing.
Especially the inhibitory effects of substrates and products on their corresponding enzymes as well as their cofactors are problematic. This was demonstrated by *Ca*Hbd and *Td*Ter work. Therefore, the substrate flux requires a definite cofactor balancing to enable efficient conversion of respective CoA intermediates towards n-butanol as the end product.
Additionally, some of our enzymes deplete NADH without substrate conversion (e.g. *Td*Ter). Over an extended time period, this causes problems in substrate conversion. A solution might be synthetic cofactor mimics, which may not inhibit the enzymes.
Alternatively, cofactor regeneration systems, like a formate dehydrogenase can be applied. In this system formate is converted to carbon dioxide (CO_2) and hydrogen (H^+), whereas one NAD^+ is oxidized to NADH. CO_2 and H^+ are gaseous and can thus leave the reaction set-up.

Furthermore, enzymes, like *Ca*Hbd, with an extremely high thermo- and solvent stability are important enzyme systems to be selected for targeted cell and cell-free n-butanol production systems.
For the reduction of crotonyl-CoA a more stable enzyme than *Td*Ter is required or its thermostability has to be improved by genetic engineering. However, high throughput screening efforts are limited by extremely expensive CoA derivates.

Additionally, an alternative n-butanol biosynthesis pathway might be designed, which may not require CoA-dependent substrates. One step in this direction was our consolidated n-butanol synthesis from the non-natural intermediate crotylalcohol with only two enzyme systems. A problem hereby is the non-productive side reaction of YqjM with molecular oxygen derived from the reaction medium. This side reaction leads to rapid depletion of the available

NADH pool and limits n-butanol yields. Initial optimisation of the reaction system indicates that NADH titration during the reaction can increase conversion efficiency of crotylalcohol to n-butanol. Alternatively, the reaction may be conducted under anaerobic conditions, thereby eliminating the reaction of oxygen with YqjM.

In conclusion, computationally predicted reaction pathways can guide the experimental development of non-natural biosynthesis and are essential for the design of molecular and cost efficient industrial processes.

9 ANNEX

9.1 MATERIALS

Table 9.1: List of devices.

Device	Unit Type	Manufacturer, Place
Autoclave	VE-150	Systec GmbH, Wettenberg, Germany
Balances	440-45N	Kern&Sohn GmbH, Balingen, Germany
	Pioneer™	Ohoaus Europe GmbH, Nänikon, Switzerland
Cell exposure	Emulsiflex-B15	Avestin, Mannheim, Germany
Centrifuges	Avanti™ J-20XP	Beckman Coulter, Krefeld, Germany
	Function Line, Labofuge 400R	Heraeus Holding GmbH, Hanau, Germany
	Biofuge fresco	Heraeus Holding GmbH, Hanau, Germany
	Centrifuge 5424	Eppendorf, Hamburg, Germany
Circular Dichroism Spectropolarimeter	J-715	Jasco GmbH, Tokyo, Japan
Clean Bench	LaminAir HB2448	Heraeus Holding GmbH, Hanau, Germany
Electrophoresis chambers:		
agarose gel-electrophoresis	Mini Sub®Cell GT	Bio-Rad Laboratories, München, Germany
SDS gel-electrophoresis	Mini Protean Tetra System	Bio-Rad Laboratories, München, Germany
IEF-gel-electrophoresis	Xcell Sure Lock™	LifeTechnologie GmbH, Darmstadt, Germany
Freezer -20 °C		Robert Bosch GmbH, Crailsheim, Germany
Freezer -80 °C	Ultra Low Temperature	New Brunswick by Eppendorf, Hamburg, Germany
Heating Block	Thermomixer comfort	Eppendorf, Hamburg, Germany
HPLC	1100 system	Agilent Technologies Deutschland GmbH, Böblingen, Germany
High-purity water system	arium® pro UV	Satorius stedim Biotech, Göttingen, Germany
Imaging System	Gel Doc™ XR+	Bio-Rad Laboratories, München, Germany
Incubator	Function Line	Thermo Scientific (former Hereaus), Schwerte, Germany
Incubator-Shaker	innova® 44	New Brunswick by Eppendorf, Hamburg, Germany

Device	Unit Type	Manufacturer, Place
Magnetic stirrer	MR Hei-Standard	Heidolph Instruments GmbH&Co.KG, Schwabach, Germany
Microliter pipettes	Research 2.5, 10, 100, 1000, 5000	Eppendorf, Hamburg, Germany
Microwave	Powertec Kitchen Mikrowelle	EFBE Elektrogeräte GmbH, Bad Blankenburg, Germany
pH-Meter	SevenGo™ pH	Mettler-Toledo GmbH, Gießen, Germany
Photometer	8453	Hewlett Packard, Palo Alto, United States of America
Power supply	EV243	Consort bvba, Turnhout, Belgium
Plate Reader	Enspire 2	Perkin Elmer, Rodgau, Germany
Thermo-Cycler	My Cycler™	Bio-Rad Laboratories, München, Germany
	Mastercycler personal	Eppendorf, Hamburg, Germany
Trace GC Ultra	DSQ II	Thermo Scientific, Schwerte, Germany
Vortex	Genie 2	Scientific Industry Inc., New York, United States of America
Waterbath		Memmert GmbH + Co.KG, Schwabach, Germany

Table 9.2: List of chemicals.

Name	Manufacturer	Place
Acetoacetyl-CoA	Sigma-Aldrich	Taufkirchen, Germany
Agarose	Applichem GmbH	Darmstadt, Germany
n-**b**utanol	Merck KG Aa	Grafing, Germany
2-Buten-1-ol cis and trans (Crotylalcohol)	VWR	Darmstadt, Germany
Butyryl-CoA	Sigma-Aldrich	Taufkirchen, Germany
Coomassie brilliant blue G250	Serva Electrophoresis GmbH	Heidelberg, Germany
Crotonaldehyde	Sigma-Aldrich	Taufkirchen, Germany
Crotonyl-CoA	Sigma-Aldrich	Taufkirchen, Germany
3-(Cyclohexylamino)-1-propanesulfonic acid **(**CAPS)	Applichem GmbH	Darmstadt, Germany
Deoxyribonucleotides	Thermo Scientificor Rapidozym	Schwerte, Germany, Berlin, Germany
Diacetyl (= 2,3 Butandione)	VWR	Darmstadt, Germany
Ethanol	Carl Roth GmbH + Co. KG	Karlsruhe, Germany
Flavin-adenin-dinucleotide	Sigma-Aldrich	Taufkirchen, Germany
Flavin-adenin-mononucleotide	Sigma-Aldrich	Taufkirchen, Germany
Glycerol	Applichem GmbH	Darmstadt, Germany

Name	Manufacturer	Place
Hepes-buffer	Carl Roth GmbH + Co. KG	Karlsruhe, Germany
ß-Hydroxybutyryl-CoA	Sigma-Aldrich	Taufkirchen, Germany
Imidazole	Carl Roth GmbH + Co. KG	Karlsruhe, Germany
IPTG	Applichem GmbH	Darmstadt, Germany
Isobutyraldehyde	Sigma-Aldrich	Taufkirchen, Germany
Kanamycin	Carl Roth GmbH + Co. KG	Karlsruhe, Germany
2-Ketoisovalerate	Sigma-Aldrich	Taufkirchen, Germany
Magnesium chloride	Carl Roth GmbH + Co. KG	Karlsruhe, Germany
2-Methylpropan-1-ol (= Isobutanol)	Sigma-Aldrich	Taufkirchen, Germany
3-Methyl-2-oxobutanoic acid	Sigma-Aldrich	Taufkirchen, Germany
Nicotinamide adenine dinucleotide disodium salt (NADH and NAD^+)	Carl Roth GmbH + Co. KG	Karlsruhe, Germany
ß-Nicotinamide adenine dinucleotide phosphate tetrasodium salt (NADPH and $NADP^+$)	Applichem GmbH	Darmstadt, Germany
Potassium permanganate	Carl Roth GmbH + Co. KG	Karlsruhe, Germany
Sodium acetate buffer	Applichem GmbH	Darmstadt, Germany
Sodium chloride	Carl Roth GmbH + Co. KG	Karlsruhe, Germany
Sodium phosphate buffer	Sigma-Aldrich	Taufkirchen, Germany
Sodium pyruvate	Carl Roth GmbH + Co. KG	Karlsruhe, Germany
Thiamine pyrophosphate	Carl Roth GmbH + Co. KG	Karlsruhe, Germany
Trichloroacetic acid	Serva Electrophoresis GmbH	Heidelberg, Germany
Tris-buffer	Carl Roth GmbH + Co. KG	Karlsruhe, Germany
Tryptone	Carl Roth GmbH + Co. KG	Karlsruhe, Germany
Urea	Carl Roth GmbH + Co. KG	Karlsruhe, Germany
Yeast Extract	Carl Roth GmbH + Co. KG	Karlsruhe, Germany

Table 9.3: List of kits.

Name	Manufacturer	Place
GeneJET™ Plasmid Miniprep Kit	Thermo Scientific	Schwerte, Germany
Genomic DNA Purification, Kit	Thermo Scientific	Schwerte, Germany
InnuPREP, DOUBLE pure Kit	Analytic Jena AG	Jena, Germany

Table 9.4: List of bought enzymes.

Name	Manufacturer	Place
Alcohol Dehydrogenase, horse liver	Evocatal	Düsseldorf, Germany
DNA-Polymerase: DreamTaq Green DNA polymerase	Thermo Scientific	Schwerte, Germany

Name	Manufacturer	Place
Phusion Polymerase	Thermo Scientific or Finnzymes	Schwerte, Germany Espoo, Finnland
Klenow Fragment	New England Biolabs GmbH	Frankfurt am Main, Germany
Lactate Dehydrogenase, porcine heart	Serva Electrophoresis	Heidelberg, Germany
Restriction enzymes	Thermo Scientific or New England Biolabs GmbH	Schwerte, Germany Frankfurt am Main, Germany
T4-DNA-Ligase	Thermo Scientific or New England Biolabs GmbH	Schwerte, Germany Frankfurt am Main, Germany
T4 Kinase	New England Biolabs GmbH	Frankfurt am Main, Germany

Table 9.5: List of markers.

Name	Manufacturer	Place
GeneRuler™, 1 kb DNA Ladder	Thermo Scientific	Schwerte, Germany
GeneRuler ™, 100 bp DNA Ladder	Thermo Scientific	Schwerte, Germany
IEF Standard (Broad Range pI 4.45 – 9.6)	Bio-Rad Laboratories,	München, Germany
Page Ruler Unstained, Protein Ladder	Thermo Scientific	Schwerte, Germany
Unstained Protein Molecular Weight Marker	Thermo Scientific	Schwerte, Germany

9.1.1 *E. coli* Strains

***E. coli* HMS174(DE3)** Merck KGaA, Darmstadt, Germany

(F^- *recA1 hsdR*(r_{K12}^- m_{K12}^+) (DE3) (Rif ^{R}))

***E. coli* XL1-Blue** Stratagene, Waldbronn, Germany

(*recA1 endA1 gyrA96 thi-1 hsdR17 supE44 relA1 lac* [F´ *proAB lacI*q*Z*Δ*M15* Tn*10* (Tetr)]

***E. coli* BL21DE3** Novagen, Nottingham, UK

(*fhuA2 [lon] ompT gal (γ DE3) [dcm]* Δ*hsdS*λ *DE3 =* λ *sBamHIo* Δ*EcoRI-B int::(lacI::PlacUV5::T7 gene1) i21* Δ*nin5)*

***E. coli* BL21 pLysS** New England Biolabs (Frankfurt, Germany)

(F-ompT hsdSB(rB-mB-) gal dcm (DE3) pLysS (CamR)

9.1.2 Vectors

Table 9.6: List of basic vectors.

vector name	base	characteristics	origin	IBK_P_
pET28a		kan^R, His	Novagen	4
pCBR_HisC	pET28a	kan^R, His	Guterl, et al., 2012	23
pCBR_HisN	pET28a	kan^R, His	Guterl, et al., 2012	24
pCBR_HisNo	pET28a	kan^R,	Guterl, et al., 2012	22
pETGST1a	pET28a	kan^R, His	Günther Stierl	121
pETGST1a_BamHI	pET28a	kan^R, His	Günther Stierl	198
p613		kan^R, His	Clariant GmbH	170
pTXB3		amp^R, GryA	New England Biolab	191

Table 9.7: List of provided and bought vectors.

vector name	base	characteristics	origin	IBK_P_
Dü-pDRIVE_CRT+BCDII	n. a.	kan^R, amp^R	Clariant GmbH	42
Dü-pDRIVE_ ETFB+ETFA+HBD	n. a.	kan^R, amp^R	Clariant GmbH	/
pMA_GthBcdI	pMA	amp^R	GeneArt	/
pMA_TdTCR	pMA	amp^R	GeneArt	95
pMA_SsAAS	pMA	amp^R	GeneArt	98
pMS-RQ-BS_BsuAls	pMS-RQ	spectinomycin	GeneArt	104

n. a. - not available;

Table 9.8: List of vectors with genes out of the n-butanol pathway.

vector name	base	characteristics	origin	IBK_P_
pCBR_HisC_bcdI	pCBR_HisC	kan^R, His	this work	83
pCBR_HisN_bcdI	pCBR_HisN	kan^R, His	this work	82
pCBR_HisNo_bcdI	pCBR_HisNo	kan^R	this work	84
pCBR_HisC_hbd	pCBR_HisC	kan^R, His	this work	85
pCBR_HisNo_hbd	pCBR_HisNo	kan^R	this work	86
pCBR_HisNo_BCDII	pCBR_HisNo	kan^R	this work	87
pCBR_HisC_BCDII	pCBR_HisC	kan^R, His	this work	203
pCBR_HisC_ETFA	pCBR_HisC	kan^R, His	this work	88

vector name	base	characteristics	origin	IBK_P_
pCBR_HisNo_ETFA	pCBR_HisNo	kan^R	this work	89
pCBR_HisC_ETFB	pCBR_HisN	kan^R, His	this work	91
pCBR_HisN_ETFB	pCBR_HisC	kan^R, His	this work	90
pCBR_HisNo_ETFB	pCBR_HisNo	kan^R	this work	92
pCBR_HisC_TCR	pCBR_HisC	kan^R, His	this work	96
pCBR_HisNo_TCR	pCBR_HisNo	kan^R	this work	97
pET28a_YqjM	pET28a	kan^R	this work	120

Table 9.9: List of vectors with genes out of the isobutanol pathway.

vector name	base	characteristics	origin	IBK_P_
pCBR_HisC_AlsSs	pCBR_HisC	kan^R, His	this work	99
pCBR_HisNo_AlsSs	pCBR_HisNo	kan^R	this work	100
pCBR_HisNo_IlvBN	pCBR_HisNo	kan^R	this work	101
pCBR_HisC_IlvB	pCBR_HisC	kan^R, His	this work	102
pCBR_HisC_IlvN	pCBR_HisC	kan^R, His	this work	103
pCBR_HisNo_IlvN	pCBR_HisNo	kan^R	this work	126
pET28a_IlvBN_HisN	pET28a	kan^R, His	this work	119
pETGST1a_IlvBN	pETGST1a	kan^R, His, GST	this work	124
pETGST1a_IlvN	pETGST1a	kan^R, His, GST	this work	125
pET_GST1a_IlvB	pETGST1a	kan^R, His, GST	this work	128
p613_IlvN	p613	kan^R, His	this work	172
pET28a_IlvBN_ E185A_E186A_NoHis	pET28a	kan^R, His	this work	183
pET28a_IlvBN_E185A_E186A_ E491A_K492A_HisNo	pET28a	kan^R, His	this work	184
pET28a_IlvBN_Q28E_E30A_NoHis	pET28a	kan^R, His	this work	186
pET28a_IlvBN_E491A_K492A_ NoHis	pET28a	kan^R, His	this work	187
pET28a_IlvBN_Q28A_E30A_ E491A_K492A_NoHis	pET28a	kan^R, His	this work	188
pET28a_IlvBN_Q28A_E30A_ E195A_E196A_NoHis	pET28a	kan^R, His	this work	189
pET28a_IlvBN_Q28A_E30A_ E195A_E196A_E491A_K492A_ NoHis	pET28a	kan^R, His	this work	190
pTXB3_IlvB_shortened	pTXB3	amp^R, GryA	this work	192
pTXB3_IlvB	pTXB3	amp^R, GryA	this work	193
pTXB3_IlvN	pTXB3	amp^R, GryA	this work	194
pET28a_ IlvBN_shortened_NoHis	pET28a	kan^R, His	this work	195

vector name	base	characteristics	origin	IBK_P_
pETGST1a_IlvB_shortened	pETGST1a	kan^R, His, GST	this work	196
pET28a_IlvB_8xA_IlvN_N-His	pET28a	kan^R, His	this work	197
pETGST1a_IlvG_R136C	pETGST1a	kan^R, His, GST	this work	199
pETGST1a_IlvB_8xA_IlvN	pETGST1a	kan^R, His, GST	this work	200
pETGST1a_IlvG	pETGST1a	kan^R, His, GST	this work	201
pCBR_HisNo_IlvG_C-His	pCBR_HisNo	kan^R, His	this work	202
pCBR_HisC_AlsS	pCBR_HisC	kan^R, His	this work	105
pCBR_NoHis_AlsS	pCBR_HisNo	kan^R	this work	106
pET_GST1a_AlsS	pETGST1a	kan^R, His, GST	this work	129
pET28a_AlsS_Q487S	pET28a	kan^R, His	this work	137
pETGST1a_AlsS_Q487S	pETGST1a	kan^R, His, GST	this work	138
pET28a_AlsS_Q424S	pET28a	kan^R, His	this work	139
pETGST1a_AlsS_Q424S	pETGST1a	kan^R, His, GST	this work	140
pET28a_AlsS_Q487S_Q424S	pET28a	kan^R, His	this work	141
pETGST1a_AlsS_Q487S_ Q424S	pETGST1a	kan^R, His, GST	this work	142
pET28a_AlsS_K40H	pET28a	kan^R, His	this work	173
pET28a_AlsS_K40I	pET28a	kan^R, His	this work	174
pET28a_AlsS_K40Y	pET28a	kan^R, His	this work	175
pET28a_AlsS_P87A	pET28a	kan^R, His	this work	176
pET28a_AlsS_Q124S	pET28a	kan^R, His	this work	177
pET28a_AlsS_Y481A	pET28a	kan^R, His	this work	178
pET28a_AlsS_M483N	pET28a	kan^R, His	this work	179
pET28a_AlsS_A39P_K40H	pET28a	kan^R, His	this work	180
pET28a_AlsS_A342K_A344E_ A347E	pET28a	kan^R, His	this work	181
pETGST1a_AlsS_A342K_ A344E_A347E	pETGST1a	kan^R, His, GST	this work	182
pET28a_AlsS_T84V	pET28a	kan^R, His	this work	204

9.1.3 Deoxyribonucleotides

Sequences of restriction sites are underlined and mutations are printed in blue.

Table 9.10: Vector specific primers for amplification and sequencing.

primer name	sequence (5′ → 3′)	restriction enzyme	IBK_O_
T7 promotor	TAA TAC GAC TCA CTA TAG GG (20 bp)	/	41
T7 term	CTA GTT ATT GCT CAG CGG T (19 bp)	/	42
5′ pETGST_1a	CAT CCT CCA AAA GGA TCT GGC AGT GGT (27 bp)	/	59

Table 9.11: Primers for amplification of the used enzymes out of the butanol pathway.

primer name	sequence (5′ → 3′)	restriction enzyme	IBK_O_
5′ BcdI pCBR	CAG CAA GGT CTC TCA TAT GGA TTT TAG CCT GAC (33 bp)	*Bsa*I	/
3′ BcdI pCBR	ACA ACC CAG CTG ACG TGC AAT (21 bp)	/	/
5′ BcdII pCBR	CAG CAA GGT CTC TCA TAT GGA TTT TAA TTT AA (32 bp)	*Bsa*I	/
3′ BcdII pCBR	TCT AAA AAT TTT TCC TGA AAT AAC TAA TTT CTG AAC (36 bp)	/	/
5′ EtfA pCBR	CAG CAA GGT CTC TCA TAT GAA TAA AGC AGA TTA CAA GGG (39 bp)	*Bsa*I	/
3′ EtfA pCBR	ATT ATT AGC AGC TTT AAC TTG AGC TAT TAA TTC (33 bp)	/	/
5′ EtfB pCBR	CAG CAA GGT CTC TCA TAT GAA TAT AGT TGT TTG TTT A (37 bp)	*Bsa*I	/
3′ EtfB pCBR	AAT ATA GTG TTC TTC TTT TAA TTT TGA GAC AAC (33 bp)	/	/
5′ Hbd pCBR	CAG CAA GGT CTC TCA TAT GAA AAA GGT ATG TGT TAT AGG T (40 bp)	*Bsa*I	/
3′ Hbd pCBR	TTT TGA ATA ATC GTA GAA ACC TTT TCC TGA TTT TCT TCC (39 bp)	/	/
5' YqjM pET 28a	GCG CCA TGG CCA GAA AAT TAT TTA CAC CTA TTA (33 bp)	*Nco*I	49
3' YqjM pET 28a	ATA TCT CGA GCC AGC CTC TTT CGT ATT GAA CAG GG (35 bp)	*Xho*I	50

Table 9.12: Primers for amplification of the used enzymes out of the isobutanol pathway.

primer name	sequence (5′ → 3′)	restriction enzyme	IBK_O
5′ IlvBN_pCBR	CAG CAA GGT CTC TCA TAT ATG GCA AAG ATG (30 bp)	*Bsa*I	/
3′ IlvBN_pCBR	TTA AAT GAT AAA CGC CGT TTT TTG GTT GG (29 bp)	/	/
5' IlvBN pET28a	CAG CAA CAT ATG GCA AAG ATG (21 bp)	*Nde*I	48
3′ IlvBN-Stop_pET28a	ATA TGC TCG AGC TAT TAA ATG ATA AAC GCC GTT TTT TG (38 bp)	*Xho*I	47
5′ IlvBN_middle	TTC TTG GCC TTG GCG GCT TCC CA (23 bp)	/	51
5' IlvBN_ pETGST_1a	GGC GCC ATG GCA AAG ATG AAC GTG GAG GA (29 bp)	*Nco*I	56
3' IlvB_ pETGST1a	GCG CCT CGA GTT ACT ATT CTT CGC ACG CTT TCA C (34 bp)	*Xho*I	61
3' IlvN_ pETGST_1a	GCG CCT CGA GCT ACT AAA TGA TAA ACG CCG TTT TT (35 bp)	*Xho*I	58
5' IlvN_ pETGST1a	ACG GCC ATG GCG ATC ACG ATG ACG GTC AA (29 bp)	*Nco*I	60
5' IlvB_ 13AS_*Nco*I	GGC GCC ATG GCA AGC GGG TCG ATG ATG TTG AT (32 bp)	*Nco*I	195
5' IlvN_p613	GCG GCC CGG GAT GAT CAC GAT GAC GCT CAA CAA CCG CCC AGG CGT GTT A (49 bp)	*Sma*I	112
5' IlvN p613 6V	GCG GCC CGG GAT GAT CAC GAT GAC GGT CAA CAA CCG CCC AGG CGT GTT A (49 bp)	*Sma*I	131
3' IlvN p613I	TAT ACC TCG AGA ATG ATA AAC GCC GTT TTT TGG TTG GCT GC (41 bp)	*Xho*I	113
5' IlvN_ AAAAAAAA	GCA GCA GCA GCA GCA GCA GCA GCA ATG ATC ACG ATG ACG GTC AAC (45 bp)	/	126
3' IlvB_ AAAAAAAA	TGC TGC TGC TGC TGC TGC TGC TGC TTC TTC GCA CGC TTT CAC CCC CA (47 bp)	/	127
3' IlvB_8xA_2	CGC GGC GGC CGC GGC TGC CGC TGC TTC TTC GCA CGC TTT CAC CCC CA (47 bp)	/	193
5' 8xA_IlvN_2	GCA GCG GCA GCC GCG GCC GCC GCG ATG ATC ACG ATG ACG GTC AAC (45 bp)	/	194
3' IlvB_16xA	GGC CGC TGC TGC CGC CGC GGC GGC CGC GGC GGC CGC GGC TGC CGC TGC TTC TTC (54 bp)	/	204
5' IlvN_16xA	GCC GCC GCG GCG GCA GCA GCG GCC ATG ATC ACG ATG ACG (39 bp)	/	205
5′ IlvBN_Q28A_ E30A_f	GAA GGC GGA GGC AGT CGC AGT CAT TTT C (28 bp)	/	132
3′ IlvBN_Q28A_ E30A_r	GAA AAT GAC TGC GAC TGC CTC CGC CTT C (28 bp)	/	133
5′ IlvBN_E185A_ E186A_f	GCA AGC AAA CTG CTG CAT CGT AAT C (25 bp)	/	134

primer name	sequence (5′ → 3′)	restriction enzyme	IBK_O
3′ IlvBN_E185A_ E186A_r	GCA AGC AAA CTG CTG CAT CGT AAT C (25 bp)	/	135
5′ IlvBN_E491A_ K492A_f	CTG TTT TAC GCA GCA CGG TAC TCC C (25 bp)	/	136
3′ IlvBN_E491A_ K492A_r	GGG AGT ACC GTG CTG CGT AAA ACA G (25 bp)	/	137
3' IlvB_PTXB3	GCG CCT CGA GTT CTT CGC ACG CTT TCA C (28 bp)	*Xho*I	198
3' IlvN_PTXB3	GCG CCT CGA GAA TGA TAA ACG CCG TTT TTT GC (32 bp)	*Xho*I	199
5' IlvG_*BamH*I	ATA TGG ATC CAT GAA TGG CGC ACA GTG GGT G (31 bp)	*Bam*HI	196
3' IlvG_*Xho*I	GCG GCT CGA GTG ATA ATT TCT CCA ACA TTT CTG AA (35 bp)	*Xho*I	197
5' IlvG_875_at	GCC GTT AAA TCA ATA TGA CTG GCA GCA ACA CTG CGC G (37 bp)	/	200
3' IlvG_875_at	CGC GCA GTG TTG CTG CCA GTC ATA TTG ATT TAA CGG C (37 bp)	/	201
3' IlvG_Stop_ *Xho*I	GCG CCT CGA GTC ATC ATG ATA ATT TCT CCA ACA TTT C (37 bp)	*Xho*I	202
5' IlvG_*Bsa*I	ATA TGG TCT CAA TGA ATG GCG CAC AGT GGG TG (32 bp)	*Bsa*I	203
5′ AlsSs_pCBR	CAG CAA GGT CTC TCA TAT ATG CCG ACC GGT GCA CGT A (37 bp)	*Bsa*I	/
3′ AlsSs_pCBR	GCT GCT TTT ACG CGG ATC (18 bp)	/	/
5′ AlsS_pCBR	CAG CAA CGT CTC TCA TAG TCT TGA CAA AAG CAA CAA AAG (39 bp)	*Bsa*I	/
3′ AlsS_pCBR	GAG AGC TTT CGT TTT CAT GAG TTC CCC GAA TT (32 bp)	/	/
5' AlsS_GST_1a	ACT GCC ATG GCC CTG ACC AAA GCA ACC AA (29 bp)	*Nco*I	63
3' AlsS_GST_1a	GCG CCT CGA GTT ACT ACA GGG CTT TGG TTT TCA T (34 bp)	*Xho*I	62
3' AlsS_pET28a	GCG CCT CGA GCA GGG CTT TGG TTT TCA T (28 bp)	*Xho*I	83
3' AlsS K40H	ATC AAA AAC TGC ATC AAT AAT GGC ACC CGG AAT ACC A (37 bp)	/	121
3' AlsS K40I	ATC AAA AAC TGC ATC AAT AAT TGC ACC CGG AAT ACC A (37 bp)	/	120
3' AlsS K40Y	ATC AAA AAC TGC ATC AAT ATA TGC ACC CGG AAT ACC A (37 bp)	/	119
3' AlsS P84A	TTG CCA GAT TGC TTG CAC CTG CAC CGC TGG TAA (33 bp)	/	122
3' AlsS T87V	GCA CCC GGA CCG CTA ACA ACC AGA ACA ACA (30 bp)	/	246

primer name	sequence (5′ → 3′)	restriction enzyme	IBK_O
3' AlsS Q124S	CAG TGC TGC ATT ATC CAG GCT GCT ATG GGT ACG TTT CAG (39 bp)	/	125
5' AlsS Q424S	GAT GAT TAG CAA TGG TAT GTC GAC CTG GGT GTT GC (36 bp)	/	111
5' AlsS Q487S	ACC TAT GAT ATG GTT GCA TTT AGC CAG CTG AAA AAA TAT A (40 bp)	/	82
5' AlsS M483N	GAA CGA TAG CAC CTA TGA TAA TGT TGC ATT TCA GCA G (37 bp)	/	124
5' AlsS Y481A	TTG GAA CGA TAG CAC CGC AGA TAT GGT TGC ATT TCA G (37 bp)	/	123

9.2 NUCLEOTIDE SEQUENCES

Butyryl-CoA dehydrogenase from *Geobacillus thermodenitrificans* (*Gthbcd*)

```
1    ATG GAT TTT AGC CTG ACC AAA GAA CAG CAG ATG ATT AAA
40   GAA ATG GTG CGC GAT TTT GCA GAA AAA GAA ATT GCA CCG
79   TAT GCA GCA AAA TGG GAT GAA GAA GCC TAT TTT CCT CGC
118  GAA GTT TTT CGT AAA ATG GGT GAA CTG GGT CTG CTG GGC
157  CTG CCG TTT CCG GAA AGC TAT GGT GGT GCC GGT GGT GAT
196  ACC ATT AGC TAT GCC ATT GCC GTT GAA GAA ATT GGT CGT
235  GCA TGT GGT GGC ACC GGT CTG AGC TAT GCA GCA GCA GTT
274  AGC CTG GGT GCA AGC CCG ATT TAT TAT TTT GGC AGC GAA
313  GAA CAG AAA CAG ACC TGG CTG GTT CCG ATG GCA AAA GGT
352  GAA ACC CTG GGT GCA TTT GGT CTG ACC GAA CCG AAT GCC
391  GGT TCT GAT GCC GGT GGC ACC CGT ACC ACC GCA GTT CTG
430  GAT GGT GAT GAA TAT GTG ATC AAC GGC GAA AAA TGT TGG
469  ATT ACC AAT GCA CAG TAT GCA CGT CAG GTT ATT GTT ACC
508  GCA GTT ACC GGT AAA GAT GCC CGT GGC AAA AAT ATT ATT
547  ACC GCA CTG ATT GTT CCG ACC GAT TCT CCG GGT TTT ACC
586  ATT CGC AGC AAT TAT GAC AAA ATG GGT GTT CGT GCA AGC
625  AAT ACC TGT GAA CTG GTG TTT GAA AAT GTT CGC GTG CCG
664  AAA GAA AAT GTT CTG GGT GAT CCG CAG AAA GGT TTT AAA
703  CAG TTT CTG TAT ACC CTG GAT GGT GGT CGT ATT AGC ATT
742  GCA GCA CTG GCA GTT GGT ATT GCA CAG GCA GCA TTT GAA
781  AAA GCA CTG CAG TAT GCA AAA GAA CGT GTT CAG TTT GGT
820  CAG AGC ATT AGC AAA TTT CAG GCC ATT CAG TTT AAA CTG
859  GCA GAT ATG GCC ATG GAA ATT GAA CTG GCA CGC AAT ATG
898  GTT TAT AAA GCA GCC TGG CTG AAA GAT CAG GGT AAA CCG
937  TTT ACC AAA GAA GCA AGC TTT GCA AAA CTG TTT GCC AGC
```

976 GAA ATG GGT TTT CGT GTT TGT AAT CAG GCG ATT CAG ATT
1015 CAT GGT GGC TAT GGC TAT ATG AAA GAA TAT GGT GTT GAA
1054 CGT CAT CTG CGC GAT ATT AAA CTG ATG GAA ATT GGC GAA
1093 GGC ACC AGC GAA ATT CAG CGT CTG GTT ATT GCA CGT CAG
1132 CTG GGT TGT

Butyryl CoA dehydrogenase from *Clostridium acetobutylicum* ATCC 824 (*Cabcd*)

1 ATG GAT TTT AAT TTA ACA AGA GAA CAA GAA TTA GTA AGA
40 CAG ATG GTT AGA GAA TTT GCT GAA AAT GAA GTT AAA CCT
79 ATA GCA GCA GAA ATT GAT GAA ACA GAA AGA TTT CCA ATG
118 GAA AAT GTA AAG AAA ATG GGT CAG TAT GGT ATG ATG GGA
157 ATT CCA TTT TCA AAA GAG TAT GGT GGC GCA GGT GGA GAT
196 GTA TTA TCT TAT ATA ATC GCC GTT GAG GAA TTA TCA AAG
235 GTT TGC GGT ACT ACA GGA GTT ATT CTT TCA GCA CAT ACA
274 TCA CTT TGT GCT TCA TTA ATA AAT GAA CAT GGT ACA GAA
313 GAA CAA AAA CAA AAA TAT TTA GTA CCT TTA GCT AAA GGT
352 GAA AAA ATA GGT GCT TAT GGA TTG ACT GAG CCA AAT GCA
391 GGA ACA GAT TCT GGA GCA CAA CAA ACA GTA GCT GTA CTT
430 GAA GGA GAT CAT TAT GTA ATT AAT GGT TCA AAA ATA TTC
469 ATA ACT AAT GGA GGA GTT GCA GAT ACT TTT GTT ATA TTT
508 GCA ATG ACT GAC AGA ACT AAA GGA ACA AAA GGT ATA TCA
547 GCA TTT ATA ATA GAA AAA GGC TTC AAA GGT TTC TCT ATT
586 GGT AAA GTT GAA CAA AAG CTT GGA ATA AGA GCT TCA TCA
625 ACA ACT GAA CTT GTA TTT GAA GAT ATG ATA GTA CCA GTA
664 GAA AAC ATG ATT GGT AAA GAA GGA AAA GGC TTC CCT ATA
703 GCA ATG AAA ACT CTT GAT GGA GGA AGA ATT GGT ATA GCA
742 GCT CAA GCT TTA GGT ATA GCT GAA GGT GCT TTC AAC GAA
781 GCA AGA GCT TAC ATG AAG GAG AGA AAA CAA TTT GGA AGA
820 AGC CTT GAC AAA TTC CAA GGT CTT GCA TGG ATG ATG GCA
859 GAT ATG GAT GTA GCT ATA GAA TCA GCT AGA TAT TTA GTA
898 TAT AAA GCA GCA TAT CTT AAA CAA GCA GGA CTT CCA TAC
937 ACA GTT GAT GCT GCA AGA GCT AAG CTT CAT GCT GCA AAT
976 GTA GCA ATG GAT GTA ACA ACT AAG GCA GTA CAA TTA TTT
1015 GGT GGA TAC GGA TAT ACA AAA GAT TAT CCA GTT GAA AGA
1054 ATG ATG AGA GAT GCT AAG ATA ACT GAA ATA TAT GAA GGA
1093 ACT TCA GAA GTT CAG AAA TTA GTT ATT TCA GGA AAA ATT
1132 TTT AGA TAA

Electron transfer protein A from *Clostridium acetobutylicum* ATCC 824 (*CaetfA*)

```
1    ATG AAT AAA GCA GAT TAC AAG GGC GTA TGG GTG TTT GCT
40   GAA CAA AGA GGC GGA GAA TTA CAA AAG GTA TCA TTG GAA
79   TTA TTA GGT AAA GGT AAG GAA ATG GCT GAG AAA TTA GGC
118  GTT GAA TTA ACA GCT GTT TTA CTT GGA CAT AAT ACT GAA
157  AAA ATG TCA AAG GAT TTA TTA TCT CAT GGA GCA GAT AAG
196  GTT TTA GCA GCA GAT AAT GAA CTT TTA GCA CAT TTT TCA
235  ACA GAT GGA TAT GCT AAA GTT ATA TGT GAT TTA GTT AAT
274  GAA AGA AAG CCA GAA ATA TTA TTC ATA GGA GCT ACT TTC
313  ATA GGA AGA GAT TTA GGA CCA AGA ATA GCA GCA AGA CTT
352  TCT ACT GGT TTA ACT GCT GAT TGT ACA TCA CTT GAC ATA
391  GAT GTA GAA AAT AGA GAT TTA TTG GCT ACA AGA CCA GCG
430  TTT GGT GGA AAT TTG ATA GCT ACA ATA GTT TGT TCA GAC
469  CAC AGA CCA CAA ATG GCT ACA GTA AGA CCT GGT GTG TTT
508  GAA AAA TTA CCT GTT AAT GAT GCA AAT GTT TCT GAT GAT
547  AAA ATA GAA AAA GTT GCA ATT AAA TTA ACA GCA TCA GAC
586  ATA AGA ACA AAA GTT TCA AAA GTT GTT AAG CTT GCT AAA
625  GAT ATT GCA GAT ATC GGA GAA GCT AAG GTA TTA GTT GCT
664  GGT GGT AGA GGA GTT GGA AGC AAA GAA AAC TTT GAA AAA
703  CTT GAA GAG TTA GCA AGT TTA CTT GGT GGA ACA ATA GCC
742  GCT TCA AGA GCA GCA ATA GAA AAA GAA TGG GTT GAT AAG
781  GAC CTT CAA GTA GGT CAA ACT GGT AAA ACT GTA AGA CCA
820  ACT CTT TAT ATT GCA TGT GGT ATA TCA GGA GCT ATC CAG
859  CAT TTA GCA GGT ATG CAA GAT TCA GAT TAC ATA ATT GCT
898  ATA AAT AAA GAT GTA GAA GCC CCA ATA ATG AAG GTA GCA
937  GAT TTG GCT ATA GTT GGT GAT GTA AAT AAA GTT GTA CCA
976  GAA TTA ATA GCT CAA GTT AAA GCT GCT AAT AAT
```

Electron transfer protein B from *Clostridium acetobutylicum* ATCC 824 (*CaetfB*)

```
1    ATG AAT ATA GTT GTT TGT TTA AAA CAA GTT CCA GAT ACA
40   GCG GAA GTT AGA ATA GAT CCA GTT AAG GGA ACA CTT ATA
79   AGA GAA GGA GTT CCA TCA ATA ATA AAT CCA GAT GAT AAA
118  AAC GCA CTT GAG GAA GCT TTA GTA TTA AAA GAT AAT TAT
157  GGT GCA CAT GTA ACA GTT ATA AGT ATG GGA CCT CCA CAA
196  GCT AAA AAT GCT TTA GTA GAA GCT TTG GCT ATG GGT GCT
235  GAT GAA GCT GTA CTT TTA ACA GAT AGA GCA TTT GGA GGA
274  GCA GAT ACA CTT GCG ACT TCA CAT ACA ATT GCA GCA GGA
313  ATT AAG AAG CTA AAA TAT GAT ATA GTT TTT GCT GGA AGG
352  CAG GCT ATA GAT GGA GAT ACA GCT CAG GTT GGA CCA GAA
391  ATA GCT GAG CAT CTT GGA ATA CCT CAA GTA ACT TAT GTT
430  GAG AAA GTT GAA GTT GAT GGA GAT ACT TTA AAG ATT AGA
```

469 AAA GCT TGG GAA GAT GGA TAT GAA GTT GTT GAA GTT AAG
508 ACA CCA GTT CTT TTA ACA GCA ATT AAA GAA TTA AAT GTT
547 CCA AGA TAT ATG AGT GTA GAA AAA ATA TTC GGA GCA TTT
586 GAT AAA GAA GTA AAA ATG TGG ACT GCC GAT GAT ATA GAT
625 GTA GAT AAG GCT AAT TTA GGT CTT AAA GGT TCA CCA ACT
664 AAA GTT AAG AAG TCA TCA ACT AAA GAA GTT AAA GGA CAG
703 GGA GAA GTT ATT GAT AAG CCT GTT AAG GAA GCA GCT GCA
742 TAT GTT GTC TCA AAA TTA AAA GAA GAA CAC TAT ATT TAA

Trans-2-enoyl CoA dehydrogenase from *Treponema denticola* (*Tdter*)

1 ATG ATT GTT AAA CCG ATG GTG CGC AAT AAC ATT TGT CTG
40 AAT GCA CAT CCG CAG GGT TGT AAA AAA GGT GTT GAA GAT
79 CAG ATT GAA TAT ACC AAA AAA CGC ATC ACC GCT GAA GTT
118 AAA GCC GGT GCA AAA GCA CCG AAA AAT GTT CTG GTT CTG
157 GGT TGT AGC AAT GGT TAT GGT CTG GCA AGC CGT ATT ACC
196 GCA GCA TTT GGT TAT GGT GCA GCA ACC ATT GGT GTG AGC
235 TTT GAA AAA GCA GGT AGC GAA ACC AAA TAT GGT ACA CCG
274 GGT TGG TAT AAT AAC CTG GCA TTT GAT GAA GCA GCC AAA
313 CGT GAA GGT CTG TAT AGC GTT ACC ATT GAT GGT GAT GCC
352 TTT AGC GAC GAA ATT AAA GCA CAG GTT ATC GAA GAA GCC
391 AAA AAA AAA GGC ATT AAA TTT GAT CTG ATT GTG TAC AGC
430 CTG GCA AGT CCG GTT CGT ACC GAT CCG GAT ACC GGT ATT
469 ATG CAT AAA AGC GTT CTG AAA CCG TTC GGT AAA ACC TTT
508 ACC GGT AAA ACC GTT GAT CCG TTT ACC GGT GAA CTG AAA
547 GAA ATT AGC GCA GAA CCG GCA AAT GAT GAA GAA GCA GCA
586 GCA ACC GTT AAA GTT ATG GGT GGT GAA GAT TGG GAA CGT
625 TGG ATT AAA CAG CTG AGC AAA GAA GGT CTG CTG GAA GAA
664 GGT TGT ATT ACC CTG GCA TAT AGC TAT ATT GGT CCG GAA
703 GCA ACC CAG GCA CTG TAT CGT AAA GGC ACC ATT GGT AAA
742 GCA AAA GAA CAT CTG GAA GCA ACC GCA CAT CGT CTG AAT
781 AAA GAA AAT CCG AGC ATT CGT GCC TTT GTG AGC GTT AAT
820 AAA GGT CTG GTT ACC CGT GCA AGC GCA GTT ATT CCG GTG
859 ATT CCG CTG TAT CTG GCA AGC CTG TTT AAA GTG ATG AAA
898 GAA AAA GGC AAC CAC GAA GGT TGC ATT GAG CAG ATT ACC
937 CGT CTG TAT GCA GAA CGT CTG TAT CGC AAA GAT GGC ACC
976 ATT CCG GTT GAT GAA GAA AAT CGT ATT CGC ATT GAT GAT
1015 TGG GAA CTG GAA GAA GAT GTT CAG AAA GCA GTT AGC GCA
1054 CTG ATG GAA AAA GTT ACC GGT GAA AAT GCA GAA AGC CTG
1093 ACC GAT CTG GCA GGT TAT CGT CAT GAT TTT CTG GCA AGC
1132 AAT GGC TTT GAT GTG GAA GGC ATT AAT TAT GAA GCC GAA
1171 GTG GAA CGT TTC GAT CGT ATT TTA TAA

ß-Hydroxybutyryl CoA dehydrogenase from *Clostridium acetobutylicum ATCC 824* (*Cahbd*)

```
1    ATG AAA AAG GTA TGT GTT ATA GGT GCA GGT ACT ATG GGT
40   TCA GGA ATT GCT CAG GCA TTT GCA GCT AAA GGA TTT GAA
79   GTA GTA TTA AGA GAT ATT AAA GAT GAA TTT GTT GAT AGA
118  GGA TTA GAT TTT ATC AAT AAA AAT CTT TCT AAA TTA GTT
157  AAA AAA GGA AAG ATA GAA GAA GCT ACT AAA GTT GAA ATC
196  TTA ACT AGA ATT TCC GGA ACA GTT GAC CTT AAT ATG GCA
235  GCT GAT TGC GAT TTA GTT ATA GAA GCA GCT GTT GAA AGA
274  ATG GAT ATT AAA AAG CAG ATT TTT GCT GAC TTA GAC AAT
313  ATA TGC AAG CCA GAA ACA ATT CTT GCA TCA AAT ACA TCA
352  TCA CTT TCA ATA ACA GAA GTG GCA TCA GCA ACT AAA AGA
391  CCT GAT AAG GTT ATA GGT ATG CAT TTC TTT AAT CCA GCT
430  CCT GTT ATG AAG CTT GTA GAG GTA ATA AGA GGA ATA GCT
469  ACA TCA CAA GAA ACT TTT GAT GCA GTT AAA GAG ACA TCT
508  ATA GCA ATA GGA AAA GAT CCT GTA GAA GTA GCA GAA GCA
547  CCA GGA TTT GTT GTA AAT AGA ATA TTA ATA CCA ATG ATT
586  AAT GAA GCA GTT GGT ATA TTA GCA GAA GGA ATA GCT TCA
625  GTA GAA GAC ATA GAT AAA GCT ATG AAA CTT GGA GCT AAT
664  CAC CCA ATG GGA CCA TTA GAA TTA GGT GAT TTT ATA GGT
703  CTT GAT ATA TGT CTT GCT ATA ATG GAT GTT TTA TAC TCA
742  GAA ACT GGA GAT TCT AAG TAT AGA CCA CAT ACA TTA CTT
781  AAG AAG TAT GTA AGA GCA GGA TGG CTT GGA AGA AAA TCA
820  GGA AAA GGT TTC TAC GAT TAT TCA AAA TAA
```

2-Enoate reductase from *Bacillus subtilis* (*yqjM*)

```
1    ATG GCC AGA AAA TTA TTT ACA CCT ATT ACA ATT AAA GAT
40   ATG ACG TTA AAA AAC CGC ATT GTC ATG TCG CCA ATG TGC
79   ATG TAT TCT TCT CAT GAA AAG GAC GGA AAA TTA ACA CCG
118  TTC CAC ATG GCA CAT TAC ATA TCG CGC GCA ATC GGC CAG
157  GTC GGA CTG ATT ATT GTA GAG GCG TCA GCG GTT AAC CCT
196  CAA GGA CGA ATC ACT GAC CAA GAC TTA GGC ATT TGG AGC
235  GAC GAG CAT ATT GAA GGC TTT GCA AAA CTG ACT GAG CAG
274  GTC AAA GAA CAA GGT TCA AAA ATC GGC ATT CAG CTT GCC
313  CAT GCC GGA CGT AAA GCT GAG CTT GAA GGA GAT ATC TTC
352  GCT CCA TCG GCG ATT GCG TTT GAC GAA CAA TCA GCA ACA
391  CCT GTA GAA ATG TCA GCA GAA AAA GTA AAA GAA ACG GTC
430  CAG GAG TTC AAG CAA GCG GCT GCC CGC GCA AAA GAA GCC
469  GGC TTT GAT GTG ATT GAA ATT CAT GCG GCG CAC GGA TAT
508  TTA ATT CAT GAA TTT TTG TCT CCG CTT TCC AAC CAT CGA
547  ACA GAT GAA TAT GGC GGC TCA CCT GAA AAC CGC TAT CGT
```

586 TTC TTG AGA GAG ATC ATT GAT GAA GTC AAA CAA GTA TGG
625 GAC GGT CCT TTA TTT GTC CGT GTA TCT GCT TCT GAC TAC
664 ACT GAT AAA GGC TTA GAC ATT GCC GAT CAC ATC GGT TTT
703 GCA AAA TGG ATG AAG GAG CAG GGT GTT GAC TTA ATT GAC
742 TGC AGC TCA CGC GCC CTT GTT CAC GCA GAC ATT AAC GTA
781 TTC CCT GGC TAT CAG GTC AGC TTC GCT GAG AAA ATC CGT
820 GAA CAG GCG GAC ATG GCT ACT GGT GCC GTC GGC ATG ATT
859 ACA GAC GGT TCA ATG GCT GAA GAA ATT CTG CAA AAC GGA
898 CGT GCC GAC CTC ATC TTT ATC GGC AGA GAG CTT TTG CGG
937 GAT CCA TTT TTT GCA AGA ACT GCT GCG AAA CAG CTC AAT
976 ACA GAG ATT CCG GCC CCT GTT CAA TAC GAA AGA GGC TGG
1015 TAA

Acetolactate synthase from *Sulfolobus solfataricus* (*Ssals*)

1 ATG CCG ACC GGT GCA CGT ATT CTG GTT GAT AGC CTG AAA
40 CGT GAA GGT GTT AAA GTG GTT TTT GGT ATT CCG GGT CTG
79 AGC AAT ATG CAG ATT TAT GAT GCC TTT GTT GAA GAT CTG
118 GCC AAT GGT GAA CTG CGT CAT GTT CTG ATG CGT CAT GAA
157 CAG GCA GCA GCA CAT GCA GCA GAT GGT TAT GCA CGT GCA
196 AGC GGT GTT CCG GGT GTT TGT ACC GCA ACC AGC GGT CCG
235 GGT ACA ACC AAT CTG ACC ACC GGT CTG ATT ACC GCA TAT
274 TGG GAT AGC AGT CCG GTT ATT GCA ATT ACA GGT AAT GTT
313 CCG CGT AGC GTT ATG GGT AAA ATG GCA TTT CAA GAA GCA
352 GAC GCA ATG GGC GTT TTT GAA AAT GTG ACC AAA TAT GTG
391 ATT GGC ATT AAA CGC ATT GAT GAA ATT CCG CAG TGG ATT
430 AAA AAT GCC TTT TAT ATT GCA ACC ACC GGT CGT CCG GGT
469 CCG GTT GTT GTT GAT ATT CCG CGT GAT ATC TTT TAT GAA
508 AAA ATG GAA GAA ATC AAA TGG CCT GAA AAA CCG CTG GTT
547 AAA GGT TAT CGT GAT TTT CCG ACC CGT ATT GAT CGT CTG
586 GCA CTG AAA AAA GCA GCC GAA ATT CTG ATT AAT GCC GAA
625 CGT CCG ATT ATT CTG GTT GGC ACC GGT GTT GTT TGG GCA
664 AAT GCA ACA CCG GAA GTA CTG GAA CTG GCA GAA CTG CTG
703 CAT ATT CCG ATT GTT AGC ACC TTT CCG GGT AAA ACC GCA
742 ATT CCG CAT GAT CAT CCG CTG TAT TTT GGT CCG ATG GGT
781 TAT TAT GGT CGT GCC GAA GCA AGC ATG GCA GCA CTG GAA
820 AGT GAT GCA ATG CTG GTT GTT GGT GCA CGT TTT AGC GAT
859 CGT ACC TTT ACC AGC TAT GAT GAA ATG GTT GAA ACC CGC
898 AAA AAA TTT ATT ATG GTG AAT ATT GAT CCG ACC GAT GGC
937 GAA AAA GCC ATT AAA GTT GAT GTT GGT CTG TAT GGC AAT
976 GCC AAA ATT ATT CTG CGC GAA CTG ATT AAA GCC ATT ATT
1015 ACC CTG GGT CAG AAA CGT GAT AAA AGC GCA TGG ATT AAA

1054 CGC GTG AAA GAA TAC AAA GAA TAT TAC AGC CAG TTT TAT
1093 TAT ACC GAA GAA AAT GGC AAA CTG AAA CCG TGG AAA ATT
1132 ATG AAA ACC ATT CGT CAG AGC CTG CCG CGT GAT GCA ATT
1171 GTT ACC ACC GGT GTT GGT CAG CAT CAG ATG TGG GCA GAA
1210 GTT TTT TGG GAA GTT CTG GAA CCG CGT ACC TTT CTG ACC
1249 AGC AGC GGT ATG GGC ACC ATG GGT TTT GGT CTG CCG GCT
1288 GCA ATG GGT GCA AAA CTG GCA CGT CCG GAT AAA ATT GTT
1327 GTT GAT CTG GAT GGT GAT GGC AGC TTT CTG ATG ACC GGC
1366 ACC AAT CTG GCA ACC GCA GTT GAT GAA CAC ATT CCG GTT
1405 ATT AGC GTG ATT TTT GAT AAT CGT ACC CTG GGT CTG GTT
1444 CGT CAG GTT CAG GAC CTG TTT TTT GGT CGT CGT ATT GTT
1483 GGT GTT GAT TAT GGT CCG AGT CCG GAT TTT GTT AAA CTG
1522 GCC GAA GCA TTT GGT GCA CTG GGT TTT AAT GCA ACC ACC
1561 TAT GAA GAA ATT GAA AAA AGC ATT AAA AGC GCC ATT AAA
1600 GAA GAT ATT CCG GCA GTT ATT CGT GTT CCG GTT GAT AAA
1639 GAA GAA CTG GCA CTG CCG ACC CTG CCT CCG GGT GGT CGT
1678 CTG AAA CAG GTT ATT CTG CGT GAT CCG CGT AAA AGC AGC

Acetolactate synthase from *Bacillus subtilis* (*alsS*)

1 ATG CTG ACC AAA GCA ACC AAA GAA CAG AAA AGC CTG GTG
40 AAA AAT CGT GGT GCA GAA CTG GTT GTT GAT TGT CTG GTT
79 GAA CAG GGT GTT ACC CAT GTT TTT GGT ATT CCG GGT GCA
118 AAA ATT GAT GCA GTT TTT GAT GCC CTG CAG GAT AAA GGT
157 CCG GAA ATT ATT GTT GCA CGC CAT GAA CAG AAT GCA GCA
196 TTT ATG GCA CAG GCA GTT GGT CGT CTG ACC GGT AAA CCG
235 GGT GTT GTT CTG GTT ACC AGC GGT CCG GGT GCA AGC AAT
274 CTG GCA ACC GGT CTG CTG ACC GCA AAT ACC GAA GGT GAT
313 CCG GTT GTT GCA CTG GCA GGT AAT GTT ATT CGT GCA GAT
352 CGT CTG AAA CGT ACC CAT CAG AGC CTG GAT AAT GCA GCA
391 CTG TTT CAG CCG ATT ACC AAA TAT TCA GTT GAA GTG CAG
430 GAT GTG AAA AAT ATT CCG GAA GCA GTT ACC AAT GCC TTT
469 CGT ATT GCA AGC GCA GGT CAG GCA GGC GCA GCA TTT GTT
508 AGC TTT CCG CAG GAT GTT GTT AAT GAA GTG ACC AAT ACC
547 AAA AAT GTT CGT GCA GTT GCA GCA CCG AAA CTG GGT CCG
586 GCA GCA GAT GAT GCA ATT AGC GCA GCA ATT GCA AAA ATT
625 CAG ACC GCA AAA CTG CCG GTT GTT CTG GTG GGT ATG AAA
664 GGT GGT CGT CCG GAA GCA ATT AAA GCA GTT CGT AAA CTG
703 CTG AAA AAA GTT CAG CTG CCG TTT GTT GAA ACC TAT CAG
742 GCA GCA GGC ACC CTG AGC CGT GAT CTG GAA GAT CAG TAT
781 TTT GGT CGT ATT GGT CTG TTT CGT AAT CAG CCT GGT GAT
820 CTG CTG CTG GAA CAG GCA GAT GTT GTT CTG ACC ATT GGT

859 TAT GAT CCG ATT GAG TAT GAT CCG AAA TTT TGG AAC ATT
898 AAT GGC GAT CGC ACC ATT ATT CAC CTG GAT GAA ATT ATT
937 GCC GAT ATC GAT CAT GCA TAT CAG CCG GAT CTG GAA CTG
976 ATT GGT GAT ATT CCG AGC ACC ATT AAC CAT ATT GAA CAT
1015 GAT GCC GTG AAA GTG GAA TTT GCA GAA CGT GAA CAG AAA
1054 ATT CTG AGC GAT CTG AAA CAG TAT ATG CAT GAA GGT GAA
1093 CAG GTT CCG GCA GAT TGG AAA AGC GAT CGT GCA CAT CCG
1132 CTG GAA ATT GTT AAA GAA CTG CGT AAT GCC GTG GAT GAT
1171 CAT GTT ACC GTT ACC TGT GAT ATT GGT AGC CAT GCA ATT
1210 TGG ATG AGC CGT TAT TTT CGT AGC TAT GAA CCG CTG ACC
1249 CTG ATG ATT AGC AAT GGT ATG CAG ACC CTG GGT GTT GCA
1288 CTG CCG TGG GCA ATT GGT GCA AGC CTG GTT AAA CCG GGT
1327 GAA AAA GTT GTT AGC GTT AGC GGT GAT GGT GGT TTT CTG
1366 TTT AGC GCA ATG GAA CTG GAA ACC GCA GTT CGT CTG AAA
1405 GCA CCG ATT GTT CAT ATT GTT TGG AAC GAT AGC ACC TAT
1444 GAT ATG GTT GCA TTT CAG CAG CTG AAA AAA TAT AAT CGT
1483 ACC AGC GCA GTG GAT TTT GGC AAT ATT GAC ATT GTG AAA
1522 TAC GCC GAA AGC TTT GGT GCC ACC GGT CTG CGT GTT GAA
1561 AGT CCG GAT CAG CTG GCA GAT GTT CTG CGT CAG GGT ATG
1600 AAT GCA GAA GGT CCG GTT ATT ATT GAT GTT CCG GTT GAT
1639 TAT AGC GAT AAC ATT AAT CTG GCC AGC GAT AAA CTG CCG
1678 AAA GAA TTT GGT GAA CTG ATG AAA ACC AAA GCC CTG

Acetohydroxyacid synthase (large subunit) from *Geobacillus stearothermophilus* (*ilvB*)

1 ATG GCA AAG ATG AAC GTG GAG GAG CAG ACG AAG ACG AAG
40 ATG AGC GGG TCG ATG ATG TTG ATC GAA GCG CTG AAG GCG
79 GAG CAA GTC GAA GTC ATT TTC GGC TAT CCG GGC GGC GCG
118 GTG CTT CCG CTT TAC GAT GAG CTG TAT AAA GCC GGT GTG
157 TTT CAC GTC TTG ACG CGG CAC GAG CAG GGA GCC ATT CAT
196 GCG GCG GAA GGG TAC GCC CGC ATT TCG GGA AAA CCG GGG
235 GTC GTC ATC GCG ACA TCG GGG CCG GGA GCG ACC AAC ATC
274 GTC ACC GGA CTG ACC GAC GCC ATG ATG GAT TCG TTG CCG
313 CTC GTC GTG TTC ACT GGG CAA GTA GCG ACG AGC GTC ATC
352 GGC TCG GAC GCC TTT CAG GAA GCC GAT GTC GTC GGG ATT
391 ACG ATG CCG ATT ACG AAA CAC AAC TAC CAA GTG CGC GAC
430 ATC AGT GAG CTG CCG AAA ATC ATC AAA GAG GCG TTC CAC
469 ATC GCA ACG ACT GGA CGA CCG GGA CCG GTG TTG ATC GAT
508 ATT CCG AAA GAC ATC ACA ACG GCC GAA GGG GAA TTC GAT
547 TAC GAT GAA GAA GTT TGC TTG CCT GGG TAT CAG CCG ACG
586 ACA CAG CCG AAC CAT TGG CAA ATC CGC CGT CTT GTC GAG

625 GCG GTC AGC CAG TCG AAG CGG CCG GTC ATT TTA GCC GGC
664 GCC GGC GTC TTG CAC GCC GAC GCG GCA AAC GAA TTG CGG
703 CAG TAC GCC GAG CAG CAA AAC ATT CCG GTC GTT CAT ACG
742 CTT CTT GGC CTT GGC GGC TTC CCA GCA GAC CAT CCG CTT
781 TTC TTG GGG ATG GCG GGC ATG CAC GGG ACG TAC ACG GCG
820 AAC ATG GCG CTC TAT GAG TGC GAT TTG CTT ATC AAC ATC
859 GGC GCC CGT TTT GCC GAC CGG GTC ACT GGC AAC TTG AAA
898 TAC TTC GCG CCA AAG GCG ACT GTC GCT CAT ATC GAC ATC
937 GAC CCG GCG GAA ATC GGC AAA AAC GTG CCG ACC AAA ATT
976 CCG ATT GTC AGC GAC GCC AAA GCG GCG CTG CAG GAA CTG
1015 ATC GCC CAG CAA GGC AAA CCG GCT GAC AAC GCG GCG TGG
1054 CTC GAA CAG CTC AAT GAG TGG AAG CGG CGC TTC CCG CTC
1093 CAT TAC GAG CCG GAA GCC GGG ACG ATC AAG CCG CAA AAG
1132 CTT ATC GAA ATG ATT TAC GAA TTG ACA AAT GGC GAA GCG
1171 ATC GTC ACA ACG GAC GTC GGC CAG CAC CAA ATG TGG GCG
1210 GCG CAA TAT TAC AAG TTC AAT CGA CCG AAC CGG TGG GTG
1249 ACG TCC GGG GGG CTC GGC ACA ATG GGC TTT GGG CTT CCG
1288 GCA GCG ATC GGC GCC CAG CTG GCG GAT CGG AGC GCG ACC
1327 GTC GTT TCC ATC GTC GGC GAC GGC GGT TTC CAA ATG ACG
1366 CTT CAA GAG CTG TCG GTC ATT CAA GAG CTG GGG TTG CCA
1405 ATT AAA ATC GTC ATC GTC AAC AAC CAG GCG CTC GGC ATG
1444 GTG CGG CAA TGG CAG GAA CTG TTT TAC GAA AAA CGG TAC
1483 TCC CAT TCG CTC ATC CCG AAT CAT CCG GAT TTT GTA AAA
1522 CTC GCT GAA GCA TAC GGC ATA CCG GGG CTG CGG GCG AAG
1561 ACG GAG GCG GAA GCA GCT GAA GTG TTA AAA CAA GCG TTT
1600 GCG ATG GAC GGC CCG GTG CTG TTG GAT TTC CAC GTC CGC
1639 GCC GAC GAG AAC GTG TAT CCG ATG GTG TCG CCT GGC AAA
1678 GGG CTT CAT GAA ATG GTG GGG GTG AAA GCG TGC GAA GAA

Acetohydroxyacid synthase (small subunit) from *Geobacillus stearothermophilus* (*ilvN*)

1 ATG ATC ACG ATG ACG GTC AAC AAC CGC CCG GGC GTG TTA
40 AAC CGC ATC ACC GGG CTG TTT ACG AAG CGG CAT TAC AAT
79 ATC GAA AGC ATC ACC GTC GGG CAT ACG GAA ATC GAT GGA
118 GTC TCG CGG ATG ACA TTT GTC GTC AAT GTC GAC GAC GAA
157 CGG ACC GCG GAA CAA ATT ATC AAA CTG CTA AAC AAG CAG
196 ATC GAT GTA TTG AAA GTC AAT GAC ATC ACG GAT CAG GCG
235 ATC GTC GCC CGT GAG CTG GCG CTT GTG AAA GTG TCG GCT
274 GCT CCG GCG ATC CGC CAA GAA ATC TAC ACG CTC ATT GAG
313 CCG TTC CGC GCC TCG ATC GTC GAC GTC AGC AAA GAC AGC
352 CTC GTC ATT CAA GTC ACC GGC GAG CCG GAA AAA GTC GAG

391 GCG TTG ATT GAG CTG TTG CGC CCC TAT GGC ATC AAA GAA
430 GTG GCG CGC ACC GGT ACA ACC GCG TTC ACC CGC GGG GCG
469 CAA AAA GCG GCA GCC AAC CAA AAA ACG GCG TTT ATC ATT

Acetohydroxyacid synthase (big subunit) from *E. coli* (*ilvG*)

1 ATG AAT GGC GCA CAG TGG GTG GTA CAT GCG TTG CGG GCA
40 CAG GGT GTG AAC ACC GTT TTC GGT TAT CCG GGT GGC GCA
79 ATT ATG CCG GTT TAC GAT GCA TTG TAT GAC GGC GGC GTG
118 GAG CAC TTG CTA TGC CGA CAT GAG CAG GGT GCG GCA ATG
157 GCG GCT ATC GGT TAT GCT CGT GCT ACC GGC AAA ACT GGC
196 GTA TGT ATC GCC ACG TCT GGT CCG GGC GCA ACC AAC CTG
235 ATA ACC GGG CTT GCG GAC GCA CTG TTA GAT TCC ATC CCT
274 GTT GTT GCC ATC ACC GGT CAA GTG TCC GCA CCG TTT ATC
313 GGC ACT GAC GCA TTT CAG GAA GTG GAT GTC CTG GGA TTG
352 TCG TTA GCC TGT ACC AAG CAC AGC TTT CTG GTG CAG TCG
391 CTG GAA GAG TTG CCG CGC ATC ATG GCT GAA GCA TTC GAC
430 GTT GCC TGC TCA GGT CGT CCT GGT CCG GTT CTG GTC GAT
469 ATC CCA AAA GAT ATC CAG TTA GCC AGC GGT GAC CTG GAA
508 CCG TGG TTC ACC ACC GTT GAA AAC GAA GTG ACT TTC CCA
547 CAT GCC GAA GTT GAG CAA GCG CGC CAG ATG CTG GCA AAA
586 GCG CAA AAA CCG ATG CTG TAC GTT GGC GGT GGC GTG GGT
625 ATG GCG CAG GCA GTT CCG GCT TTG CGT GAA TTT CTC GCT
664 GCC ACA AAA ATG CCT GCC ACC TGT ACG CTG AAA GGG CTG
703 GGC GCA GTA GAA GCA GAT TAT CCG TAC TAT CTG GGC ATG
742 CTG GGG ATG CAC GGC ACC AAA GCG GCA AAC TTC GCG GTG
781 CAG GAG TGT GAC CTG CTG ATC GCC GTG GGC GCA CGT TTT
820 GAT GAC CGG GTG ACC GGC AAA CTG AAC ACC TCC GCG CCA
859 CAC GCC AGT GTT ATC CAT ATG GAT ATC GAC CCG GCA GAA
898 ATG AAC AAG CTG CGT CAG GCA CAT GTG GCA TTA CAA GGT
937 GAT TTA AAT GCT CTG TTA CCA GCA TTA CAG CAG CCG TTA
976 AAT CAA TAT GAC TGG CAG CAA CAC TGC GCG CAG CTG CGT
1015 GAT GAA CAT TCC TGG CGT TAC GAC CAT CCC GGT GAC GCT
1054 ATC TAC GCG CCG TTG TTG TTA AAA CAA CTG TCG GAT CGT
1093 AAA CCT GCG GAT TGC GTC GTG ACC ACA GAT GTG GGG CAG
1132 CAC CAG ATG TGG GCT GCG CAG CAC ATC GCC CAC ACT CGC
1171 CCG GAA AAT TTC ATC ACC TCC AGC GGT TTA GGT ACC ATG
1210 GGT TTT GGT TTA CCG GCG GCG GTT GGC GCA CAA GTC GCG
1249 CGA CCG AAC GAT ACC GTT GTC TGT ATC TCC GGT GAC GGC
1288 TCT TTC ATG ATG AAT GTG CAA GAG CTG GGC ACC GTA AAA
1327 CGC AAG CAG TTA CCG TTG AAA ATC GTC TTA CTC GAT AAC
1366 CAA CGG TTA GGG ATG GTT CGA CAA TGG CAG CAA CTG TTT

1405 TTT CAG GAA CGA TAC AGC GAA ACC ACC CTT ACT GAT AAC
1444 CCC GAT TTC CTC ATG TTA GCC AGC GCC TTC GGC ATC CAT
1483 GGC CAA CAC ATC ACC CGG AAA GAC CAG GTT GAA GCG GCA
1522 CTC GAC ACC ATG CTG AAC AGT GAT GGG CCA TAC CTG CTT
1561 CAT GTC TCA ATC GAC GAA CTT GAG AAC GTC TGG CCG CTG
1600 GTG CCG CCT GGC GCC AGT AAT TCA GAA ATG TTG GAG AAA
1639 TTA TCA TGA

LIST OF PUBLICATIONS

Guterl JK, Garbe D, Carsten J, Steffler F, Sommer B, Reisse S, Philipp A, Haack M, Rühmann B, Koltermann A, Kettling U, Brück T, Sieber V. 2012. Cell-free metabolic engineering: production of chemicals by minimized reaction cascades. ChemSusChem **5:**2165-2172.

Sommer B, Garbe D, Schrepfer P, Brück T. 2013. Characterization of a highly thermostable ß-hydroxybutyryl CoA dehydrogenase from Clostridium acetobutylicum ATCC 824. Journal of Molecular Catalysis B: Enzymatic 98: 138-144.

Sommer B, Haack M, Garbe D, Brück T. 2013. Catalytic Modules in Non-Natural Butanol Biosynthesis: Conversion of the Key Intermediate Crotylalcohol to n-Butanol via a Designed Enzyme Cascade. JSM Biotechnol Bioeng 1(2): 1010

Sommer B, Waege I, Pöllmann D, Seitz T, Thomm M, Sterner R, Hausner W. 2013. Activation of a chimeric Rpb5/RpoH subunit using library selection. Plos One. Accepted.

Sommer B, Moeller H, Langner C, Bourenkov G, Garbe D, Loll B, Brück T. 2013. Detailed structure-function correlations of Bacillus subtilis Acetolactate Synthase. Manuscript in Preperation.